The cellular, chemical, and molecular response of the sponge *Aplysina aerophoba* to grazing

Dissertation

in fulfilment of the requirements for the degree of Doctor in Natural Sciences

of the Faculty of Mathematics and Natural Sciences

at Kiel University

Submitted by

Yu-Chen Wu

Kiel, 2019

First examiner:	Prof. Dr. Ute Hentschel Humeida
Second examiner:	Prof. Dr. Martin Wahl

Date of the oral examination: 11th December, 2019

Statutory Declaration

Declaration according to § 9 (2) of the Doctoral Degree Regulations of the Faculty of Mathematics and Natural Sciences and the Faculty of Engineering at Christian-Albrechts-Universität zu Kiel from 9 August 2018

I, Yu-Chen Wu, herewith declare that the PhD thesis entitled “The cellular, chemical, and molecular response of the sponge *Aplysina aerophoba* to grazing” is an original report of my research, has been written by me, has not been submitted for any previous degree or publication, and has been prepared subject to the Rules of Good Scientific Practice of the German Research Foundation. I declare that all my academic degrees have never been withdrawn. The experimental work is almost entirely my own work except where explicitly stated otherwise in the text; the collaborative contributions have been indicated clearly and acknowledged. Due references have been provided on all supporting literatures and resources. Furthermore, I declare that the submitted written (bound) copies of the present thesis and the version submitted on a data carrier are consistent with each other in contents.

Place, Date: _____ Signature:_____

Abstract

Sponges (Phylum Porifera) are sessile invertebrates that produce secondary metabolites to defend against predators, competition and bio-fouling. Nevertheless, certain sea slugs (Phylum Mollusca: Class Opistobranchia) have specialized in grazing on specific sponge species, which leaves the sponge tissue exposed. To date, no study has examined the response of sponges upon grazing. In the present PhD thesis, I investigated the Mediterranean sponge *Aplysina aerophoba* which produces brominated alkaloids with antibacterial and deterrence properties against generalist predators. These brominated compounds are enriched in a particular cell type, so-called spherulous cells. However, *A. aerophoba* is the main food source for a specialist grazer – the sea slug *Tylodina perversa* – which tolerates brominated compounds and also exploits them for its own defense. By ways of microscopic technologies, MALDI-imaging MS, and RNA-Seq, I aimed to investigate the cellular processes, the potential role of secondary metabolites, and molecular mechanisms in the response of the sponge to grazing. I hypothesized that grazing can induce signaling pathways for a recruitment of spherulous cells with secondary metabolites. Three treatments were applied: control, grazing, and mechanical damage. Samples were collected 3 hours, 1 day, 3 days, and 6 days after treatment. My results showed that spherulous cells were recruited to the wounded site in a time-dependent manner. MALDI-imaging MS showed that both brominated compounds (aerophobin-2 and aeroplysinin-1) localized usually at the sponge surface and accumulated at the damaged surface upon wounding. The expression of key potential candidate genes for cell migration, wound sealing, and immune response were activated also in a time-dependent manner based on RNA-Seq data. Compared to mechanical damage, grazing triggered a relatively lower degree of stimulus perception, inflammatory response, and oxidative stress, and induced a relatively higher degree of chemical perception, phagocytosis, and mucus production. As spherulous cells are common in many members of the class Demospongiae, the recruitment of defensive cells may also occur in other sponges for protecting these filter-feeders. My PhD thesis contributes to understanding the evolutionary mechanisms in sponges for facing grazing and wounding.

Zusammenfassung

Schwämme sind sessile Invertebraten, die Sekundärmetaboliten produzieren um sich gegen Feinde, Konkurrenz und das Überwachsenwerden durch Biofilme (sogenanntes „bio-fouling“) zu verteidigen. Bestimmte Meeresschnecken haben sich jedoch als Fraßfeinde auf bestimmte Schwammarten spezialisiert. Bisher gibt es keine Untersuchungen, wie ein Schwamm auf den Befall durch Schnecken als Fraßfeinde reagiert. Im Rahmen meiner Doktorarbeit untersuchte ich den Mittelmeerschwamm *Aplysina aerophoba*, der bromierte Alkaloide mit antibakteriellen und abschreckenden Eigenschaften gegen generalistische Feinde produziert. Diese bromierten Verbindungen reichern sich in einem bestimmten Zelltyp, den sogenannten Rosettenzellen, an. *A. aerophoba* ist jedoch auch die Hauptnahrungsquelle für einen spezialisierten Fraßfeind, die Meeresschnecke *Tylodina perversa*, die bromierte Verbindungen toleriert und diese zur eigenen Abwehr ausnutzt. Mein Ziel im Rahmen meiner Doktorarbeit war es, mittels Mikroskopie, MALDI-Imaging-MS und Transkriptom-Analysen („RNA-Seq“) die zellulären Prozesse, die mögliche Rolle von Sekundärmetaboliten sowie die molekularen Mechanismen des Schwamms nach der Beweidung durch die Schnecke zu untersuchen. Ich stellte die Hypothese auf, dass die Beweidung des Schwamms durch die Schnecke Signalwege für die Rekrutierung von Rosettenzellen mit Sekundärmetaboliten hervorrufen kann. Es wurden drei Behandlungen angewendet: Kontrolle, Beweidung und mechanische Verletzung. Die Proben wurden 3 Stunden, 1 Tag, 3 Tage und 6 Tage nach der Behandlung gesammelt. Meine Ergebnisse zeigten, dass sich die Rosettenzellen und die beiden bromierten Verbindungen Aerophobin-2 and Aeroplysinin-1 zeitabhängig an der verletzten Stelle ansammelten. Potentielle Kandidatengene für Zellmigration, Wundversiegelung und Immunantwort wurden aktiviert. Im Vergleich mit der mechanischen Verletzung löste die Beweidung die Schnecke einen relativ geringen Grad an Reizwahrnehmung, Entzündungsreaktion und oxidativem Stress aus und induzierte einen hohen Grad an chemischer Wahrnehmung, Phagozytose und Schleimproduktion. Da Rosettenzellen bei vielen Schwammarten der Klasse Demospongiae vorkommen, kann die Rekrutierung von Abwehrzellen auch bei anderen Schwämmen zum Schutz dieser filtrierenden Organismen erfolgen. Diese Promotionsarbeit trägt zum Verständnis der evolutiven Mechanismen zwischen sessilen Schwämmen und spezialisierten Fraßfeinden bei.

Acknowledgements

First and foremost I want to say a very big “thank you” to my supervisor Prof. Dr. Ute Hentschel Humeida (GEOMAR) for the friendly reception in her laboratory, for founding and supporting me over the PhD years. I appreciate all her guidance and encouragement to make my PhD thesis meaningful. I want to thank her for all of the opportunities I was given to conduct my research.

Many thanks also to Prof. Dr. Martin Wahl (GEOMAR) for taking over the second expert opinion, for serving on my PhD dissertation committee, for his scientific advice and valuable knowledge. I am also very grateful to his insightful comments, suggestions, and inspirational discussions during advisory committee meetings.

I would also like to thank my oral defense committee members, Prof. Dr. Dietrich Ober (Kiel University) for taking over the examiner role and Prof. Dr. Mirjam Perner for agreeing to serve as my committee chair.

Special thanks go to Dr. Lucía Pita Galán (GEOMAR) for the support of all the work during my PhD life. Without all her experimental contributions and endless support, expertise in RNA-Seq data analysis, advisory role and valuable input, many helpful and critical discussions, passionate attitude and encouragement, this PhD thesis would not have been achieved.

My deep appreciation goes to Dr. María García-Altares (HKI, Jena) for her wonderful collaboration and expert advice in MALDI-imaging MS. I gratefully acknowledge Dr. Mark Lenz (GEOMAR) for sharing his expert knowledge in statistics. I also thank Dr. Sören Franzenburg (IKMB) for his friendly collaboration in RNA sequencing. I am very appreciative of Dr. Carsten Thoms (OVGU, Magdeburg) for sharing his tremendous experience in studying sponges and sea slugs.

I am also very grateful to Dr. Marta Ribes and Marc Catllà (CSIC, Barcelona, Spain), Dr. Laura Rix (University of Queensland, Brisbane, Australia), Dr. Rafel Coma (CSIC, Blanes, Spain), as well as Berta Pintó, Dr. Creu Palacín Cabañas, and Dr. Manuel Ballesteros (University of Barcelona, Spain) for excellent collaboration, for collections of sponges and sea slugs, and for supporting my experiments.

My thanks also go out to the support I received from all members of the working group Marine Symbioses (GEOMAR). I greatly appreciate the support of a thousand little things of everyday life in the lab and for the pleasant working atmosphere. My sincere thanks also go to all members of the Central Microscopy (Kiel University) for their friendly and expert support.

Many thanks go to my family: my parents, who always give me motivation with their encouragement and warm love. I want to thank my mother-in-law, all my family and my friends who always give me their love and stand by my side. I also thank my dear daughters, who bring happiness, joy and laughter to my life every day.

Lastly, my special thanks go to my husband for his ongoing support. He has brought so much understanding when I sat for long hours at the work desk. I express my deepest gratitude to him for creating happiness during this challenging time.

Table of Contents

List of Tables

List of Figures

List of Materials and Equipments

Materials

Sponge *Aplysina aerophoba*

Sea slug *Tylodina perversa*

Sterile scalpels (B. Braun, Germany)

Sterile steel blades (Schreiber Instrumente, Germany)

Sterile cryotubes (Greiner Bio-one, Germany)

Tweezers (Plano, Germany)

Aluminum

Embedding capsules (Plano, Germany)

Microscope glass slides (Superfrost Plus, Menzel, Germany)

Microscope cover slips (Menzel, Germany)

MALDI-imaging MS glass slide Indium-Tin-Oxide (ITO, Bruker Daltonics, Bremen, Germany)

Double-sided adhesive conductive carbon tape (Plano, Germany)

Pioloform coated grids (Plano, Germany)

Cryomold (22 mm in diameter, 5 mm in height, Tissue-Tek@ Cryomold@, Plano, Germany)

Chemicals and Kits

25 % glutaraldehyde (Carl Roth, Germany)

Cacodylic acid sodium salt trihydrate (cacodylate, Carl Roth, Germany)

D(+)-sucrose (Carl Roth, Germany)

Osmium tetroxide (Carl Roth, Germany)

100% ethanol Rotipuran (Carl Roth, Germany)

LR White resin (Plano, Germany)

Mounting medium (Biomount 2, BBI Solutions)

Richardson solution (provided by the Central Microscopy of University of Kiel, Germany)

Uranyl acetate replacement stain (Science Services, Germany)

Reynold´s lead citrate (provided by the Central Microscopy of University of Kiel, Germany)

Liquid nitrogen

Embedding medium, Optimal Cutting Temperature (OCT, Tissue-Tek@, Plano, Germany)

Universal MALDI matrix (1:1 mixture of 2,5-dihydroxybenzoic acid and α-cyano-4-hydroxy-cinnamic acid; Bruker Daltonics, Germany)

Acetonitrile/methanol (70:30, v/v)

Peptide Calibration Standard II (Bruker Daltonics)

Standard reference aerophobin-2 (Santa Cruz Biotechnology, Germany)

Standard reference aeroplysinin-1 (Santa Cruz Biotechnology, Germany)

RNA*later*TM (Invitrogen, Thermo Fisher Scientific, Germany)
RNaseZapTM (Invitrogen, Thermo Fisher Scientific, Germany)
ß-mercaptoethanol (Sigma-Aldrich, Germany)
RLTplus buffer (Qiagen, Germany)
AllPrep DNA/RNA Mini Kit (Qiagen, Germany)
Buffer EB (Qiagen, German)
DNA-free DNase Treatment and Removal Reagent (Ambion, Germany)
TruSeq stranded mRNA library prep kit (Illumina, Inc., USA)

Equipments

Aquaria (6L)
Flow-through system for aquaria experiments (provided by ICM-CSIC, Spain)
GoPro Hero 4 camera
Hood
4 ºC fridge
-20 °C freezer
-80 °C freezer
Incubator (59 °C)
Microscope (ZEISS Axio Observer, version 1.1, Zeiss, Germany)
Transmission electron microscope (Tecnai G2 Spirit BioTwin, 80 kV, FEI, USA)
Ultramicrotome (Reichert Ultracut S, Leica, Austria)
Cryostat (CM3050 S, Leica, Germany)
ImagePrep device 2.0 (Bruker Daltonics)
UltrafleXtreme MALDI TOF/TOF (Bruker Daltonics)
PowerLyzerTM24 (Mobio, Qiagen, Germany)
Biometra TRIO kombi PCR (Biometra, Germany)
NanoDrop 2000c Spectrophotometer (peolab, Germany)
Qubit 2.0 (Life Technologies, Carlsband, CA)
ExperionTM Electrophoresis Station (Bio-Rad, Hercules, CA)
HiSeq 4000 system (Illumina, Inc., USA)

Software

ImageJ (version 1.51j8, Java 1.8.0_112, Schneider *et al.*, 2012)
R (Version R 3.6.0, R Core Team, 2019)
RStudio (version 1.2.1335, RStudio Team, 2019)
SCiLS Lab 2015b (SCiLS, Bremen, Germany)
Trimmomatic-version 0.38
FastQC-version 0.11.7

Kaiju-version 1.6.2

Trinity-version 2.6.6

TransRate-version 1.0.3

BUSCO-version 3

Trinotate-version 3.0.2

RSEM bowtie2- version 1.2.19

edgeR implemented in Trinity-version 2.6.5

List of Abbreviations

1d	Time point 1 day after stop of treatment
3d	Time point 3 days after stop of treatment
3h	Time point 3 hours after stop of treatment
6d	Time point 6 days after stop of treatment
1d-2016	Experiment for the sampling time point 1 day after stop of treatment in 2016
1d-2017	Experiment for the sampling time point 1 day after stop of treatment in 2017
3d-2016	Experiment for the sampling time point 3 days after stop of treatment in 2016
3h-2017	Experiment for the sampling time point 3 hours after stop of treatment in 2017
6d-2016	Experiment for the sampling time point 6 days after stop of treatment in 2016
ADAMTS	A disintegrin and metalloproteinase with thrombospondin motifs family-like gene
BAG	BAG domain-containing gene
bHLH	helix-loop-helix DNA-binding domain-containing gene
Buffer	2.5 % glutaraldehyde in 0.1 M cacodylate buffer/11 % sucrose
CaMK	Calcium/calmodulin-dependent protein kinase-like gene
Calx-beta	Calx-beta domain-containing gene
Cdk5 activator	cyclin-dependent kinase 5 activator protein domain-containing gene
CLOCK	Circadian locomoter output cycles protein kaput-like
Collagen	Collagen triplex helix repeat domain-containing gene
DBH	dopamine beta-hydroxylase
DEG	Differentially-expressed gene
DnaJ	DnaJ homolog subfamily B member 1-like gene
DVL	Segment polarity protein dishevelled homolog family-like gene
ECM	Extracellular matrix
FDR	False Discovery Rate
Fibrinogen	Fibrinogen beta and gamma chains, C-terminal globular domain-containing gene
Fibronectin	Fibronectin type III domain-containing gene
$GABA_BR$	Gamma-aminobutyric acid type B receptor subunit family-like gene
glmmPQL	Generalized Linear Mixed-effects Model via Penalized Quasi-Likelihood
GPCR	G protein-coupled receptor
GST	Glutathione S-transferase domain-containing genes
HIF	Hypoxia-inducible factor-like gene
HSP16	Hsp20/alpha crystallin family domain-containing gene
IgGFcBP	IgGFc binding protein
ITO	Indium-Tin-Oxide

Immuno-globulin	Immunoglobulin domain-containing gene
Kunitz	Kunitz-type protease inhibitor-like gene
MALDI-imaging MS	Matrix-assisted laser desorption/ionization imaging mass spectrometry
MAPK	Mitogen-activated protein kinase
MAPKKK	Mitogen-activated protein kinase kinase kinase
MOXD	DBH-like monooxygenase protein homolog-like gene
MUSK	Muscle, skeletal receptor tyrosine-protein kinase
NF-kB	Nuclear factor NF-kappa-B
OCT	Optimal Cutting Temperature
PLPL9	85/88 kDa calcium-independent phospholipase A2-like
PXDN	Animal haem peroxidase containing gene
RNA-Seq	RNA sequencing
ROI	Region Of Interest
TEM	Transmission electron microscopy
TGFß	Transforming growth factor beta
TGM	Transglutaminase/ protein-glutamine gamma-glutamyltransferase family-like gene
THAP	THAP domain-containing protein 11-like gene
TRAF	TNF receptor-associated factor family-like gene
TRPA1	Transient receptor potential cation channel subfamily A member 1
TSN	tetraspanin family domain-containing gene
SRCR	Scavenger receptor cysteine-rich domain-containing gene

"The performances of nature are unique:

generators of precious chemical systems and adaptable to extreme conditions."

-- Book Chemical Ecology, Wiley-ISTE, 2016

1. Introduction

1.1 Secondary metabolites mediate ecological interactions

Prey-predator interactions have been well studied in terrestrial plant-herbivore model systems (reviewed in Baldwin, 1990; Schuman and Baldwin, 2016; Wang *et al.*, 2016a; Erb and Reymond, 2019). Predation acts as the selection pressure that triggers the production of diverse secondary metabolites in sessile preys for their defense and survival. This concept “secondary metabolites” was defined by Nobel Prize winner Kossel (1891). Kossel stated that those substances vary from organism to organism and are not included in the basic metabolism in living cells present (Kossel, 1891; reviewed in Firn and Jones, 2009). Secondary metabolites are particular relevant for marine sessile organisms in the context of chemical defense (Hay, 1996; Cronin, 2001; Thoms and Schupp, 2007; Pawlik, 2011; Rohde and Schupp, 2018). The number of publications in marine secondary metabolites (or marine natural products) increased dramatically in the last 60 years (reviewed in Blunt, *et al.*, 2018). However, ecological roles of these compounds, the “how, when and why” are they produced remain understudied.

1.2 Sponges as basal animal phyla

Sponges (Phylum Porifera) constitute one of the oldest animal groups (Metazoa; Dunn *et al.*, 2015; Moroz and Kohn, 2016; Cavalier-Smith, 2017) and exist since 600 million years in time (Li *et al.*, 1998; Yin *et al.*, 2015). Sponges inhabit freshwater as well as marine ecosystems, but are more commonly found in oceans, from tidal zones to the deep-sea as well as from tropical to cold-waters (Hooper and Van Soest, 2002; Van Soest *et al.*, 2012). Until now, 9,194 sponge species are recorded in the World Porifera Database (Van Soest *et al.*, 2019). Adult sponges are sessile and play important roles in many marine ecosystems (Bell, 2008; Pawlik and McMurray, 2020). Sponges have no true tissues and sensory organs, but different types of cells with diverse functions (Simpson 1984; De Vos *et al.*, 1991; Ereskovsky, 2010). The outer

layer of sponges is the thin pinacoderm consisting of pinacocytes. Flagellated choanocytes are organized in choanocyte chambers and create a flow of water through the sponge body. Food particles are taken up and passed through the choanocytes into the mesohyl interior where they are digested by the amoeboid-like archeocytes. Both archeocytes and choanocytes contribute to the stem cell system capable to differentiate into all of the other types of sponge cells (Funayama, 2010; 2018). Archeocytes are found in the mesohyl which is a space between the pinacoderm and choanocyte chambers. The mesohyl fills the main interior space of sponges and contains skeletal elements (spicules or spongin fibers) and other cell types such as spherulous cells. Besides, the sponge mesohyl can harbor symbiotic microbes that contribute up to 35 % of the animal´s biomass (reviewed in Hentschel *et al.*, 2012).

1.3 Survival strategies of sponges throughout evolution

The long evolutionary history and the abundance in different ecological habitats of sponges indicate their ability to respond and adapt to different environmental conditions. They face multiple challenges, such the abundance and diversity of pathogens in the marine environment, the presence of predators and fouling organisms, as well as competition for space. These driving forces were instrumental for sponges to develop defenses protecting these sessile, soft-bodied invertebrates throughout evolution (Loh and Pawlik, 2014). Some species have evolved to be capable of rapid growth and recovery (Ayling, 1983). Some have the cryptic mimicry to hide themselves effectively under corals (Bakus and Green, 1974). Some have hard structures like spicules to damage gut of predators (Gemballa and Schermutzki, 2004). But the species of the largest sponge class Demospongiae rely on chemical defenses with probed deterrent effect that could be the source of secondary metabolites (Blunt *et al.*, 2018; El-Demerdash *et al.*, 2019; Shady *et al.*, 2019).

It is hypothesized, that maintenance of the interactions with other organisms plays a major selective role throughout evolution, leading to the accumulation of bioactive secondary metabolites in marine sponges. Secondary metabolites have three major ecological functions: – antimicrobial activities, – antifouling effects, and – defense against predators (Hay, 1996; Becerro *et al.*, 2003a; Thoms and Schupp, 2007;

Pawlik, 2011; Rohde and Schupp, 2018). Surveys revealed that feeding on chemically-protected sponges by fishes is indeed rare (Randall and Hartmann, 1968; Carpenter, 1986; Braekman and Daloze, 1986; Wulff, 2006). However, sponge secondary metabolites may serve as stimuli or attractants for specialized consumers.

1.4 Specific associations between sponges and sea slugs

A prominent example of specific interactions is the group of shell-free molluscs – opisthobranchs – which are often found on marine sponges (Faulkner and Ghiselin, 1983; Willan, 1984; Proksch, 1994). These sea slugs may benefit by living on sponges that are unpalatable by fishes. In general, they are specialized in a chemically-defended sponge species so they also avoid competition for food.

Opisthobranchs can take secondary metabolites from sponges and incorporate them or *de novo* synthesize them for their own defense (reviewed in Bornancin *et al.*, 2017). This specific interaction benefits the opisthobranch to keep their population growing. Feeding on opisthobranchs by fishes has not yet been observed. The selective feeding on marine sponges and the chemistry of sea slugs have been already addressed (see review by Pawlik 1993; Proksch, 1994; Bornancin *et al.*, 2017), however, the evolutionary and ecological implications of the association remain unclear.

1.5 The interaction between the sponge *Aplysina aerophoba* and the sea slug *Tylodina perversa*: a case study

In this PhD thesis, I study the interaction between the opisthobranch *Tylodina perversa* and the sponge *Aplysina aerophoba* to understand the sponge´s response in response to sea slug grazing (**Figure 1**). The Mediterranean sponge *A. aerophoba* accumulates “brominated alkaloids” as secondary metabolites up to 12 % of its dry weight (Teeyapant *et al.*, 1993a). Those brominated compounds play ecological roles as protection against microbes and defense against consumers (Teeyapant *et al.*, 1993b; Weiss *et al.*, 1996; Koulman *et al.*, 1996; Thoms *et al.*, 2004; Niemann *et al.*, 2015).

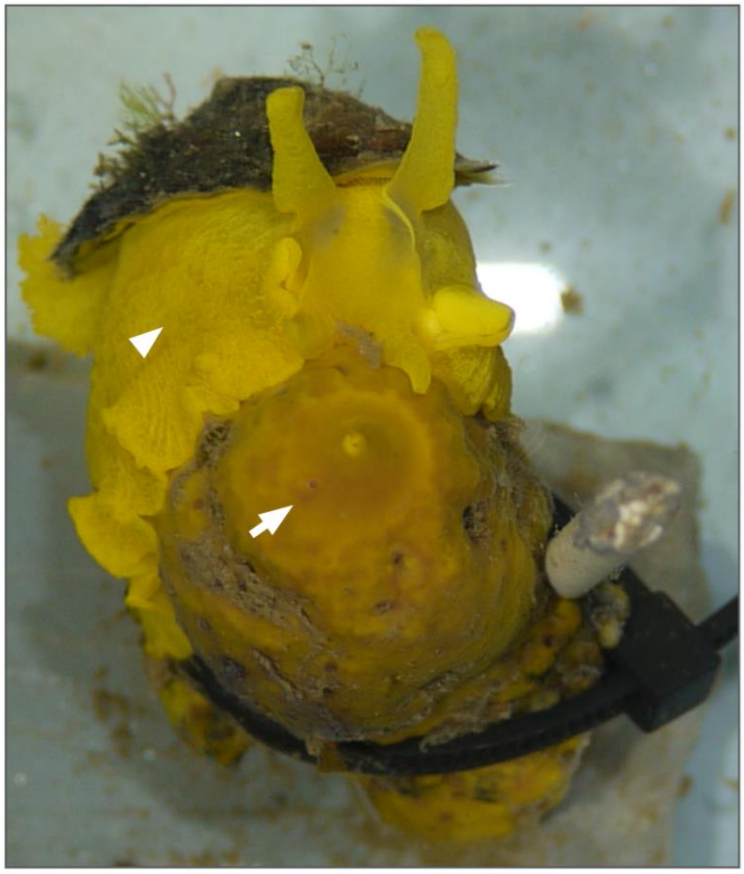

Figure 1. An image of the sponge and the opistobranch grazing on it. *A. aerophoba* (**arrow**) was grazed by *T. perversa* (**arrowhead**).

The sea slug *T. perversa* can take up and store the saffron-colored pigment uranidine which contributes the coloration of *T. perversa* as well as *A. aerophoba* (Chimino *et al.*, 1984). For this reason, *T. perversa* is also called “yellow Tylodina.” As a result, this sponge-feeding opisthobranch blends in the yellow *A. aerophoba* so that it becomes unvisible and thus minimizes its chance to be preyed on by fishes or crabs. *Tylodina perversa* feeds preferentially on the ectoderm found in 1-2 mm in the outer layer of *A. aerophoba* which is packed with cyanobacteria (Becerro *et al.*, 2003b). Becerro and colleagues suggested that *T. perversa* may be preferentially feeding on cyanobacteria and rather than on the sponge *A. aerophoba* itself. Ebel and colleagues (1999) reported that after feeding on *A. aerophoba*, the opisthobranch *T. perversa* could not only accumulate but also selectively sequester toxic sponge-derived brominated alkaloids including aerophobin-2 and isofistularin-3, in which aerophobin-2 concentration was higher (about 70 % of all identified alkaloids) in mantles, mucus, and egg masses of the opisthobranch than isofistularin-3. It seems possible that the ecological survival strategies of the opisthobranch *T. perversa* rely, in part, on tolerance to, accumulation and sequestering of selective

secondary metabolites including uranidine and brominated alkaloids from its prey (Ebel *et al.*, 1999; Thoms *et al.*, 2003; Becerro *et al.*, 2003b; Thoms *et al.*, 2006a).

1.6 Brominated alkaloids in *Aplysina aerophoba*

There are two groups of brominated compounds in *A. aerophoba*. The first group is so called “precursors,” its major compounds are aerophobin-2, isofistularin-3, and aplysinamisin-1. They are all derived from tyrosine (reviewed in Peng *et al.*, 2005; Niemann *et al.*, 2015). Brominated precursors have been showed to have repellency activity against marine fishes (Becerro *et al.*, 2003a; Thoms *et al.*, 2004). Teeyapant and Proksch (1993) have detected a transformation of these brominated precursors to nitrile aeroplysinin-1 and dienone by tissue extraction under an aqueous condition. Ebel and colleagues (1997) have showed in *in vitro* assays that the transformation of brominated alkaloids was induced within 40-50 seconds after mechanical damage on one piece tissue obtained from *A. aerophoba* (**Figure 2**). When sponge tissue (in aqueous condition) was heated, no transformation could be detected, suggesting that the transformation is an enzymatic process (Teeyapant and Proksch, 1993). However, until now, no enzymes which may involve in this transformation in *A. aerophoba* can be found, except that Lipowicz and colleagues have reported a transformation of aeroplysinin-1 into the dienone in sister group *Aplysina cavernicola* through an enzyme nitrile hydratase (Lipowicz *et al.*, 2013).

These second group “converted products” have multiple functions. They showed repellency and cytotoxic activities (Teeyapant *et al.*, 1993b; Weiss *et al.*, 1996; Ebel *et al.*, 1997; Koulman *et al.*, 1996; Niemann *et al.*, 2015). Besides, they present stronger antibiotic activity than the precursors aerophobin-2 and isofistularin-3, and can protect sponges against bacterial invasion (Teeyapant *et al.*, 1993b; Thoms *et al.*, 2006b). It is hypothesized that the sponges have evolved this transformation as a defensive mechanism against bacterial pathogen in exposed tissues after wounding and breakdown of the cellular compartmentation (Thoms *et al.*, 2006b).

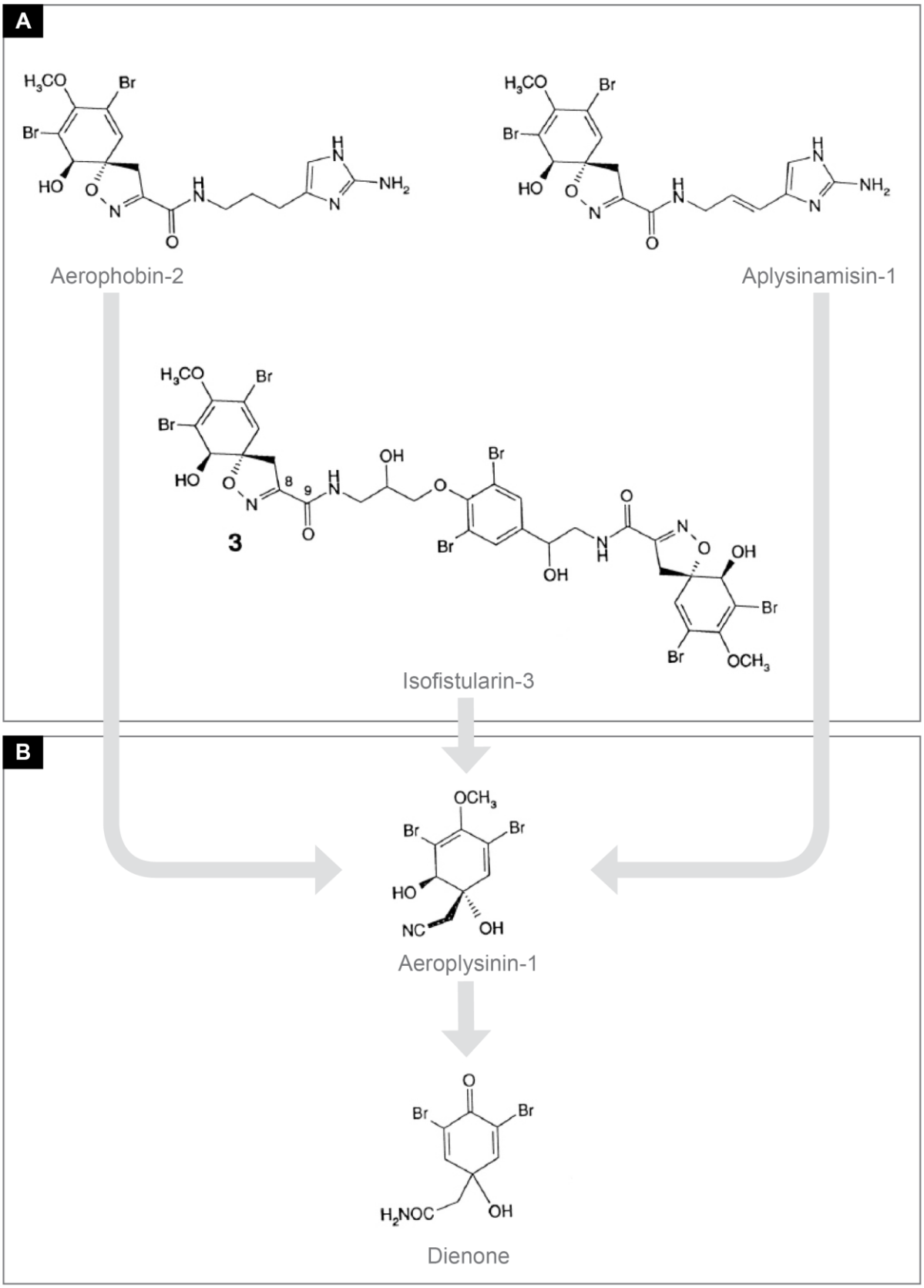

Figure 2. Transformation of brominated alkaloids in *A. aerophoba*. Brominated precursors (**A**) can be converted to aeroplysinin-1 which is further converted to dienone (**B**), modified from Ebel *et al*. (1997).

This transformation also occurs in other species in the genus *Aplysina* including *A. cavernicola, A. archeri, A. cauliformis, A. fistularis, A. fulva, and A. lacunose* (Ebel *et al.*, 1997). The first evidence of the localization of brominated compounds in the genus *Aplysina* was provided by Thompson and colleagues (1983). They detected two brominated alkaloids aerothionin and homoaerothionin in a specialized cell type, so called spherulous cells, in *A. fistularis*. Interestingly, 17 years later, the cellular localization of brominated compounds in *A. aerophoba* has been shown in the spherulous cells with electron-dense spherules and the outer layer of spongin fibers (Turon *et al.*, 2000).

Studies on spherulous cells in the genus *Aplysina* have reported that this specialized cell type had an average length of 12 µm, contained membrane-bound spherules with numerous granules, and were often found near collagen fibrils (De Vos *et al.*, 1991), beneath the pinacoderm, and near excurrent canals (Vacelet, 1967; Thompson *et al.*, 1983; Becerro *et al.*, 1997; Turon *et al.*, 2000; Maldonado 2016). Spherulous cells have been found to degenerate in the mesohyl and release their toxic compounds into the mesohyl, indicates their defensive role (Thompson *et al.*, 1983; Uriz *et al.*, 1996a; Turon *et al.*, 2000).

1.7 Aims

This PhD thesis aims to characterize the response of *A. aerophoba* to *T. perversa* at cellular, chemical, and molecular levels. I performed controlled experiments to expose the sponge to grazing by opistobranchs. To further elucidate if the sponge response specifically evolved from the grazing interaction, all my experiments included a treatment in which a genetically identical sponge specimen was mechanically-damaged with a scalpel (abbreviated as mechanical damage).

Aim 1: Assess the role of spherulous cells in the response to grazing

I hypothesize that grazing induces a recruitment of spherulous cells – brominated alkaloid containing cells – to wounded sites in order to protect damaged areas. To test this hypothesis, I compared the number of spherulous cells between grazed and control sponges by microscopy.

Aim 2: Characterize the distribution and transformation of brominated alkaloids upon wounding

Second, I hypothesize that (i) brominated alkaloids localize mainly at the surface in healthy sponges as a way to ensure constitutive defense of most vulnerable areas, and that (ii) brominated precursors are converted to more toxic forms at grazed sites. I applied Matrix-Assisted Laser Desorption/Ionization Imaging Mass Spectrometry (MALDI-imaging MS) in collaboration with colleagues (Dr. María García-Altares, HKI) to visualize spatial patterns of two brominated compounds in the sponge, i.e., the most abundant brominated precursor aerophobin-2 and the most abundant converted product aeroplysinin-1.

Aim 3: Decipher the molecular responses of the sponge to grazing

Third, I hypothesize that grazing triggers signaling pathways which activates the recruitment of spherulous cells to wounded sites. To test my hypothesis, I compared gene expression between treatments based on RNA sequencing (RNA-Seq) data.

2. Methods and Materials

2.1 Field collection

The sponge *Aplysina aerophoba* and the sea slug *Tylodina perversa* were collected by scuba diving in June 2016 (13 sponges and 4 sea slugs) and May 2017 (12 sponges and 4 sea slugs) at the Mediterranean coast of Spain (42.29408 N, 3.28944 E in 2016 and 42.1145863 N, 3.168486 E in 2017), at a depth between 2 to 10 m. The collections were performed by Lucía Pita Galán (Geomar, Germany), Marta Ribes (CSIC, Spain), Rafel Coma (CEAB-CSIC, Spain), Marc Catllà (CSIC, Spain), Laura Rix (University of Queensland, Australia), and Berta Pintó (University of Barcelona, Spain).

After collection, animals were transported to the Experimental Aquaria Zone (ZAE) at the Institute of Marine Science (ICM-CSIC) in Barcelona (Spain). Each sponge individual was then divided into 2-3 specimens which each having its own osculum. Each specimen was placed into individual aquaria (6 L) for 1 week acclimatization. The aquaria were maintained in a flow-through system with direct intake of seawater and a circadian cycle of 12 h light/12 h dark using artificial light sources. This set-up was designed by Lucía Pita Galán and Marta Ribes.

2.2 Experimental set-up

The specimens from each sponge individual were randomly assigned to one of the following three treatments (i) control: no treatment, (ii) grazing: one sea slug, which starved for 24 hours, was placed in direct contact to the sponge specimen and was allowed to feed for 24 hours, and (iii) mechanical damage: the specimen was clipped with a scalpel for 3 minutes every half hour of the first 3 hours and the last 3 hours (**Figure 3**).

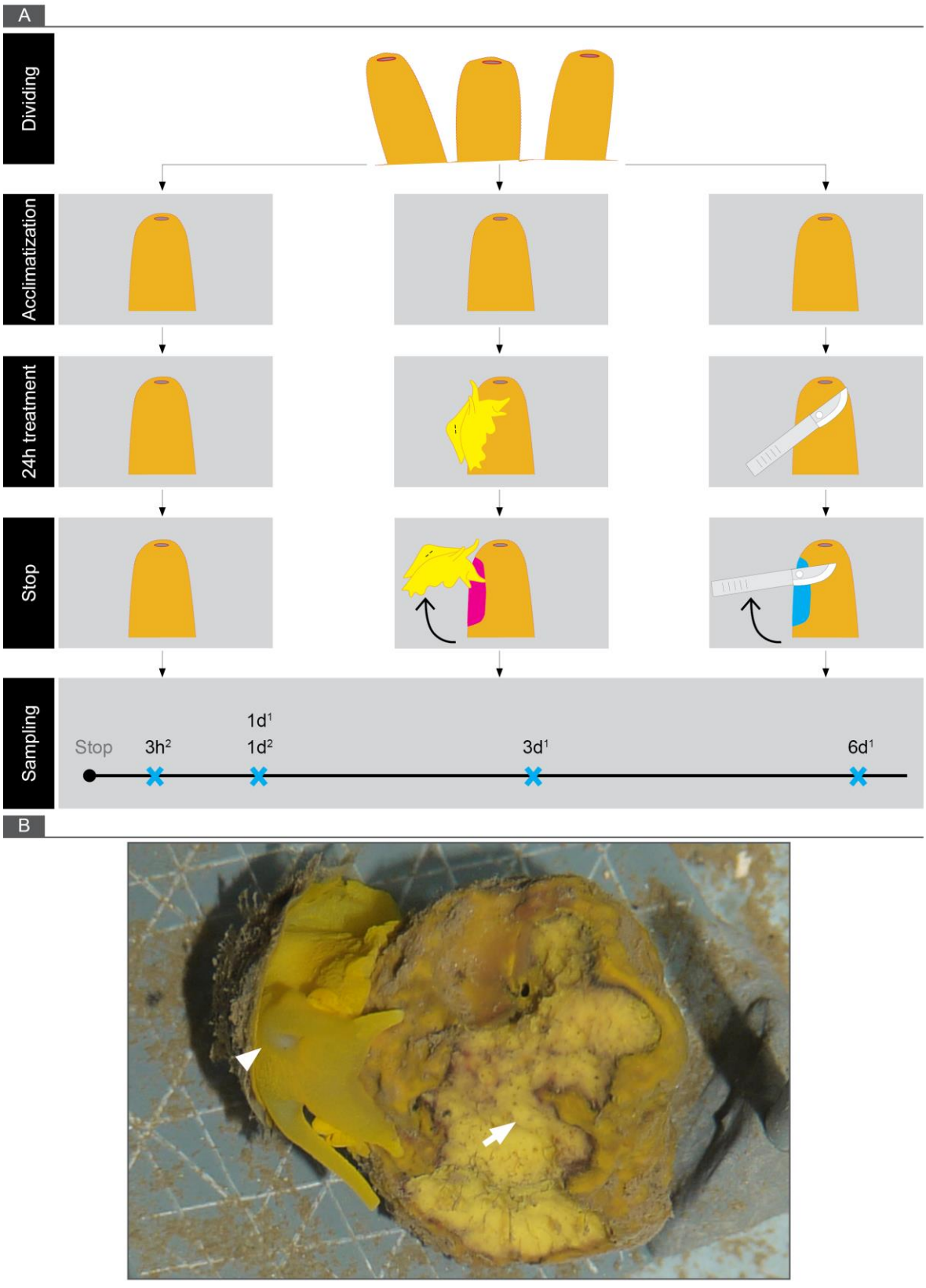

Figure 3. Experimental design. (**A**) Sponge individuals were divided into specimens. The specimens were randomly assigned to either control (**left panel**), or grazing (**middle panel**), or mechanical damage (**right panel**). Treatment was applied for 24 hours. This design was applied in consecutive experiments to collect samples at different time points: at 3 hours (**3h**), 1 day (**1d**), 3 days (**3d**), and 6 days (**6d**) after stop of treatments. Superscript number 1 and 2 denotes experiments performed in 2016 and 2017, respectively. (**B**) An example of photographical recording of grazed scars (**arrow**) by the sea slug (**arrowhead**). The grazed scar was light yellow-colored compared to orange-yellow-colored intact surface.

The behavior of sea slugs after directly contact with sponge specimen was recorded by using a GoPro Hero 4 camera with the program time lapse (1 picture every 5 sec) for 1.5 to 2 hours. Osculum aperture, positions of sea slugs and generated scars were recorded photographically. All treatments were stopped after 24 hours. This design was applied in independent experiments that differ in the sampling time points to avoid repetitive sampling of the same specimen (**Figure 3**). Three consecutive experiments were performed in 2016: 1 day, 3 days, and 6 days after stop of the treatment (abbreviated as 1d-2016, 3d-2016, and 6d-2016, respectively). The 1 day-experiment was repeated in 2017 and, in addition, an experiment with an early sampling time point, 3 hours after stop of the treatment, was performed (abbreviated as 1d-2017 and 3h-2017, respectively). Due to availability of sponges, no mechanical damage group was performed for 3d-2016.

2.3 Microscopy

2.3.1 Preparation of samples for microscopy

A total of 53 samples were collected for counting of spherulous cells at the microscope (**Table 1**). The collection position on the sponge specimen is described in **Appendix A**. After collection, samples were immediately fixed in 2.5 % glutaraldehyde in 0.1 M cacodylate buffer/11 % sucrose (abbreviated as buffer; 4 °C) and stored at 4 ºC. Later, samples were washed with buffer three times (4 °C) and post-fixed in 2 % solution of osmium tetroxide in buffer for 1.5 hours at room temperature (RT). Following three times wash with buffer (4 °C), samples were dehydrated in a graded ethanol series (30 %, 2 x 50 %, 70 %, 90 % and 2 x 100 %, 4 °C) and transferred into 100 % ethanol. After gradual infiltration with LR White resin (33.3 %, 50 %, 66.7 %, 2 x 100 %, RT), samples were maintained in this resin at 4 °C for 24 hours. They were then transferred into fresh resin and polymerized in embedding capsules at 59 °C for at least 24 hours until they solidified. Semi-thin (0.35 µm) sections were prepared with an ultramicrotome (Reichert Ultracut S, Leica, Austria), deposited on Superfrost Plus glass slides (Menzel) with Biomount 2 mounting medium (BBI Solutions), stained with Richardson solution, and imaged at a resolution of 100x with a ZEISS Axio Observer microscope (version 1.1, Zeiss, Germany).

Table 1. Number of biological replicates for microscopy, MALDI-imaging MS, and RNA-Seq. For RNA-Seq, one grazed sample collected at 3h-2017 with low-qualitative reads was filtered from the data after *de novo* reference assembly and the correspondent number is shown in brackets. **C**: control; **G**: grazing; **M**: mechanical damage.

	Microscopy			MALDI-imaging MS			RNA-Seq		
Experiment	**C**	**G**	**M**	**C**	**G**	**M**	**C**	**G**	**M**
3h-2017	4	4	3				4	4 (3)	3
1d-2017	4	4	4	4	4	4	6	6	6
1d-2016	4	4	3						
3d-2016	4	4	0						
6d-2016	4	4	3				4	4	3
Total	53			12			40 (39)		

2.3.2 Automatic counting of spherulous cell at the surface

Microscopic images at a resolution of 100x were analyzed by using ImageJ (version 1.51j8, Java 1.8.0_112, Schneider *et al.*, 2012). The first 100 µm depth from the surface was defined as the Region Of Interest (ROI 1, **Figure 4**) and the area of ROI 1 was measured excluding aquiferous canals. Adjustment of Image type, Substract background, Threshold, and Watersheld parameters enabled to select the spherulous cells which were densely-stained.

Next, those cells were automatically counted by using “Analyze Particles” ImageJ tool with criteria “Size” = 34 - 314 µm^2 (considering a round cell with a diameter from 10 to 20 µm and a sectioning at 1/8 from cell edge or through cell center) and “Circularity” = 0.20 - 1.00 (considering a cell shape from elongated/possibly motile stage to circular/possibly non-motile stage). Spherulous cells on edges of each ROI 1 were excluded from the counting.

The number of densely-stained spherulous cells pro area (50 000 µm^2) was calculated for the ROI 1 of each image. For samples in 2017 which covered a larger surface area (ca. 3 mm) than those collected in 2016 (ca. 1 mm)**,** spherulous cells were counted following the same pipeline, but for each microscopic image two regions of the same area size as ROI 1 in 2016 samples were selected (to keep measured area constant while analyzing a longer surface). Then, the average number of spherulous cells of ROI 1 from the two regions was calculated (**Figure 4B**). The automatic counting was validated by manual counting of the 2016-subset of samples (**Figure 5**).

2.3.3 Statistical comparison of spherulous cells at the surface

I compared the density of densely-stained spherulous cells between treatments for each time point by applying Generalized Linear Mixed-effects Model via Penalized Quasi-Likelihood (glmmPQL) in R (Version R 3.6.0, R Core Team, 2019) as implemented in RStudio (version 1.2.1335, RStudio Team, 2019), with treatments (control, grazing, and mechanical damage) as the fixed effect and the sponge individual as the random effect.

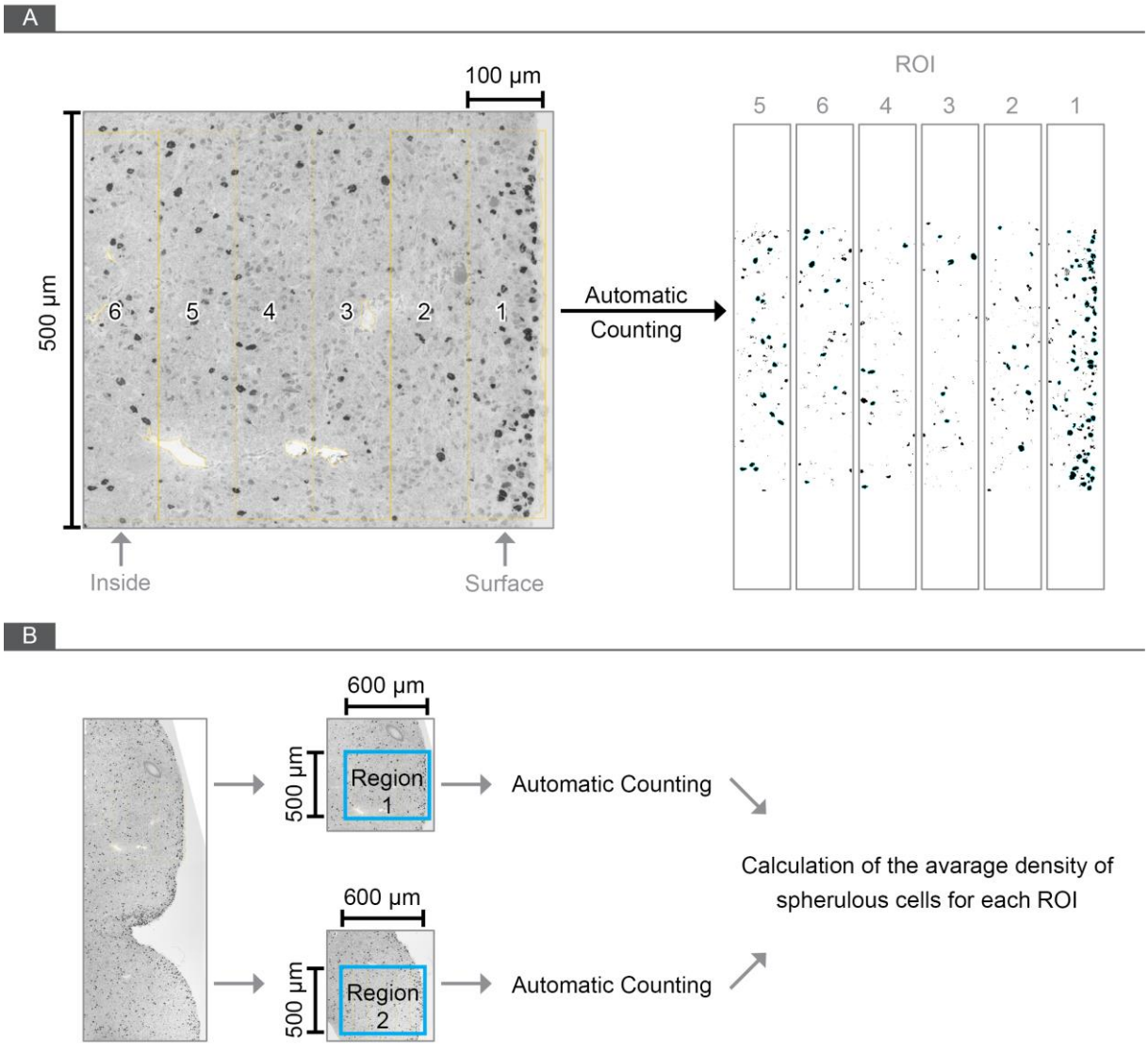

Figure 4. Automatic cell counting method. (**A**) Starting at the surface, 6 Region Of Interests (**ROI 1 - ROI 6, yellow squares**) with a depth of 100 µm and a length of 500 µm were selected in each microscopic image. Parameters were adjusted to count spherulous cells (**blue outline**). (**B**) Samples with longer surface area were collected in 2017. To keep each measured area constant with that in 2016, two regions **(Region 1 and Region 2**; each region with an area of 600 µm in depth x 500 µm in length) in each microscopic image were selected by avoiding of spongin fibers and aquiferous canals. For each region, the same counting method was applied for 6 ROIs (see A). Then, the average density of spherulous cells from these two regions was calculated for each ROI.

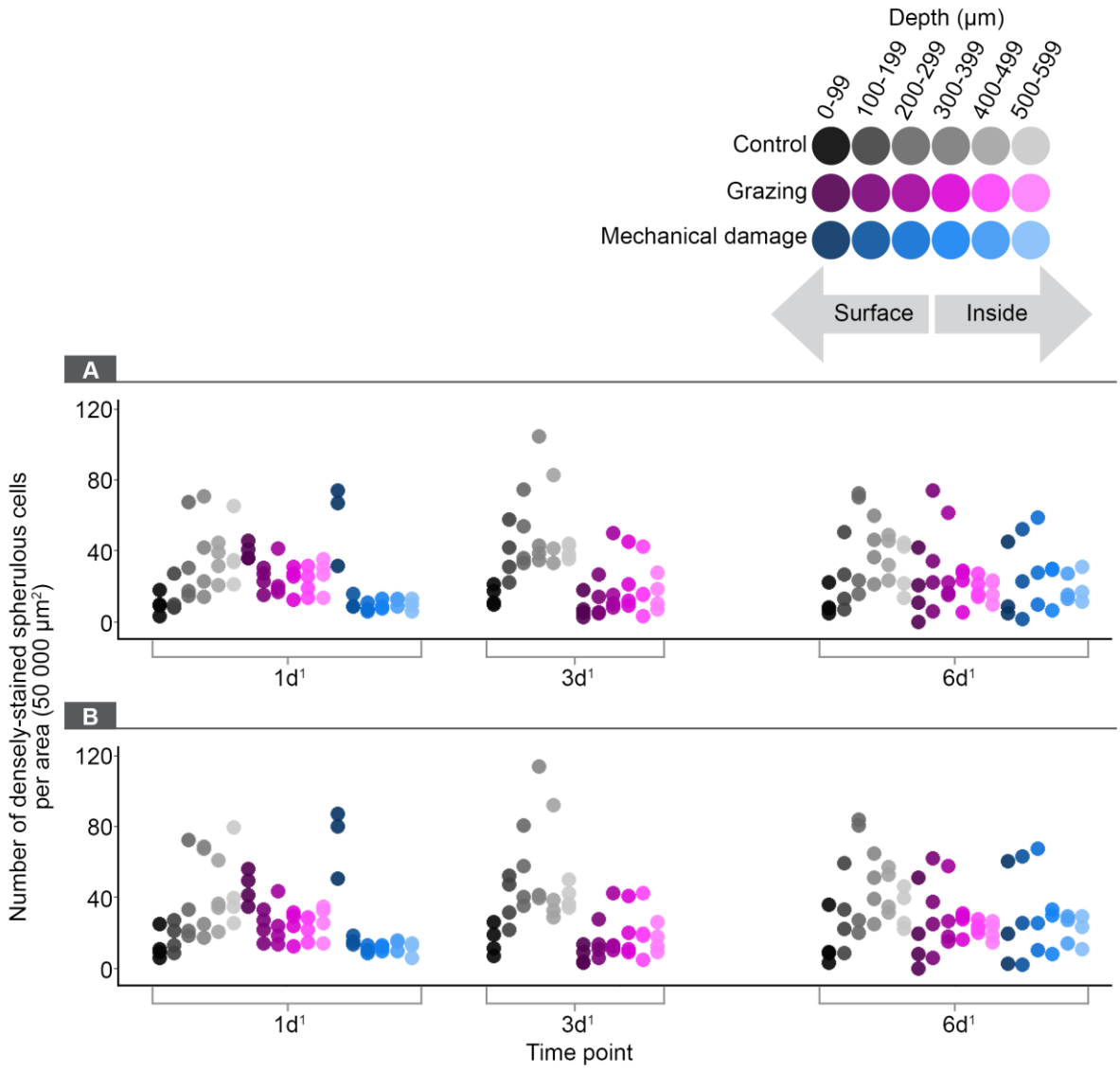

Figure 5. Comparison between automatic and manual counting method by counting samples from 2016 showing a similar pattern. (A) Automatic counting. (**B**) Manual counting by using "Multi-Point" ImageJ tool to count densely-stained spherulous cells per hand in each ROI of each microscopic image from 1d-2016 ($1d^1$), 3d-2016 ($3d^1$), and 6d-2016 ($6d^1$). Both methods showed a similar pattern of the cell density.

2.3.4 Distribution of spherulous cells from the surface to the inside of sponges

The distribution pattern of the densely-stained spherulous cells from the surface to the inside of sponge samples was investigated by defining 5 consecutive ROIs of 100 µm depth adjacent to ROI 1 (**Figure 4A**) and counting cells following the methodology described above.

2.3.5 Transmission electron microscopy (TEM)

One sponge individual from 1d-2017, with its corresponding three differently-treated specimens, was further analyzed at TEM in order to characterize in more detail the morphology of the densely-stained spherulous cells observed at the light microscopy. Embedded samples were cut into ultra-thin (70 nm) sections by using an ultramicrotome (Reichert Ultracut S, Leica, Austria). Ultra-thin sections were mounted on pioloform coated grids and contrasted with uranyl acetate replacement stain (Science Services, Germany) for 20 min and subsequently with Reynold´s lead citrate for 3 min. Ultra-thin sections were imaged with a Tecnai G2 Spirit BioTwin transmission electron microscope (80 kV, FEI, USA) at the Central Microscopy of University of Kiel (Germany).

2.4 MALDI-imaging MS

2.4.1 Preparation and cryosectioning of samples for MALDI-imaging MS

A total of 12 samples of specimens corresponding to 4 sponge individuals from 1d-2017 were collected for assessing chemical distribution pattern across sponge cross-section by MALDI-imaging MS (**Table 1**). The collection position on the sponge specimen was described in **Appendix A**. After collection, samples were immediately wrapped in aluminum with a clear annotation of the location of the wounded surface in grazing and mechanical damage groups, snap-frozen in liquid nitrogen, and immediately stored at -20 °C until cryosectioning. Samples were cryosectioned as described by Yarnold *et al.* (2012), with some modifications. In short, each sample was thawed at room temperature, then placed in a cryomold (22 mm in diameter, 5 mm in height, Tissue-Tek@ Cryomold@, Plano, Germany) with a drop of embedding medium: Optimal Cutting Temperature (OCT, Tissue-Tek@, Plano, Germany). If samples were bigger than the cryomold, exceeded sponge tissue was cut to fit the cryomold, preserving the surface. After filling with OCT, each sample was placed immediately in a cryostat (CM3050 S, Leica, Germany) at -20 °C to form a block for cryosectioning. Samples were frozen-sectioned at 14 µm and thaw-mounted onto Indium-Tin-Oxide glass slides (ITO glass slides, Bruker Daltonics, Bremen, Germany) for subsequent MALDI-imaging MS, as well as onto microscope slides (Superfrost

Plus glass slides, Menzel) for imaging at a resolution of 100x with a ZEISS Axio Observer microscope (version 1.1, Zeiss, Germany). Each ITO glass slide consisted of three sponge specimens (control, grazed, and mechanically-damaged) from the same sponge individual. Unlike Yarnold *et al.* (2012), sample sections were directly mounted onto ITO glass slides without washing with MilliQ-water, as this step caused, in my PhD thesis, an alteration of chemical distribution and mass spectrum pattern probably due to different polarity of compounds (**Appendix B**). This testing of MilliQ-water was performed by María García-Altares (HKI, Germany).

2.4.2 MALDI-imaging MS and data analysis

The MALDI-imaging MS, data analysis, and the corresponding protocol for my PhD thesis were performed by María García-Altares. In this PhD thesis, the protocol of MALDI-imaging MS was optimized by applying a non-washed step, a non-water-containing matrix, and an appropriate raster size (details see **Appendix B**). Each ITO glass slide was spray-coated with 2 ml of a saturated solution (20 mg/mL) of universal MALDI matrix (1:1 mixture of 2,5-dihydroxybenzoic acid and α-cyano-4-hydroxy-cinnamic acid; Bruker Daltonics, Germany) in acetonitrile/methanol (70:30, v/v), using the automatic system ImagePrep device 2.0 (Bruker Daltonics) in 60 consecutive cycles (the sample was rotated 180° after 30 cycles) of 41 seconds (1 s spraying, 10 s incubation time, and 30 s of active drying). The matrix solvent selection was optimized to visualize the spatial distribution of both aerophobin-2 and aeroplysinin-1, which differ in polarity. The raster width ranged from 250, to 275, and to 300 µm according to the total measured area of each ITO glass slide to preserve sensitivity and consistency during measurement (**Table 2**).

Samples were analyzed in an UltrafleXtreme MALDI TOF/TOF (Bruker Daltonics), operated in positive reflector mode using flexControl 3.0. The analysis was performed in the 100-1500 Da range, with 30 % laser intensity (laser type 4), accumulating 1000 shots by tanking 50 random shots at every raster position. Calibration of the acquisition method was performed externally using Peptide Calibration Standard II (Bruker Daltonics) containing Bradykinin1-7, Angiotensin II, Angiotensin I, Substance P, Bombesin, ACTH clip1-17, ACTH clip18-39, and Somatostatin 28. Spectra were processed with baseline subtraction in flexAnalysis

3.3 and corrected internally using the peaks of HCCA ([M+H]+ *m/z* 190.0499 and [2M+H]+ *m/z* 379.0925).

Table 2. Raster size, measured area, and number of mass spectra by MALDI-imaging MS of sponge specimens from 1d-2017. Individual: sponge individual; **C**: control; **G**: grazing; **M**: mechanical damage.

Individual	Treatment	Raster [µm^2]	Area [mm²]	Number of spectra
1	C	250 x 250	131.06	2097
1	G	250 x 250	167.06	2673
1	M	250 x 250	233.44	3735
2	C	275 x 275	131.29	1736
2	G	275 x 275	216.89	2868
2	M	275 x 275	248.20	3282
3	C	275 x 275	199.88	2643
3	G	275 x 275	235.50	3114
3	M	275 x 275	223.09	2950
4	C	300 x 300	266.40	2960
4	G	300 x 300	140.94	1566
4	M	300 x 300	309.60	3440

2D-visualization of MALDI-imaging MS data was performed by using the software SCiLS Lab 2015b (SCiLS, Bremen, Germany). Brominated compounds aerophobin-2 and aeroplysinin-1 (Santa Cruz Biotechnology, Germany) were used as standard references. The ionization yields of both standards were inspected at the same concentration. As aerphobin 2 and aeroplysinin 1, in my PhD thesis, did not show the same ionization yield in MALDI-TOF (details see **Appendix B**), thus I aimed to investigate the spatial patterns of relative intensities of each compound by itself. Brominated compounds with two bromine attoms (Br) show a specific three-peaks-pattern due to the fact that the two stable isotops (^{79}Br and ^{81}Br) have similar abundance in the nature. Based on this pattern, the brominated compounds were manually selected from the isotopic profiles. To visualize the distribution of each compound, the intensity of each compound was normalized by Root Mean Square (RMS) method, calculated as relative intensity to the highest value among all sections within each ITO glass slide, and depicted in a color scale. To visualize the co-localization of MALDI-imaging MS data with microscopic images, 2D-MALDI-images were superimposed with corresponding microscopic images.

2.5 RNA-Seq

2.5.1 RNA extraction and sequencing

A total of 40 samples from 3h-, 1d-, and 6d-experiments were collected for differential gene expression analysis by RNA-Seq (**Table 1**). Samples from wounded treatments (grazing and mechanical damage) were collected at the scar side. The collection position on the sponge specimen was described in **Appendix A**. After collection, all samples were immediately washed with artificial seawater and kept in RNA*later*™ (Invitrogen, Thermo Fisher Scientific, Germany) at 4 °C overnight. Samples were then stored at -80 °C until RNA extraction. To extract total RNA, the frozen sponge samples were thaw and ca. 30 mg (wet weight) of sample was immediately homogenized in 1 % ß-mercaptoethanol in RLTplus buffer (Qiagen, Germany) by using the PowerLyzer™24 (Mobio, Qiagen, Germany). The total RNA was obtained using an AllPrep DNA/RNA Mini Kit (Qiagen, Germany) following manufacturer's protocol and eluted in 100 µL of Buffer EB (Qiagen, German). To remove DNA contamination, the extracted total RNA was treated with DNA-free DNase Treatment and Removal Reagent (Ambion, Germany). The absence of DNA was further checked by PCR amplification of eukaryotic 18s rRNA gene (Sigma-Aldrich, Germany: forward primer - ACCTGGTTGATCCTGCCAG, reverse primer - AATTATAATACGACTCACTATAGATTCYGCAGGTTCACCTAC; Stewart *et al.* 2010). The total RNA was checked for purity by using NanoDrop 2000c Spectrophotometer (peolab, Germany), for quantity by Qubit 2.0 (Life Technologies, Carlsband, CA), and for quality by Experion™ Electrophoresis Station (Bio-Rad, Hercules, CA). Only the total RNA which was DNA-free, and presented OD260/280 >1.8 (in Nanodrop) as well as RIN > 8 (Experion) was subsequently used for RNA-Seq.

Equal amounts of the total RNA (1950 ηg in 30 µl) were used for library construction with the TruSeq stranded mRNA library prep kit (Illumina, Inc., USA), including a poly-A enrichment step. Samples were then 150 base paired-end sequenced on the HiSeq 4000 system (Illumina, Inc., USA). Library preparation and sequencing was performed by Sören Franzenburg at the IKMB Kiel.

2.5.2 Differential gene expression analysis

Differential gene expression analysis was performed following the protocol described by Pita *et al.* (2018). Raw Illumina RNA-Seq reads were qualitatively trimmed and filtered to remove adapters and low-qualitative reads in Trimmomatic-version 0.38 (parameters: TruSeq3-PE-2.fa:2:20:10 LEADING:3 TRAILING:3 SLIDINGWINDOW:4:15 MINLEN:36; Bolger *et al.*, 2014). Read quality was visualized in FastQC-version 0.11.7. Additional filtering of prokaryotic and microbial eukaryotic reads was performed in the classifier Kaiju-version 1.6.2 (Andrews, 2010), in greedy-5 mode (database accessed in February 2018; Menzel *et al.*, 2016).

The following analyses of RNA-Seq data were performed by Lucía Pita Galán (GEOMAR). The surviving reads were combined to create *de novo* reference assembly in Trinity-version 2.6.6 (Grabherr *et al.*, 2011; Haas *et al.*, 2013) because the lack of a reference genome for *A. aerophoba*. Assembly statistics were obtained in Trinity-version 2.6.6 and TransRate-version 1.0.3 (Smith-Unna *et al.*, 2016). Completeness was assessed by comparing the assembly against the Metazoa reference data in BUSCO-version 3, trans mode (Simão *et al.*, 2015; Waterhouse *et al.*, 2018). Functional annotation was performed following Trinotate-version 3.0.2 (e-values < 1 e−5; Bryant *et al.*, 2017), a comprehensive suite that includes homology search to publically available data (BLAST+/SwissProt; The UniProt Consorticum, 2019), protein domain identification (HMMER/Pfam; El-Gebali *et al.*, 2019), protein signal peptide and transmembrane domain prediction (signalP/tmHMM; Sonnhammer *et al.*, 1998; Krogh *et al.*, 2001), as well as eggNOG (Huerta-Cepas *et al.*, 2016), GO (Ashburner *et al.*, 2000; The Gene Ontology Consortium, 2019), and KEGG annotation (Kanehisa and Goto, 2000; Kanehisa *et al.*, 2019; Kanehisa, 2019). Those contigs with blast matches to Bacteria, Archaea, or Virus were further removed from the reference assembly.

Given the set of up-regulated genes in each treatment *versus* control at each time point, a GO enrichment analysis was performed in blast2GO-5 (Goetz *et al.*, 2008), based on GO annotations obtained from Trinotate. GO-annotated genes in the reference transcriptome were used as a reference. Enrichment was determined by Fisher's exact test and *p*-value was corrected by False Discovery Rate control according to Benjamini-Hochberg (significance threshold: FDR *p*-value < 0.005). Transcript abundance was estimated based on gene (Trinity component)

abundances by RSEM bowtie2-based quantification (version 1.2.19; Li and Dewey, 2011). Differential gene expression analysis within each time point (i.e., 3h, 1d, and 6d) was performed in edgeR as implemented in Trinity-version 2.6.5 (default parameters). Differentially-expressed genes (DEGs) in pairwise-treatment comparisons were defined by False Discovery Rate –corrected (FDR) *p*-value < 0.005 and log2|FC| ≥ 2 expression (4-fold change).

2.5.3 Survey of candidate genes related to biosynthesis of brominated compounds

To search for potential candidate genes related to enzymes in the biosynthesis pathways of brominated compounds in the RNA-Seq dataset, following key words were used: “bromination”, “halogenase”, “methyltransferase”, “oxime”, “arene oxide”, “hydroxylation”, “nitrile hydratase”, “histamine”, “aromatic compound catabolic process”, “nitrogen compound metabolic process”, “alkaloid biosynthetic process”, and “secondary metabolite” based on proposed putative biosynthesis of brominated compounds from the literatures (De Luca and Laflamme, 2001; Peng *et al.*, 2005; Niemann *et al.*, 2015; El-Demerdash *et al.*, 2019). Subcellular location was noted according to GO analysis and UniProt data base.

3. Results

3.1 Sea slug feeding behavior

The sea slug usually started to feed on sponge specimen within 15 - 30 minutes after starting the experiments (see the video available in Open Access library: doi.pangaea.de/10.1594/PANGAEA.907958). While the osculum of sponges in control group remained usually opened during the experiments, it was relatively smaller or even closed in grazing and mechanical damage groups compared to that before experiments started (**Figure 6A**). I observed that the sea slug tightly attached and covered the sponge by curling its body and bending the foot during grazing (**Figure 6A**). The sea slug turned around at the same place to feed the neighbor tissue (**Figure 6A**). In contrast, it flattened the body and foot during moving on the aquarium surface. In general, scars generated by grazing showed yellow-colored surface, whereas scars in mechanical damage were dark blue (**Figure 6B**). In a test study, I observed that a wounded area continuously increased dark blue materials within 2 hours after mechanical damage (**Figure 6C**).

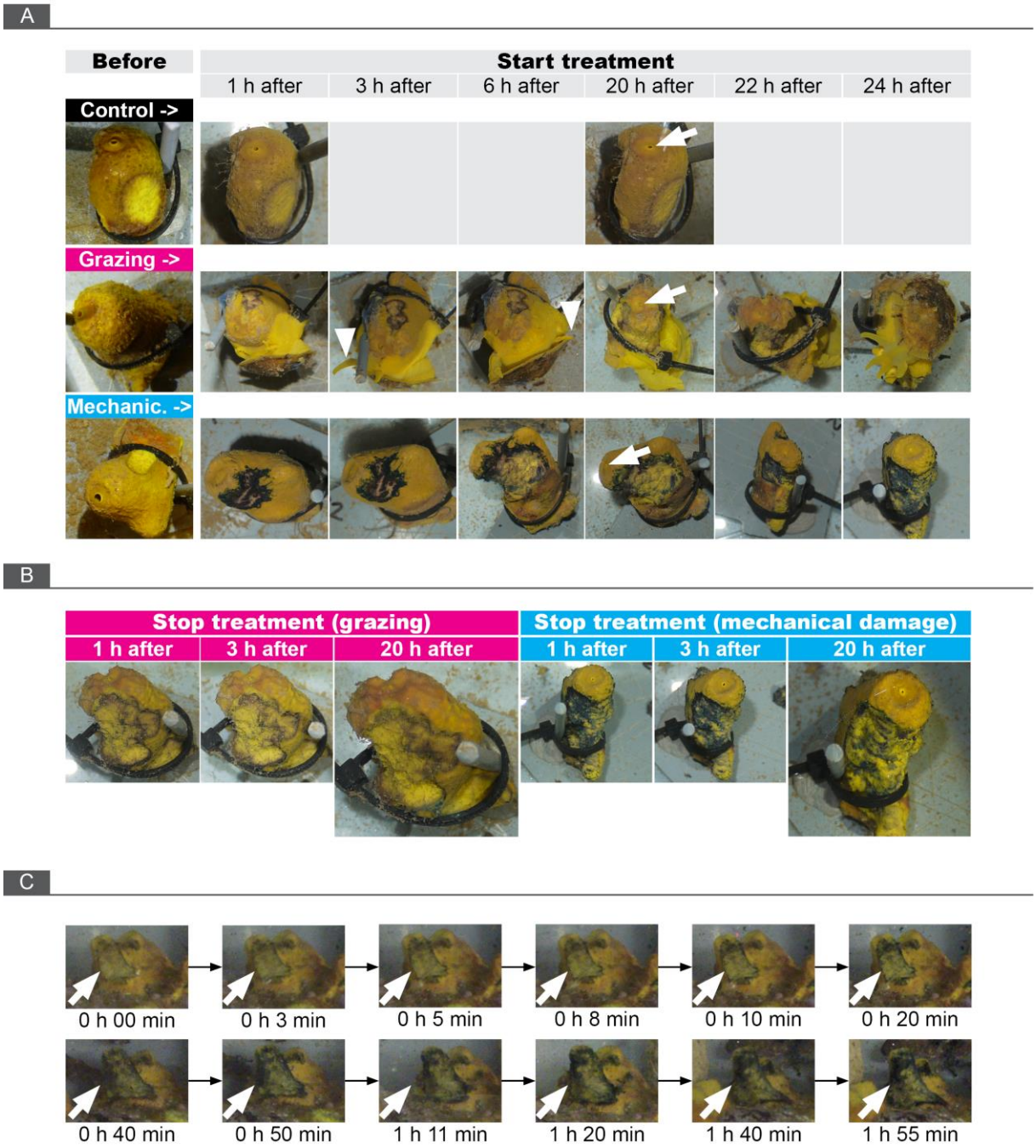

Figure 6. ***T. perversa*** **feeding behavior.** (**A**) An example of three differently-treated sponge specimens from the same individual during treatments. Sponges were photographically-recorded before the treatment (**Before**) and during the treatment (**hours after start treatment**). Note that the sea slug turned its body at 6 h after start of the experiment by covering the same place of the sponge body. **Mechanic**.= mechanical damage; **white arrow**; osculum; **white arrowhead**: rhinophores of the sea slug. (**B**) Generated scars after the stop of the experiment. (**C**) A photographical recording of 2 hours after wounding a sponge by mechanical damage. **White arrow**: increased dark blue materials.

3.2 Cellular responses

3.2.1 Time-dependent accumulation of spherulous cell at the wounded surface

Microscopic images (100x) of samples collected at 1d-2016 and 1d-2017 showed a striking accumulation of densely-stained spherulous cells at the wounded surface (first 100 µm from the wounded site to the inside of sponge specimens) in both grazing and mechanical damage groups compared to control (**Figure 7A**). Such cell accumulation was not evident in the other time point-experiments (**Figure 8**). Further inspection at TEM confirmed that those densely-stained spherulous cells at the wounded surface were spherulous cells with electron-dense spherules (abbreviated as spherulous cells for the following text; **Figure 7B**), while the surface of control group contained mostly spherulous cells with electron-lucent spherules (**Figure 7C**).

Automatic quantification of spherulous cells revealed that spherulous cells accumulated at the surface as early as 3h after grazing (glmmPQL, $p = 0.023$). At 1d, the density of spherulous cells at the surface reached the highest value in both grazing and mechanical damage groups (**Figure 9**). This increase was statistically significant except in grazing at 1d-2016 (glmmPQL, 1d-2016: grazing, $p = 0.056$ and mechanical damage, $p = 0.022$; 1d-2017: grazing, $p = 0.035$ and mechanical damage, $p = 0.013$). In contrast, 3d-2016 and 6d-2016 samples showed a similar density of spherulous cells at the surface among treatments in each experiment (glmmPQL, $p > 0.1$). Thus, the accumulation of spherulous cells was a time-dependent response. The similar results of 1d-experiments performed in different years suggest a consistent cellular response.

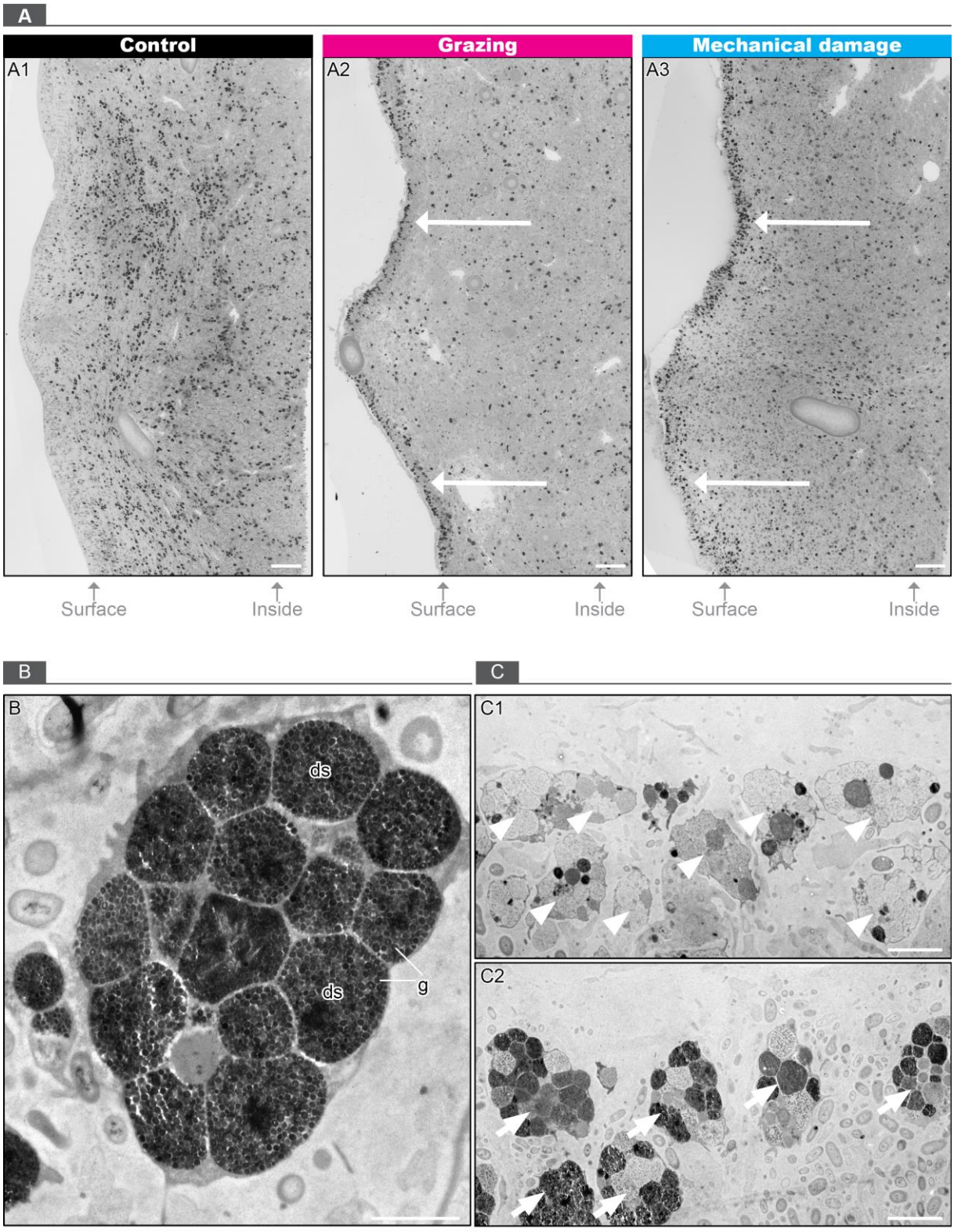

Figure 7. Accumulation of spherulous cells with electron-dense spherules at the surface at 1d time point. (A) Example of microscopic sections (100x resolution) from 1d-2017 sponges showing that densely-stained spherulous cells accumulated at the surface in grazing (**A2**) and mechanical damage (**A3**) groups compared to control (**A1**). **Arrow**: accumulated spherulous cells at the wounded surface; scale bar= 100 µm. (**B**) Example of a TEM-image at the surface of 1d-2017 sponges confirming that densely-stained spherulous cells at wounded surface were spherulous cells with electron-dense spherules which were characterized by electron-dense spherules (**ds**) with numerous electron-dense granules (**g**) within each spherule. Scale bar= 2 µm (**C**) The surface of control group contained spherulous cells with electron-lucent spherules (**C1, arrowhead**) compared to the surface of wounding group with spherulous cells with electron-dense spherules (**C2, arrow**). Scale bar= 5 µm.

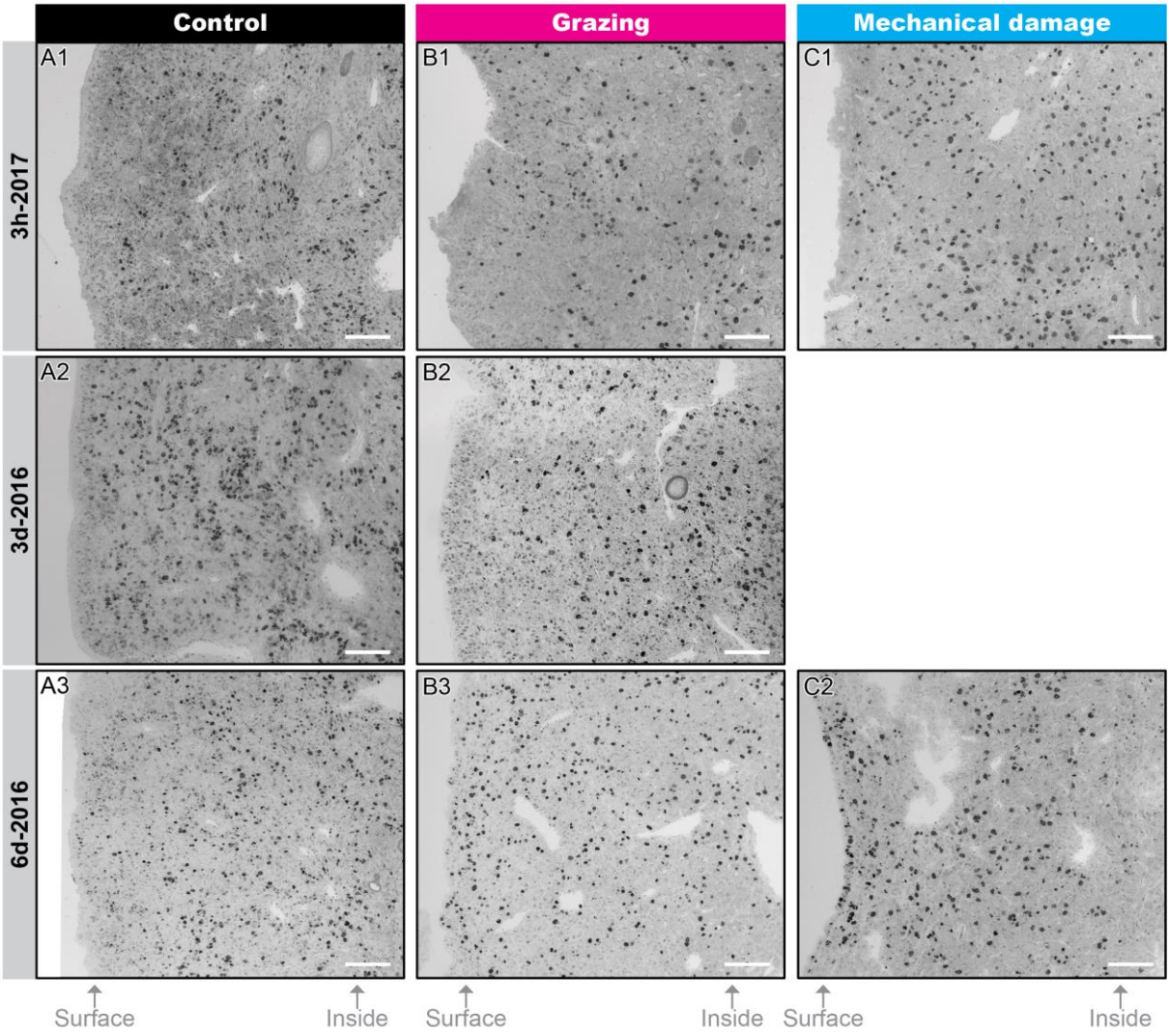

Figure 8. Example of a microscopic section of sponge samples at 3h-2017, 3d-2016, and 6d-2016 showing no clear accumulation of spherulous cells at the surface. The surface of sponge samples was at the left side of each image in the control (**A**), grazing (**B**), and mechanical damage (**C**) group. The resolution of the microscopic images was 100x. Scale bar= 100 µm.

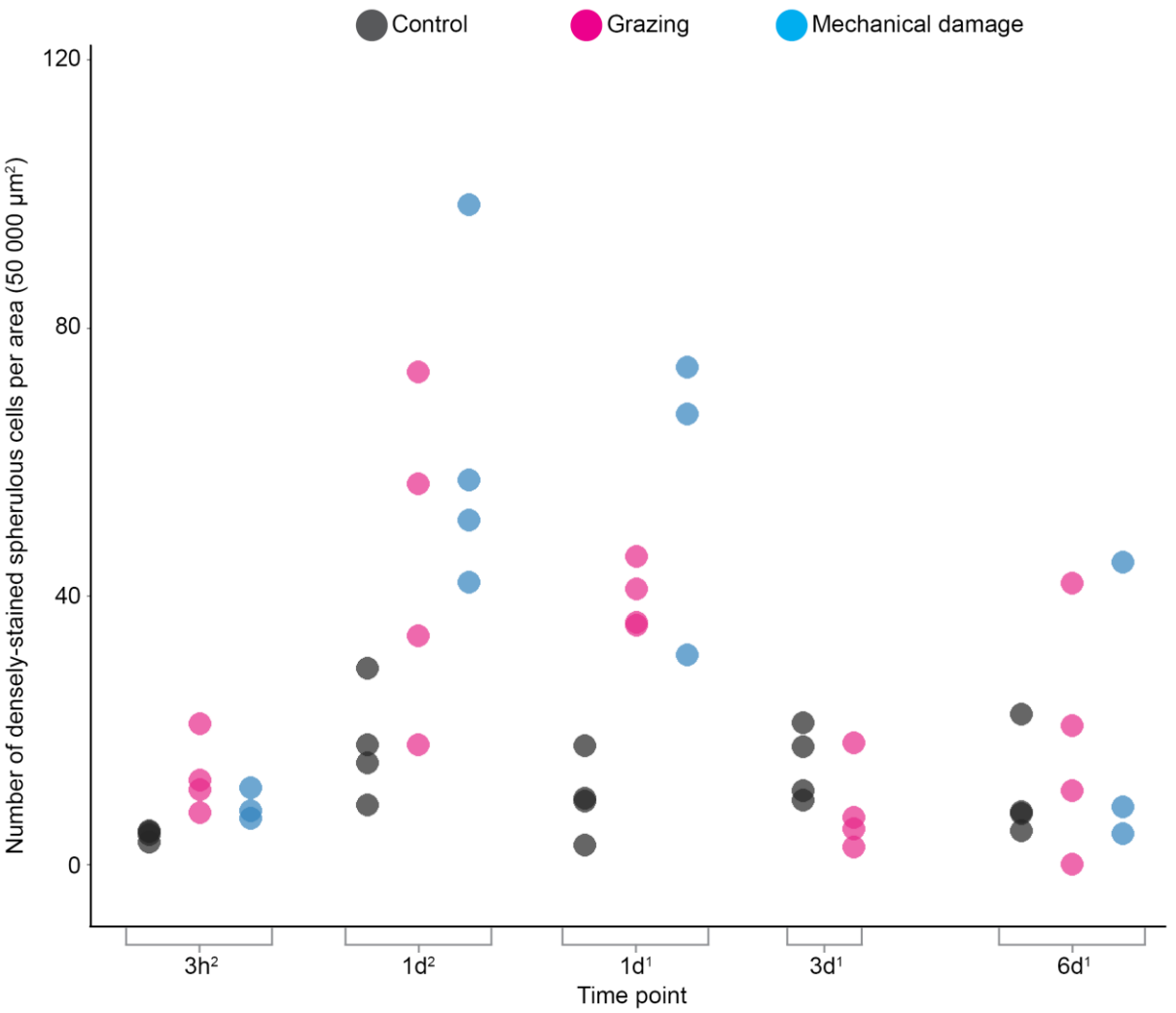

	3h²		1d²		1d¹		3d¹	6d¹	
t-value	3.249	1.530	2.703	3.501	2.481	3.262	-1.739	1.737	1.874
p-value	**0.023**	0.187	**0.035**	**0.013**	0.056	**0.022**	0.181	0.158	0.134
	*		*	*		*			

Figure 9. Time-dependent accumulation of spherulous cells at the surface (first 100 µm) upon wounding. The density of spherulous cells of each sample per each time point and treatment was calculated as the number of densely-stained spherulous cells per area (50 000 µm^2) and showed as colored circle. Differences in cell density among treatments (**black**, control; **red**, grazing; **blue**, mechanical damage) within the same experiment were tested by Generalized Linear Mixed-effects Model via Penalized Quasi-Likelihood and corresponding *t*- and *p*-values were showed at the bottom. Note that there was no mechanical damage group at 3d. Superscript number 1 and 2 denotes experiments performed in 2016 and 2017, respectively. Table 1 shows the correspondent number of biological replicates.

3.2.2 Secretion and shedding at the wounded surface at 1d

Microscopic images of 1d samples showed different degrees of sponge secretion at the wounded surface, especially in grazed sponges (**Figure 10A-B**). Compared within grazed samples from 1d-experiment, samples with more sponge secretion and a dense mesohyl at the wounded surface contained more accumulated spherulous cells (**Figure 10A *vs* 10B**). Spherulous cells or spherules were observed to be released into the space between this secretion and sponge mesohyl (**Figure 10C**). Further inspection at TEM confirmed that this secretion composited of two layers with a thick of ca. 5 µm and 150 nm, respectively (**Figure 10D**). The thicker outer layer consisted of mucus-like materials and a few attached bacteria, while the thinner inner layer formed a barrier between sponge mesohyl and the outer layer. Bacteria beneath the thinner inner layer seemed to be trapped by sponge components (**Figure 10D**). Compared to grazing group, mechanical damage group contained no or less sponge secretion at the wounded surface, and the thinner inner layer was disrupted through protruded spongin fibers out of the wounded surface (**Figure 10E**).

Besides, shedding of spherulous cells and sponge components at the wounded surface and into aquiferous canals were observed at 1d, in both grazing and mechanical damage group (**Figure 11A**). The cross-sections across sponge specimens at 1d revealed that both wounded groups contained debris (**Figure 11B**). I observed that spongin fibers became dark and protruded out of the wounded surface as well as into aquiferous canals in both wounding groups (**Figure 11B**). The frequent events of shedding and debris in both grazing and mechanical damage groups compared with the control suggest a specific response after wounding

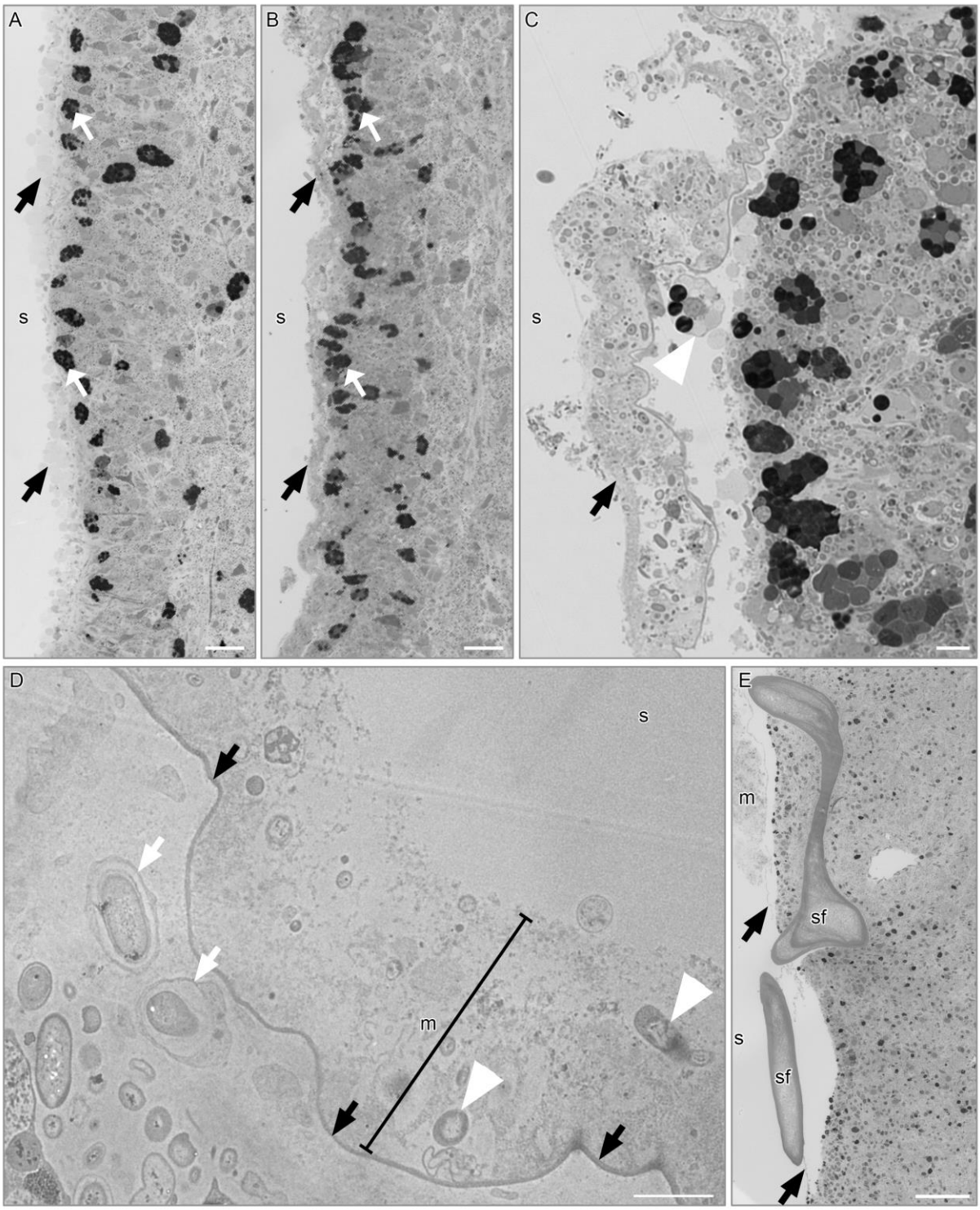

Figure 10. Example of a microscopic section of sponge samples at 1d showing secretion after wounding (**A-B**) Examples of a microscopic image at 400x of grazed samples showing different degrees of sponge secretion (**black arrow**) and accumulated spherulous cells (**white arrow**) at the wounded surface. (**C**) An example of a microscopic image at 630x of grazed samples showing released spherulous cells (**white arrowhead**) between the secretion (**black arrow**) and the sponge mesohyl. (**D**) An example of a TEM-image of grazed samples at 1d showing a mucus-like outer layer (**m**) with attached bacteria (**white arrowhead**) and a thinner inner layer (**black arrow**) with trapped bacteria beneath it (**white arrow**). (**E**) An example of a microscopic image at 100x of mechanically-damaged samples at 1d showing a part of sponge secretion including a mucus-like layer (**m**) and a thinner inner layer (**black arrow**) no longer attaching to the wounded surface probably due to protruded spongin fibers (**sf**). Scale bar= 20 µm (A-B), = 5 µm (C), = 2 µm (D), = 100 µm (E); **m**= mucus-like outer layer.**s**= wounded surface; **sf**=spongin fiber.

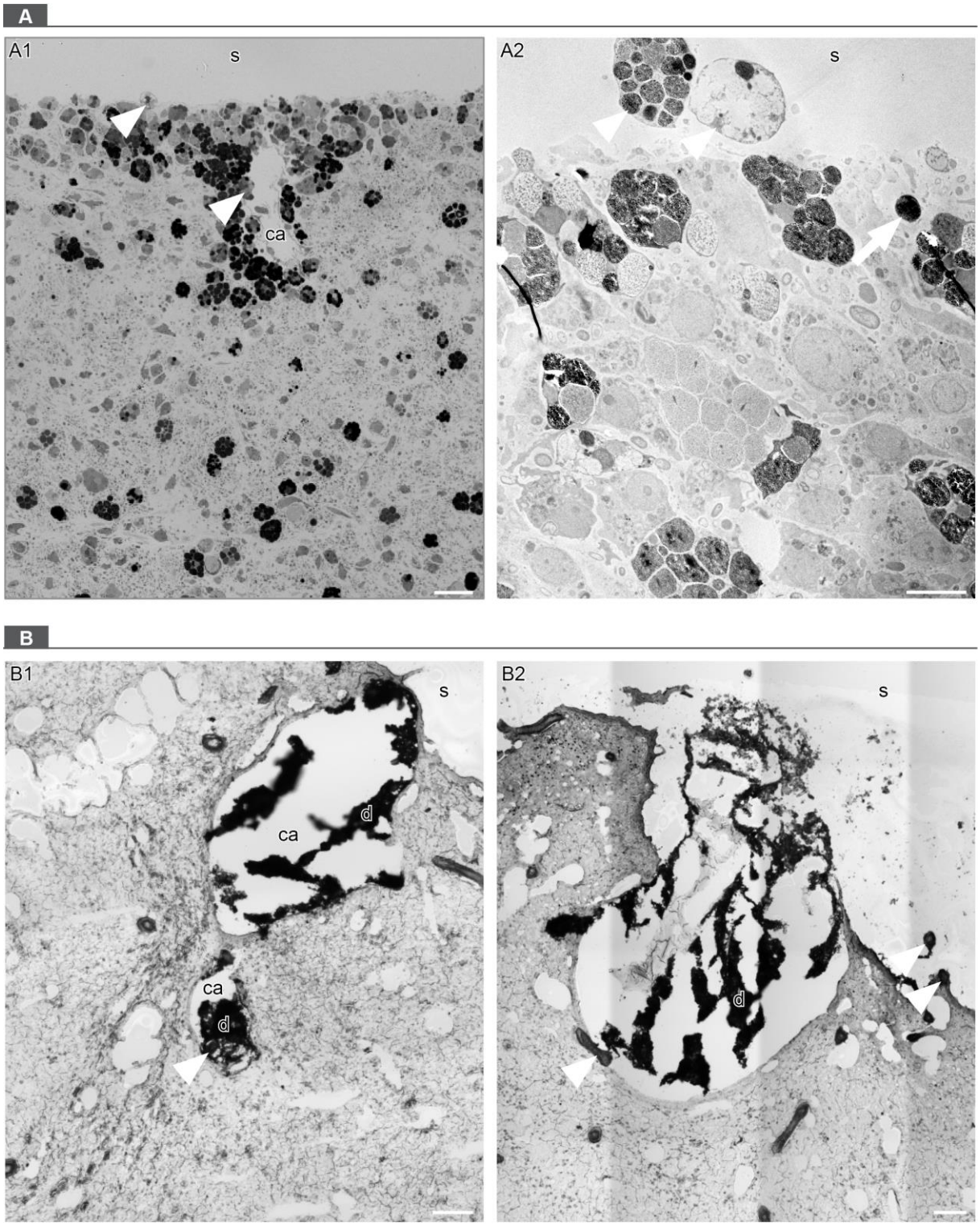

Figure 11. A microscopic section of wounded samples at 1d showing shedding and debris. (**A**) Shedding: an example of microscopic images at 400x (**A1**) showed shedding of cellular components and spherulous cells (**arrowhead**) out of the wounded surface (**s**) and into aquiferous canals (**ca**). An example of TEM-images showed shed spherulous cells (**A2, arrowhead**) out of the wounded surface (**s**) and an excreted spherule at the surface (**A2, arrow**). Scale bar=20 µm (A1), =5 µm (A2). (**B**) Debris: an example of microscopic images at 100x of cross-sections across wounded sponge samples showed debris (**d**) which were excreted into aquiferous canals (**B1**) or shed out of the wounded surface (**B2**). Spongin fibers were observed to protrude into aquiferous canals or out of the wounded surface (**arrow**). Scale bar= 200 µm; **s**= wounded surface; **ca**= aquiferous canal.

3.2.3 Time-dependent distribution pattern of spherulous cells upon wounding

I also investigated the distribution of spherulous cells beyond the surface. In the control group, the density of spherulous cells followed a depth-dependent distribution pattern with a lower value at the surface (first 100 µm) than towards the inside and the highest value at a depth from ca. 300 - 400 µm (**Figure 12A**). After grazing and mechanical damage, this distribution pattern was lost in 3h and 1d samples (**Figure 12B-C**). At 3h after wounding, sponges had similar density of spherulous cells at each depth (from the wounded surface to the inside of sponge specimens). At 1d, the cell density peaked at the wounded surface, whereas the density inside was similar to that observed at 3h. After 3d, the distribution pattern of spherulous cells resembled that observed in control group, which agrees with the beginning of regeneration (i.e., formation of new osculum 3d after treatment; **Figure 13A**). In fact, after 3 days I observed a regenerated ectosome characterized by a well-defined surface border with electron-lucent spherule cells and the presence of collagen fibrils (**Figure 13B**).

3.2.4 Other observed behaviors of spherulous cells

I also observed a stronger accumulation of spherulous cells, if the wounding reached deeper in the tissue (**Figure 14A**). In all samples, spherulous cells were usually observed to localize near aquiferous canals (**Figure 14B1**) and near spongin fibers (**Figure 14B2**). I further observed a mass of cells probably containing spherulous cells near spongin fibers by inspection of sponge cross-sections at 1d (**Figure 14B3**). Moreover, I observed potential interaction between spherulous cells with bacteria in a grazed sample (**Figure 14C1**) and archeocytes in a mechanically-damaged sample (**Figure 14C2-C3**). Furthermore, spherulous cells were observed in archeocyte-like cells with potential phagosomes either in mechanical damage group (**Figure 14C4**) or in control group (**Figure 14C5**).

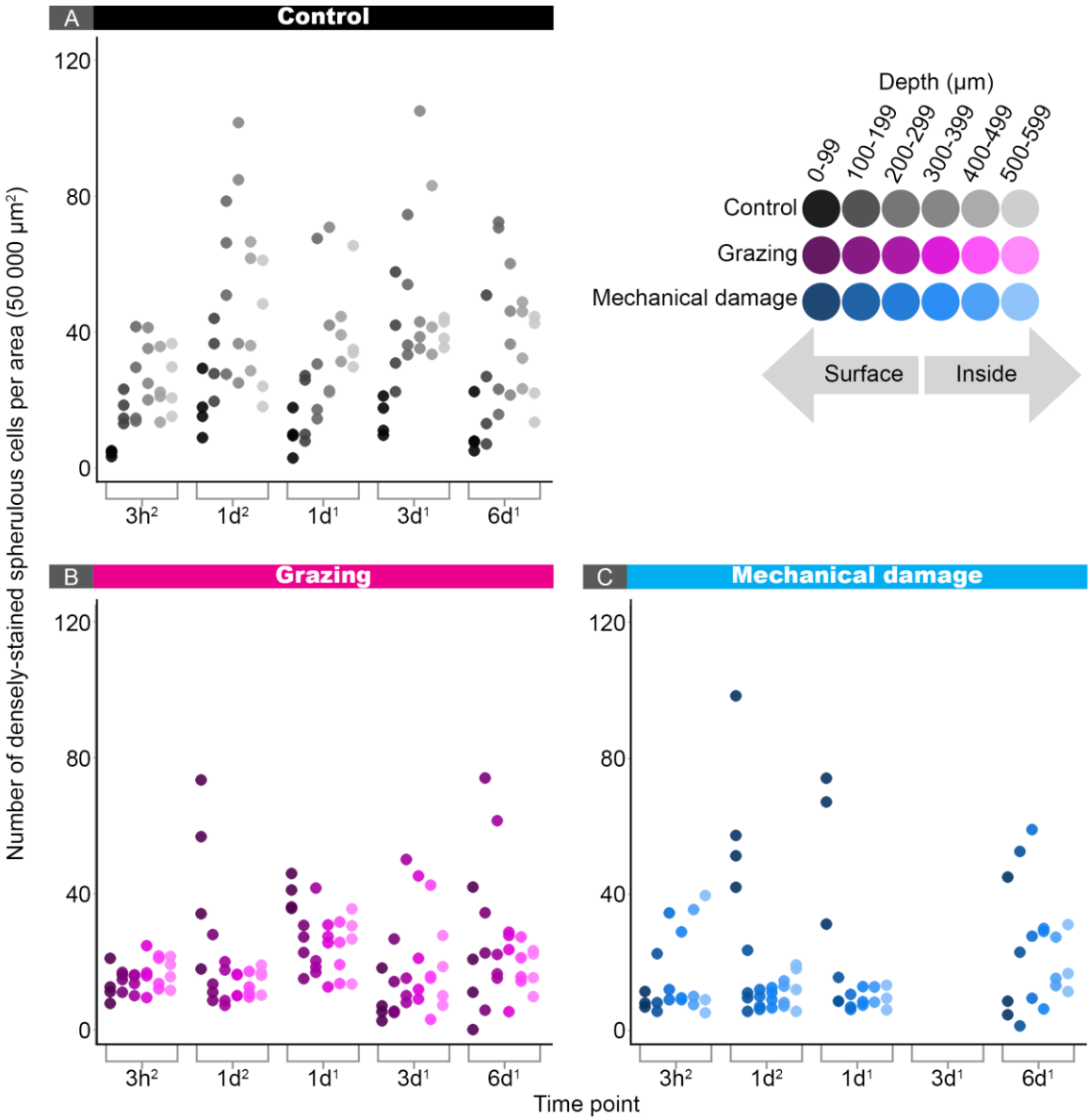

Figure 12. Distribution pattern of spherulous cells showing a time-dependent pattern after wounding. (**A, B, C**) Distribution pattern of spherulous cells from the surface to the inside in control (**A**), grazing (**B**), and mechanical damage (**C**) groups at each time point. Superscript number 1 and 2 denotes experiments performed in 2016 and 2017, respectively. Table 1 shows the correspondent number of biological replicates.

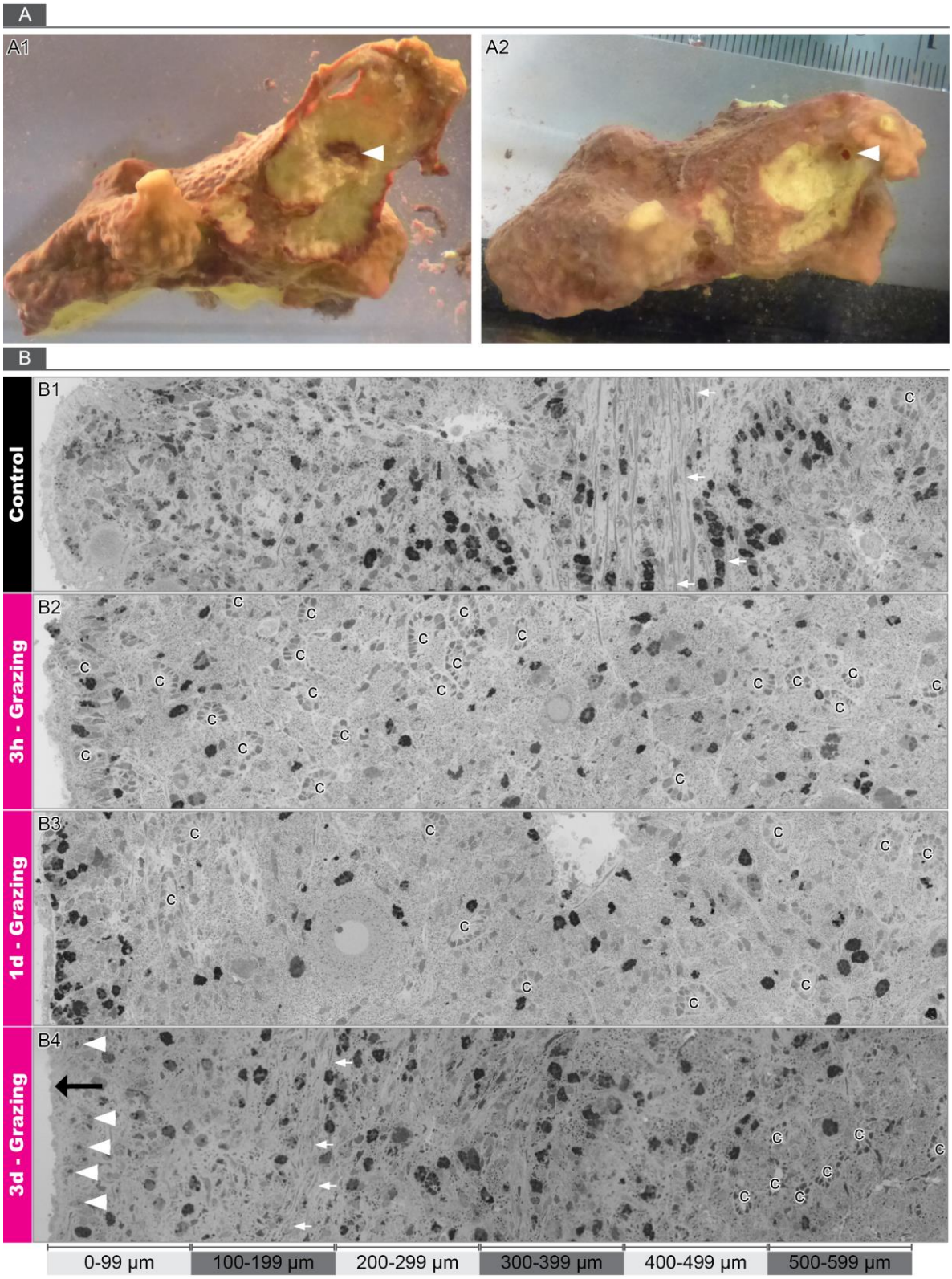

Figure 13. Microscopy and photographical recording of recovery after wounding. (**A**) Photographical recording showing an example of grazed samples directly after removal of the sea slug (**A1**). Its osculum (**white arrowhead**) and the edges between the scar and the intact tissue were regenerated after 3d (**A2**). (**B**) Example of a microscopic section at 400x of samples collected from control group (**B1**), from grazing group at 3h (**B2**), 1d (**B3**), and 3d (**B4**). Collagen fibrils and elongated sponge cells (**white arrow**) were observed in control samples and 2 out of 4 grazed samples at 3d. The area between the surface and choanocyte chambers (**c**) of the choanosome was defined as the ectosome. A sealed surface border (**black arrow**) and lucent spherulous cells (**white arrowhead**) beneath the surface were observed in all grazed samples at 3d. The surface side was at left of each image. Scales at bottom showed the depth from the surface.

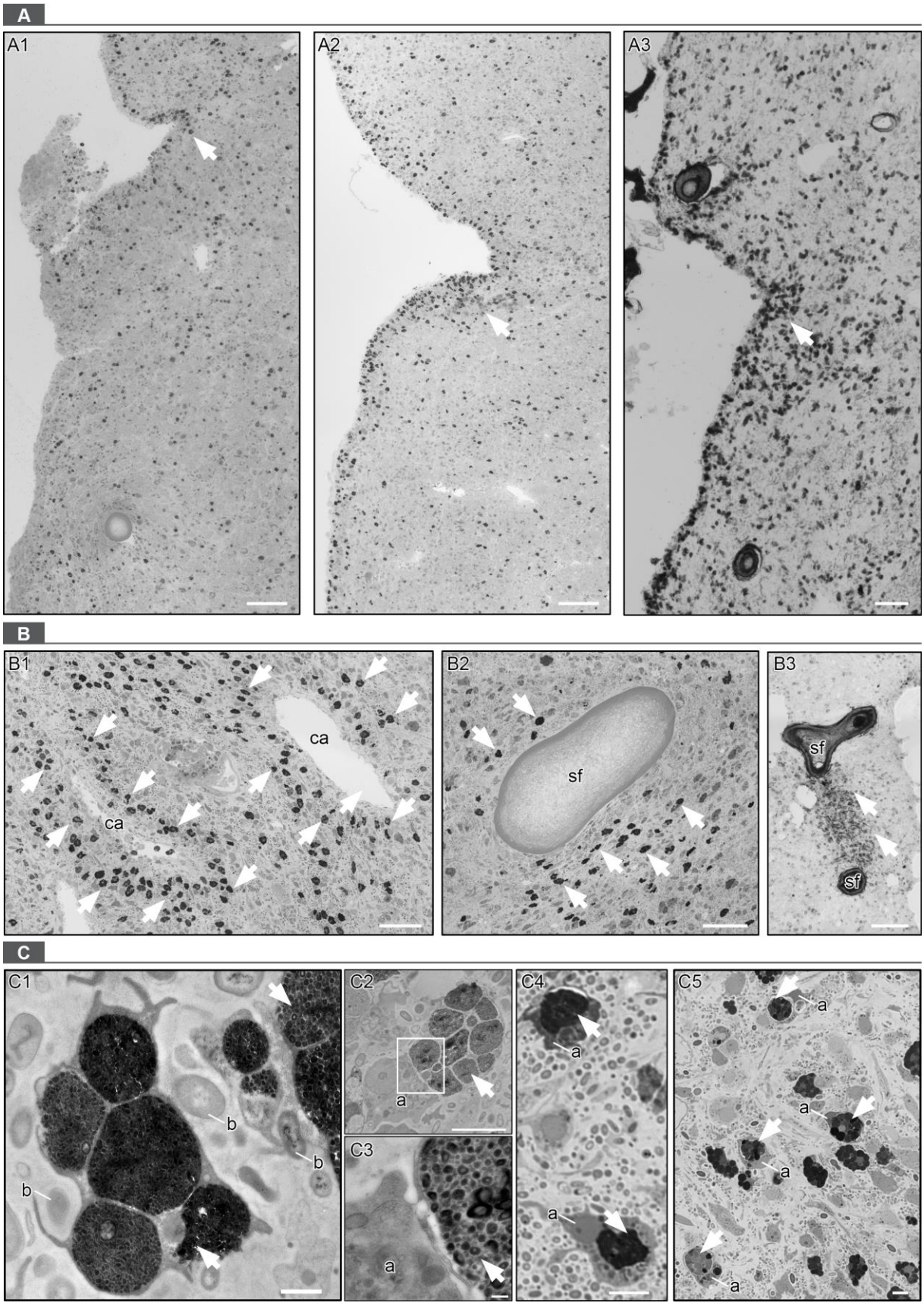

Figure 14. Observed behaviors of spherulous cells. Example of microscopic sections showing localization of spherulous cells (**arrow**) at a deeper wounded surface (**A**), near canals and spongin fibers (**B**), as well as their potential interaction with bacteria (**C1**) and archeocyte-like cells (**C2-C5**). Note C3 represents a insert of C2. Scale bar= 100 µm (A, B3), =50 µm (B1-B2), = 5 µm (C2, C4-C5), = 1 µm (C1), = 200 nm (C3); **a**= archeocyte-like cell; **b**= bacterium; **ca**= aquiferous canal; **sf**= spongin fiber.

3.3 Chemical responses

3.3.1 MALDI-imaging MS of brominated alkaloids on sponge sections

I analyzed specimens corresponding to 4 sponge individuals collected at 1d-2017 by MALDI-imaging MS. Both aerophobin-2 and aeroplysinin-1 were detected on all samples as $[M+H]^+$ ions (monoisotopic *m/z* 504.053/ 506.054/ 508.057 corresponding to $C_{16}H_{20}Br_2N_5O_4$ for aerophobin-2, and monoisotopic *m/z* 336.935/ 338.934/ 340.933 corresponding to $C_9H_{10}Br_2NO_3$ for aeroplysinin-1). The isotopic pattern of both molecules was consistent with their molecular structures containing two Br atoms, and matched the isotopic patterns of the standards (**Figure 15A-B**). Interestingly, MALDI-imaging MS also revealed other 5 unknown Br-containing compounds (**Figure 16**).

3.3.2 High inter-individual variability of the distribution of brominated compounds

MALDI-imaging MS revealed a striking biological variability of the distribution of both aerophobin-2 and aeroplysinin-1 among 4 control samples (**Figure 15C-F**). Despite this variability, the most intense signal of both compounds localized mainly at the surface (first 2 mm depth) of the cross-sections (**Figure 15C-F**). By combining 2D-MALDI-images with light microscopic sections, I observed that, in general, both compounds were most intense at places that contained a dense mesohyl, and near aquiferous canals, as well as occasionally near spongin fibers (**Figure 17A**). Also, the intra-individual variability of chemical distribution occurred concomitant with certain colouration (**Figure 17B**). Both compounds were found in connection with greenish cells whose color might due to pigment uranidine (Cimino *et al.*, 1984). Nevertheless, aerophobin-2 was usually found in brownisch areas which had more protruded spongin fibers and dark cells (**Figure 17B1-B2**), while aeroplysinin-1 was usually found in reddish area beneath subdermal spaces and around aquiferous canals (**Figure 17B3-B4**). Thus, cellular features may explain the observed individual variability in the distribution of brominated compounds.

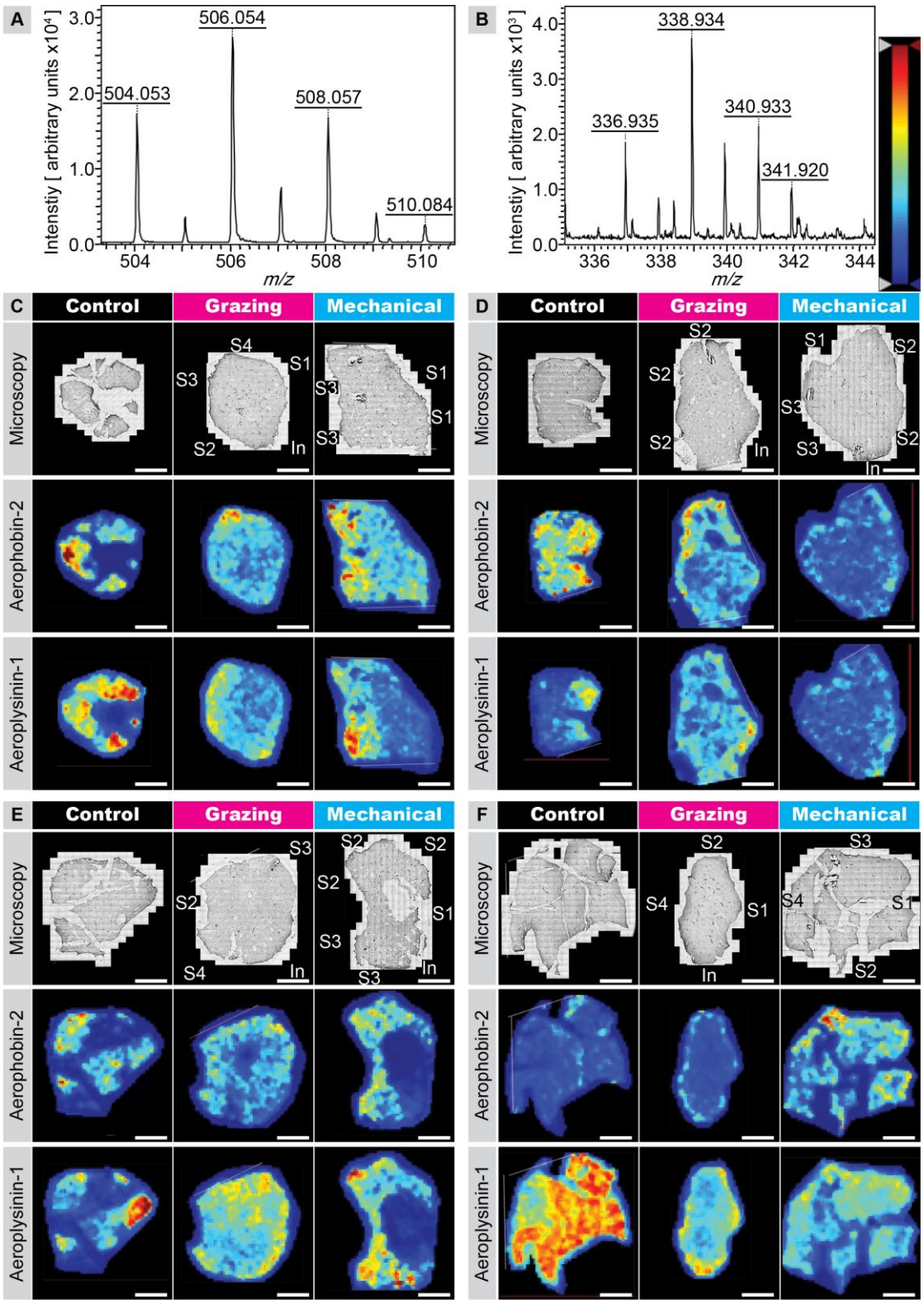

Figure 15. MALDI-imaging MS of a total of 12 samples of specimens corresponding to 4 sponge individuals at 1d. (**A-B**) The experimental isotopic pattern of aerophobin-2 (**A**) and aeroplysinin-1 (**B**). (**C-F**) Each box shows the results corresponding to the three different treatments of one biological replicate (i.e., specimens of a same sponge individual): **Control** (left panel), **Grazing** (middle panel), and **Mechanical** (mechanical damage; right panel). For each sample, the correspondent microscopic image (**Microscopy**; top panel), the distribution pattern of aerophobin-2 intensity (**Aerophobin-2**), and that of aeroplysinin-1 (**Aeroplysinin-1**) are shown. The relative intensity of each compound is depicted in a color scale (**top right**). Red color represents a relatively higher intensity, while blue color represents a relatively lower intensity of each compound. **White-dotted line**= broken or cut edges; scale bar = 5 mm; **In**= intact surface; **S1**= the first evident scar; **S2**= the second scar, and so on.

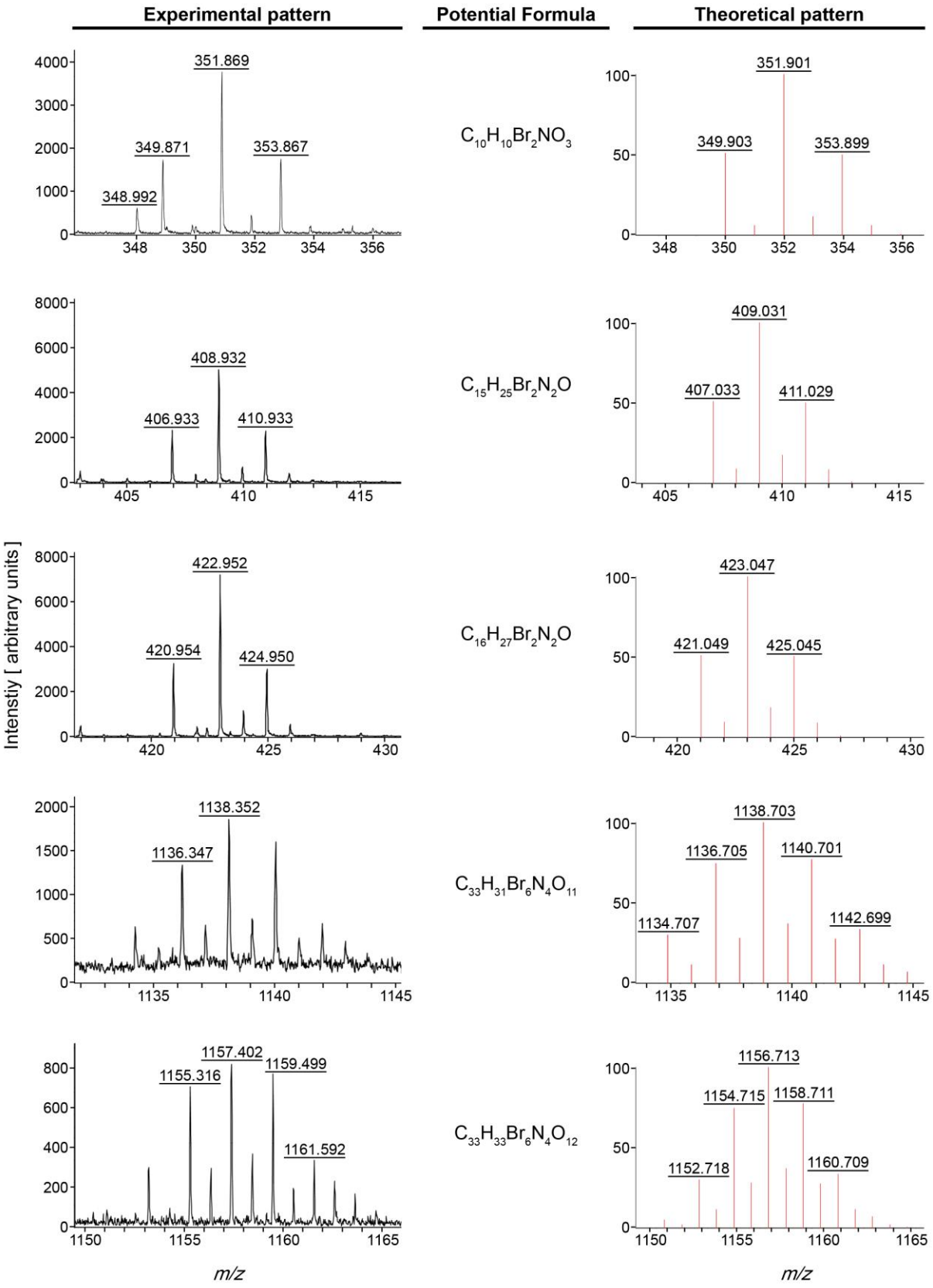

Figure 16. The spectrum for unknown brominated compounds by MALDI-imaging MS. Five further unknown Br-containing compounds were identified.

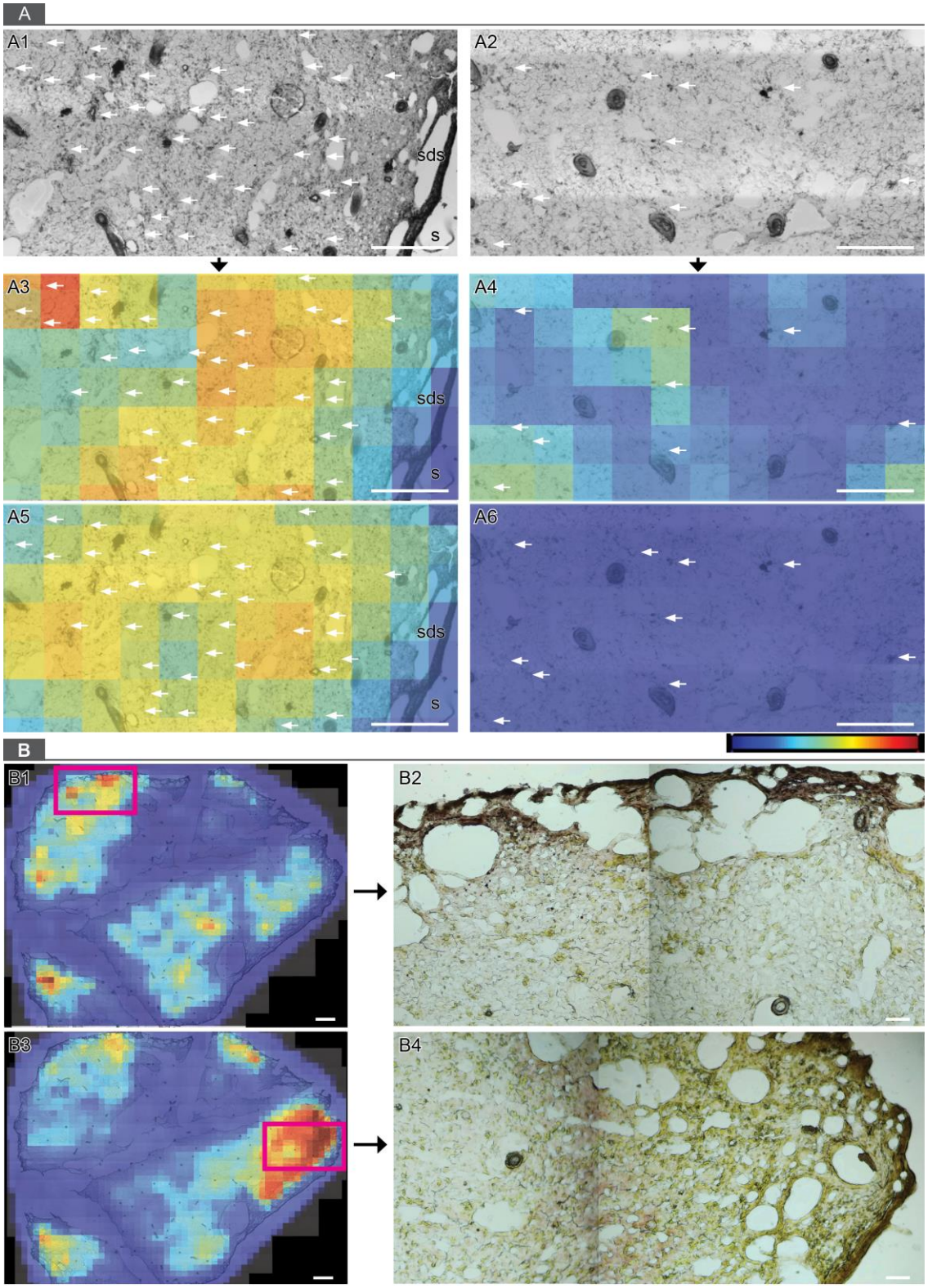

Figure 17. Correlation between presence of brominated alkaloids and cellular features of sponges at 1d-2017. (A) Example of superimposing of microscopic images (**A1, A2**) with correspondent 2D-MALDI-images of aerophobin-2 (**A3, A4**) and aeroplysinin-1 (**A5, A6**), respectively. Both compounds correlated with a dense mesohyl (left panel) which was characterized also by a great number of cell masses (**arrow**) compared to a less dense mesohyl (right panel). Scale bar= 500 µm; **sds**= subdermal spaces. (**B**) Comparison between microscopic images superimposed with correspondent 2D-MALDI-images of aerophobin-2 (**B1**) and aeroplysinin-1 (**B3**) and correspondent light microscopic images (**B2, B4**) of each insert from a same sample, respectively. Scale bar= 1 mm (B1, B3), = 100 µm (B2, B4). The relative intensity of each compound is depicted in a color scale (**middle**). Red color represents a relatively higher intensity, while blue color represents a relatively lower intensity of each compound.

3.3.3 Distinct distribution pattern of brominated compounds upon wounding

Compared to control, both grazing and mechanical damage groups showed a more consistent chemical pattern among the biological replicates: both aerophobin-2 and aeroplysinin-1 distributed mainly at the surface (first 2 mm) and were almost missing in the center of the sponge cross-sections (**Figure 15C-F**). Interestingly, aerophobin-2 mainly accumulated at recently wounded surfaces and showed lower intensity level at intact surfaces.

3.3.4 Co-localization of spherulous cells with brominated compounds

In addition to the samples from experiments, I analyzed a grazed sponge sample which was collected in the field and in which an accumulation of spherulous cells parallel to the surface was evident (**Figure 18**). MALDI-imaging MS at higher resolutions varied from 20 - 100 µm^2 showed that this track of spherulous cells co-localized with both brominated compounds (aerophobin-2 and aeroplysinin-1) investigated in this study (**Figure 18**).

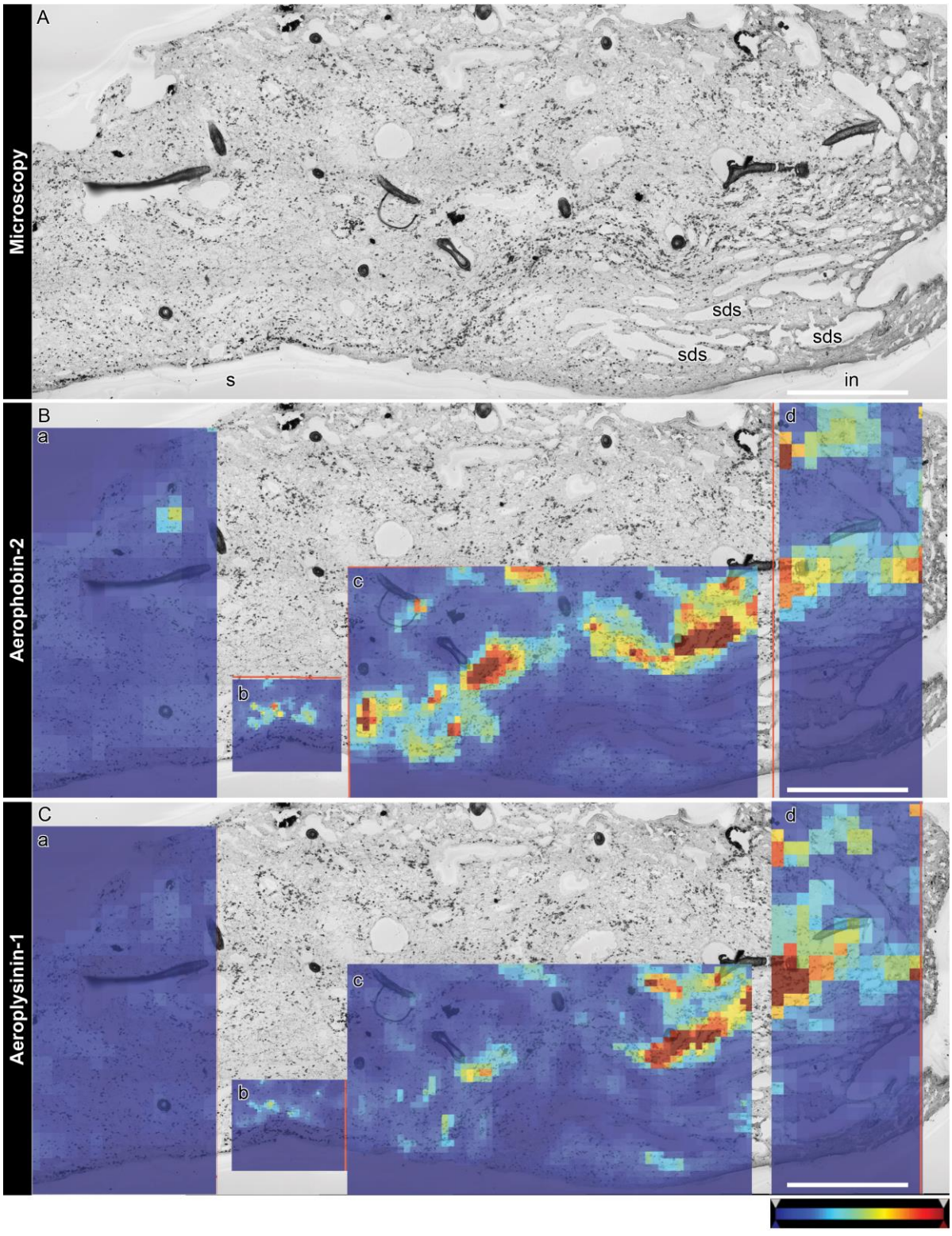

Figure 18. Correlation of cellular pattern and spatial distribution of brominated alkaloids. (**A**) Microscopic image of a grazed sample collected from the field. A track of spherulous cells was parallel to the surface in a multiple-layer beneath the subdermal spaces (**sds**) below the intact surface (**in**), and in a mono-layer at the wounded surface (**s**). The size, shape and location of the main cell type (a size from 10 – 20 µm, densely-packed spherule-like structures, location beneath subdermal spaces) resembled that of spherulous cells. (**B, C**) Superimposition of the microscopic image with 2D-MALDI-images of aerophobin-2 (**B**) and aeroplysinin-1 (**C**), respectively. The sample was measured by MALDI-imaging MS with a raster size at 100 µm (**a** and **d**), 50 µm (**c**), and 20 µm (**b**). The relative intensity of each compound is depicted in a color scale (**bottom right**). Red color represents a relatively higher intensity, while blue color represents a relatively lower intensity of each compound. Scale bar = 1 mm.

3.4 Molecular responses

3.4.1 Transcriptomic profiles of the sponge in response to wounding

Fourty samples of *A. aerophoba* were sequenced by Illumina technology, corresponding to 3 - 6 biological replicates per treatment within 3h-, 1d-, and 6d-experiments (**Table 1**). The number of paired-end Illumina reads generated in this study is summarized in **Table 3**.

Table 3. Number of read pairs (million reads). "Raw" refers to the output from sequencing; "Clean" to surviving pairs after trimming and filtering in trimmomatic-v0.38; and "Eukaryote" to pairs identified as non-prokaryotic and non-microbial eukaryote by kaiju-v1.6.2 (see Methods and Materials).

	Raw	Clean	Eukaryote
average per library (± standard error)	27.0 ± 10.9	20.0 ± 8.5	13.8 ± 5.8
total	1 115.5	825.5	553.3

BUSCO assessments revealed that 92.2 % of the 902 core Metazoan genes were detected in the *de novo* reference transcriptomic assembly generated in my study, with 31.6 % of the genes found as fragments. The reference assembly consisted of a total of 459 466 genes (Trinity components). The statistics of the resulting reference assembly are summarized in **Table 4.** Overall, 72.32 ± 3.19 % (average ± standard error) of the reads of each sample aligned to the *de novo*-assembled reference transcriptome. One grazed sample collected at 3h (H15407-L1_S56) had a lower alignment rate of 53.53 % as well as a lower number of read pairs than the other samples. Therefore, I discarded this sample for downstream analysis.

Table 4: Statistics of the *de novo* transcriptomic assembly from 40 samples. Transcripts refer to Trinity isoforms, genes refer to Trinity components. Mb: mega bases; PE: paired-end.

Statistics:	**150 PE**
Transcripts – Trinity isoforms	1 101 660
Genes – Trinity components	478 830
Transcripts with open reading frames, %	60.8
Average transcript length, nucleotides	510.8
N50	582
Total assembled bases, Mb	562.7
Filtering after Blast search:	
-Transcripts – Trinity isoforms	1 065 137
-Genes – Trinity components	459 466

Gene expression levels were then compared in grazing and mechanical damage group in relation to control, and each time point was analyzed as a separate experiment. The number of significantly differentially-expressed genes (DEGs) was higher at 3h than 1d, whereas no DEGs were detected after 6d (**Figure 19A**). At both 3h and 1d, most of DEGs were up-regulated (i.e., higher expression level than in control). In terms of number of DEGs and expression levels, the response at 3h was stronger in mechanical damage group than in grazing group (**Figure 19A-B**). At 1d, the number of DEGs in each wounding group and expression levels were more similar; yet the proportion of genes unique to grazing response increased (**Figure 19A-B**). As mentioned above, no differential gene expression between wounding groups and control was detected at 6d (FDR *p*-values were all > 0.1).

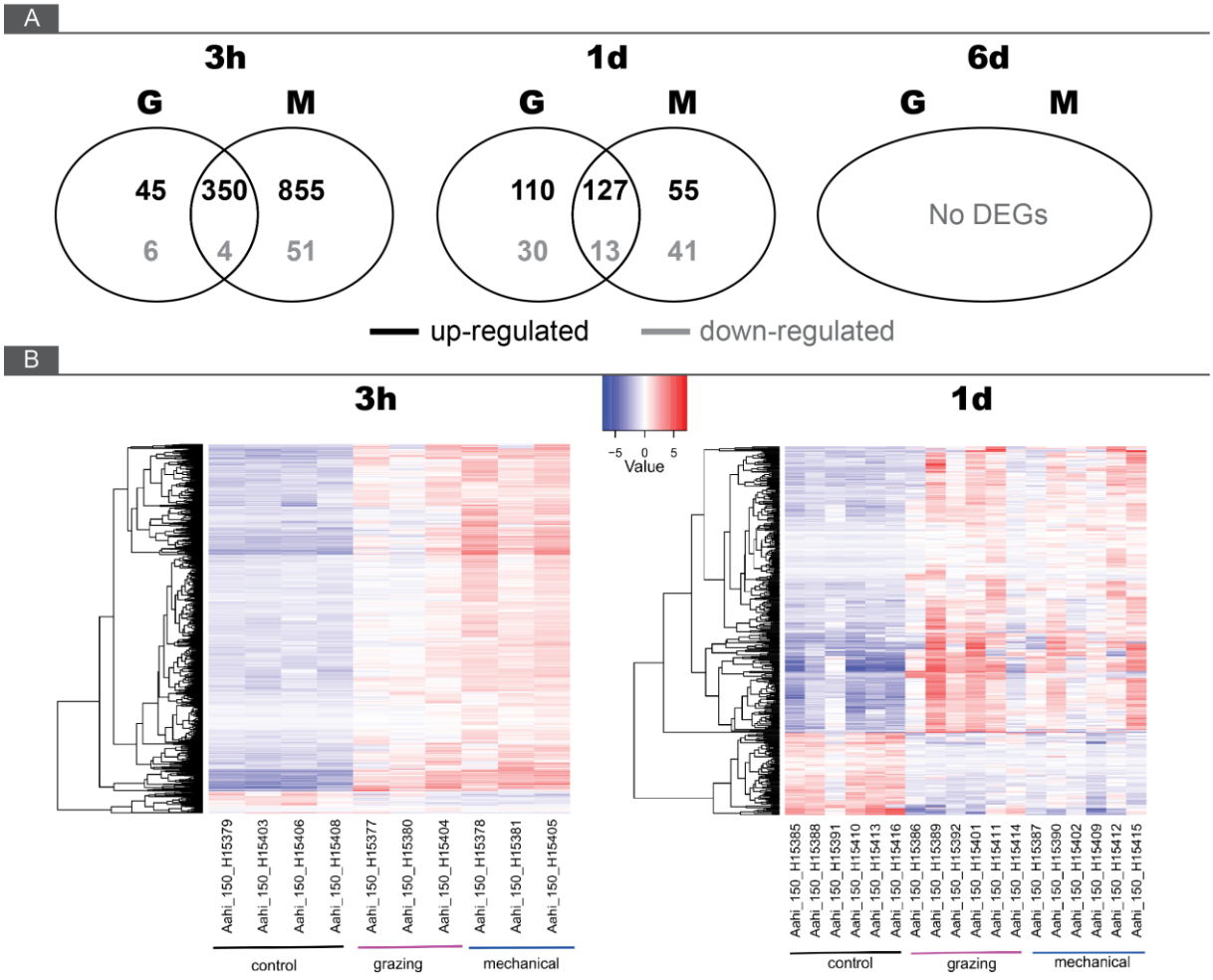

Figure 19. Overview of differentiation expression results. (A) Number of differentially-expressed genes (DEGs). The number of up- and down-regulated DEGs in grazing (**G**) and mechanical damage (**M**) groups compared to control group at different time points (**3h, 1d, and 6d**) are shown. Note that none DEG was detected at 6d. DEGs were defined according to FDR *p*-value < 0.005 and $\log_2|FC| \geq 2$ expression, as calculated in edgeR. **(B)** Heatmaps of DEGs upon wounding showing relative expression levels of each DEG (rows, hierarchically clustered) in each sample at 3h (left) and 1d (right). Expression values are log2-transformed median-centred TMM-normalised values.

The full results from the differential expression analysis in edgeR are reported in Wu *et al.* (in preparation). The full annotation report for DEGs is available in Wu *et al.* (in preparation). From now on, I present the molecular response of samples at 3h and 1d according to the set of annotated genes, which constituted ca. 44 % of the total of DEGs (**Table 5**).

Table 5. Number and percentage (%) of annotated DEGs (Annotated) compared to all DEGs (Total) upon grazing (G) or mechanical damage (M) at each time point (3h, 1d). Up: up-regulated DEGs; **Down**: down-regulated DEGs.

	Up 3h G	**Up 3h M**	**Up 1d G**	**Up 1d M**	**Down 3h G**	**Down 3h M**	**Down 1d G**	**Down 1d M**
Annotated	185	490	110	88	8	25	28	28
Total	395	1205	237	182	10	55	43	54
%	46.84	40.66	46.41	48.35	80.00	45.45	65.12	51.85

3.4.2 Common sponge responses to grazing and mechanical damage at 3h

At 3h time point, the common transcriptional profile of grazing and mechanical damage was characterized by an up-regulation of genes related to wounding response, i.e., cell migration, peptide cross-linking, extracellular matrix (ECM) remodeling, immune and stress response. Moreover, calcium-dependent signaling, lipid signaling and transcriptional factors were activated. The most predominantly up-regulated genes were transglutaminases (TGM), which were accompanied by the up-regulation of potential ECM molecules, i.e., von Willebrand factors, collagens, and fibronectins. TGMs catalyze peptide cross-linking, which was identified as an enriched function in the set of up-regulated genes (GO enrichment analysis, FDR *p*-value < 0.005). TGMs likely interacted with up-regulated TGF-beta like domain-containing gene (TGFß) and integrins, and promoted cell migration (GO:0016477; GO:0030335).

The potential activation of cell migration was further supported by the activation of ETS transcription factors and the detection of genes related to re-assembly of cytoskeleton (i.e., profilin, BTB/POZ domain-containing genes, and a tetraspanin family domain-containing gene (TSN)). I also found regulators of TGFß-mediated signaling such as alpha-2-macroglobulin (Li *et al.*, 2016; Man *et al.*, 2012), a caveolin domain-containing gene (Gvaramia *et al.*, 2013), and an astacin peptidase domain-containing gene which was identified as a tolloid-like protein 1 (Delolme *et al.*, 2015)

based on BLASTP approach. Thus, it suggests potential feedbacks on the signaling and regulation of TGFß-mediated response related to cell migration.

The up-regulation of receptors involved in immune response was detected, in particular scavenger receptor cysteine-rich domain-containing genes (SRCRs) and G-protein coupled receptors (GPCR). SRCRs were identified by the presence of one or multiple SRCR domains. GPCRs were identified and classified according to the 7 transmembrane domain (7tm). Members of the adhesion and rhodopsin GPCR families were up-regulated. Both SRCR and GPCR were up-regulated by grazing and mechanical damage. The immune response to grazing and mechanical damage was further characterized by the up-regulation of components in the complement system (i.e., alpha-2-macroglobulin domain-containing genes), a fibrocystin-L-like gene which contained repeated IPT/TIG domain, a PA14 domain and a G8 domain, lectins such as a ficolin-1-like gene which contained fibrinogen beta and gamma chains and C-terminal globular domain, a galectin-3-binding protein-like gene, and two interferon-induced transmembrane protein domain-containing genes. The up-regulation of stress-related genes was also observed, i.e., a heat shock 70 kDa protein IV-like gene (HSP74), a DnaJ homolog subfamily B member 1-like gene (DnaJ), HIG1 domain family member 2A-like genes, and a BAG domain-containing gene (BAG).

The early response to grazing and mechanical damage was further characterized by the up-regulation of calcium-dependent signaling. In particular, I detected up-regulated genes related to calcium-dependent functions, i.e., calx-beta domain-containing genes, EF-hand domain-containing genes, calcium/calmodulin-dependent protein kinase (CaMK), and death-associated protein kinase, as well as genes related to intracellular calcium concentration, i.e., voltage-dependent calcium channel family, transient receptor potential cation channel subfamily A member 1 (TRPA1), and inositol-1,4,5-trisphosphate 3-kinase activity. This transcriptomic pattern points to calcium ions as major secondary messengers following wounding. The early response to grazing and mechanical damage was further characterized by the up-regulation of genes potentially related to lipid signaling. These included an animal haem peroxidase domain-containing gene (PXDN) which was identified as a peroxidasin (based on BLASTX) belonging to peroxidase-cyclooxygenase superfamily, and a 85/88 kDa calcium-independent phospholipase A2-like gene

(PLPL9) likely belonging to members of phospholipase A2 family. They might be related with lipid metabolism and release of fatty acids.

The early transcriptional response was further characterized by the up-regulation of neurotransmitter-like receptors: nuclear hormone receptor-like genes (NHRs), and a dopamine beta-hydroxylase (DBH)-like monooxygenase protein-like gene (MOXD). I also found the up-regulation of one bHLH. Interestingly, the up-regulation of a gamma-aminobutyric acid type B receptor subunit family-like gene ($GABA_BR$) was detected. The transcriptional response was further characterized by the up-regulation of fibrinogens, a FYVE zinc finger domain-containing gene, immunoglobulin domain-containing genes, and a collagen-containing gene which was homologous to macrophage receptor with collagenous structure (MARCO). In addition, I detected the up-regulated short-chain collagen C4-like gene which likely involved in production of spongin fibers. In common responses at 3h, almost all differentially-expressed genes were up-regulated. A noticeable down-regulation was found in a galactoside-binding lectin domain-containing gene, a C2H2 type zinc finger domain-containing gene, and an ADAM-TS Spacer 1 domain-containing gene which was identified as a member of A disintegrin and metalloproteinase with thrombospondin motifs (ADAMTS).

3.4.3 Treatment-specific responses at 3h

At 3h time point, I observed differences in the response depending on treatment. In general, those common responses described in the previous sections (ECM remodeling, cell migration, calcium signaling, transcription factors, immune and stress response) were stronger (i.e., more genes) in mechanical damage than in grazing group (**Table 6**). However, more genes coding TRPA1, $GABA_BR$, and fibrinogen were induced by grazing compared to mechanical damage.

Grazing-specific responses included the up-regulation of genes related to signaling, including a GPCR receptor of the glutamate family, as identified by the 7TM domain (PF00003; TRINITY_DN163800_c3_g1). Besides, other genes related with autophagy (i.e., autophagy protein Apg5 domain-containing gene), transcription factor (i.e., THAP), cytoskeleton (i.e., intermediate filament protein domain-containing gene) and metabolism (i.e., ethylbenzene dehydrogenase domain-containing) were

also up-regulated. The grazing-specific responses were further characterized by the down-regulation of genes related to signaling (i.e., SAM domain-containing caskin-2), oxidation process (i.e., galactose oxidase central domain-containing gene) and chitin synthesis (i.e., chitin synthase).

Table 6: Comparison of DEGs of interest at 3h. The number of each DEG regulated in grazing (**Grazing**) or mechanical damage group (**Mechanical damage**), or commonly-regulated in both treatments (**Commonly-regulated**) was shown. Compared to grazing, mechanical damage triggered a higher number of DEGs, except for TRPA1, $GABA_BR$, glutamate-like GPCR, and fibrinogen (**labeled with grey-colored background**). [1]: including macrophage receptor MARCO and short-chain collagen C4; [2]: including calx-beta domain-, EF-hand domain-containing genes, and calcium-dependent protein kinase; [3]: including PXDN and PLPL9; [4]: including glutamate-like GPCR.

Gene	Grazing	Mechanical damage	Commonly-regulated
Up-regulation			
ECM remodeling			
Transglutaminase	29	31	29
von Willebrand factor	10	16	8
Collagen[1]	3	4	3
Macrophage receptor MARCO	1	1	1
Short-chain collagen C4	1	1	1
Fibronectin	8	14	8
Cell migration			
TGFß	1	2	1
Integrin	3	7	3
ETS transcriptional factor	7	8	7
Signaling			
Calcium signaling[2]	17	35	17
Lipid signaling[3]	3	3	3
Immune response			
SRCR	8	15	6
GPCR	3	10	3
Metabolism			
DBH-like monooxygenase protein	1	5	1
Other			
TRPA1	4	3	3
$GABA_BR$[4]	7	1	1
Glutamate-like GPCR	1	0	0
Fibrinogen	3	2	1
Down-regulation			
Mucin-like protein	0	1	0
Fibrinogen	0	3	0

Compared to grazing, mechanical damage specifically-triggered expression of additional genes annotated as TGM, ECM molecules, TGFß, integrin, SRCR, GPCR, RTK, Kunitz, MOXD, ETS, NHR, RFX, bHLH, and calcium signaling. Certain signaling pathways were significantly regulated only upon mechanical damage: Wnt signaling (WNT, frizzled, PI3K, DVL, and Wnt inhibitor shisa), MAPK cascade (rab protein, MAPK, and MAPKKK), patterning-related (reeler domain, ephrin receptor with RTK domain, plexin, and PDZ domain), cyclin-dependent kinase 5 activator

protein domain (Cdk5 activator), RTK (including cdc42, src42, and MUSK), latrophilin-like adhesion GPCR, teneurin-3-like, beta-adrenergic receptor kinases, 3'5'-cyclic nucleotide phosphodiesterases, phosphatase, and adenylate kinase. The mechanical damage-specific responses were further characterized by the up-regulation of genes related to immune response (NF-kB p105 subunit, TRAF, and leucine rich repeat), and oxidative stress (BTG, axin-2, oxidative stress-induced growth inhibitor 2, proline dehydrogenase, Hsp16, glutathione S-transferase, alternative oxidase, dyp-type peroxidase family, carbon-nitrogen hydrolase, SH3 domain, PB1 domain, and tetratricopeptide repeat). I also detected the up-regulation of interferon regulatory factor 2-binding protein zinc finger.

Other DEGs activated exclusively upon mechanical damage included additional transcription factors (i.e., high mobility group box, Runt, FOS, F-box, bZIP, PAS domain, HIF, CLOCK, and Tudor domain), genes related with ubiquitination (E3 ubiquitin-protein ligase TRIM71 containing filamin/ABP280 repeat domain, F-box only protein, tubby-related protein, and ubiquitin carboxyl-terminal hydrolase), proteases and protease inhibitors (ADAMTS, trypsin, tryipsin inhibitor, and Kazal-type inhibitor), and transporters (i.e., nuceloporin, mitochondrial carrier protein, and ABC-2 type transporter containing genes), as well as galectin-3-binding protein-like genes and a suprabasin-like gene. Finally, a down-regulation specific to mechanical damage was observed, in particular, ADAMTS, TSN, sulfotransferase, reeler domain, septin/AIG family domain, and mucin-like protein. Genes related to fibrinogen were additionally down-regulated by mechanical damage, but up-regulated by grazing.

In summary, the early transcriptional response to both wounding types were characterized by (i) multicellularity maintenance via the activation of ETS, NHR, bHLH, TGFß, and RTK, (ii) integrity restoration via the activation of wound sealing (in particular TGM and ECM molecules), cell migration (in particular TGFß and cytoskeleton), and skeleton formation (i.e., spongin fiber), (iii) defense and tolerance potentiation via the activation of immunity (in particular SRCR, GPCR, and complement system) and stress response (chaperones), and (iv) stimulus amplification via the activation of calcium signaling and lipid signaling. Compared the response to grazing with the response to mechanical damage, the degree of cell migration, wound sealing, inflammatory response, immune response, and stress response was relatively lower, and the degree of chemical perception (i.e.,

glutamate-like GPCR) and fibrinogen expression was relatively higher in grazing group.

3.4.4 Common sponge responses to grazing and mechanical damage at 1d

As for 3h time point, the response at 1d was also characterized by TGMs, ECM remodeling (e.g., VWF domain-, collagen domain-, and fibronectin domain-containing genes), spongin fiber-related genes (i.e., short-chain collagen C4-like gene), calcium-dependent signaling (calx-beta domain-, EF-hand domain-containing genes, and CaMK-like genes), immune response (SRCR and complement system), stress response (Hsp16), Kunitz, BTB/POZ domain, immunoglobulin, and potential MOXD gene (containing DOMON domain). However, the number of DEGs in these categories dramatically decreased compared to the 3h response, except for spongin fiber-related gene (i.e., short-chain collagen C4-like, **Table 6** and **Table 7**). Moreover, most of the genes related to cell migration, signaling (e.g., GPCRs and RTKs), lipid signaling, transcription factors, as well as proteases and protease inhibitors were almost no longer significantly regulated or were even down-regulated, suggesting a time-dependent transcriptional response upon wounding.

Nevertheless, I detected the up-regulation of genes potentially related to differentiation (i.e., NDR family), cell-cell communication (i.e., cadherin-like gene), mucus production (i.e., IgGFc binding protein, abbreviated as IgGFcBP), and metabolism (i.e., ethylbenzene dehydrogenase).

3.4.5 Treatment-specific responses at 1d

At 1d, the response to grazing was different to that in mechanical damage group in the regulation of several genes. The number of genes annotated as TGM, VWF, collagen, integrin, calx-beta (related with calcium signaling) and SRCR was higher in grazing than that in mechanical damage group (**Table 7**, and **Figure 20**). After 1 day, the responses that were specifically up-regulated by mechanical damage at 3h were no longer activated. It should note that, in general, the number of genes in these categories was still decreased in both groups at 1d compared to 3h (**Figure 20**).

Moreover, genes coding TRPA1, $GABA_BR$, and fibrinogen were only up-regulated by grazing compared to mechanical damage. The gene coding glutamate-like GPCR was still up-regulated by grazing.

Table 7: Comparison of DEGs of interest at 1d. The number of each DEG regulated in grazing (**Grazing**) or mechanical damage group (**Mechanical damage**), or commonly-regulated in both treatments (**Commonly-regulated**) was shown. Compared to mechanical damage, grazing triggered more genes listed below (**labeled with grey background**). [1]: including macrophage receptor MARCO and short-chain collagen C4; [2]: including calx-beta domain-, EF-hand domain-containing genes, and calcium-dependent protein kinase; [3]: including PXDN and PLPL9, here only PXDN was still up-regulated; [4]: including glutamate-like GPCR; [5]: containing VWD-C8-TIL domain.

Gene	Grazing	Mechanical damage	Commonly-regulated
Up-regulation			
ECM remodeling			
Transglutaminase	25	19	19
von Willebrand factor	6	2	2
Collagen[1]	4	3	3
Macrophage receptor MARCO	0	0	0
Short-chain collagen C4	2	2	2
Fibronectin	4	4	3
Cell migration			
TGFß	0	0	0
Integrin	1	0	0
ETS transcriptional factor	0	0	0
Signaling			
Calcium signaling[2]	15	14	9
Lipid signaling[3]	1	1	1
Immune response			
SRCR	8	5	4
GPCR	0	0	0
Metabolism			
DBH-like monooxygenase protein	2	2	2
Mucus production			
Cuticle collagen 90	1	0	0
IgGFcBP	4	1	1
Other			
TRPA1	1	0	0
$GABA_BR$[4]	4	0	0
Glutamate-like GPCR	1	0	0
Fibrinogen	2	0	0
Down-regulation			
Metabolism			
DBH-like monooxygenase protein	3	0	0
Neuropeptide			
PRQFV-amide	1	0	0
Mucus production			
Mucin-like protein	0	1	0
IgGFcBP[5]	0	1	0
AMOP-VWD	0	1	0
Other			
Fibrinogen	0	1	0

Interestingly, a cuticle collagen 90-like gene and two additional IgGFcBPs were up-regulated specifically upon grazing, likely involving in cuticle and/or mucus formation

(**Table 7**). Moreover, grazing up-regulated putative ephrin receptor-like domain-containing genes. Interestingly, two of them contained further upstream repeated thrombospondin type 1 domain with a signal peptide and a downstream IgGFcBP, respectively. Grazing-specific response was further characterized by the up-regulation of universal stress protein family domain-containing genes. Furthermore, the response to grazing was further characterized by a down-regulation of a wnt domain-containing gene, a caskin-2-like gene, and MOXD-like genes. I also detected in grazing group the down-regulation of one gene annotated as PRQFV-amide-like (based on BLASTX annotation; TRINITY_DN146186_c0_g1). PRQFV-amide gene was identified as a neuropeptide modulating the feeding system of the opisthobranch *Aplysia* (Furukawa *et al.*, 2003). However, the characteristic PRQFV motif was missing in the protein sequence of the gene found in my PhD thesis.

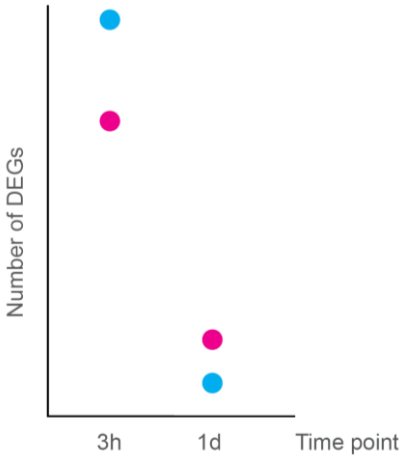

Figure 20. Comparison of the number of DEGs between treatments at 3h and 1d within the categories TGM, ECM molecules, integrin, calx-beta, and SRCR. Grazing (**red circles**) and mechanical damage group (**blue circles**) are included.

Compared to grazing, the responses to mechanical damage was characterized by the up-regulation of an apolipoprotein A1/A4/E domain-containing gene and an eukaryotic translation initiation factor 3 subunit A-like gene, and the down-regulation of genes related to fibrinogen, septin/AIG family domain, mucin-like protein, VWD-C8-TIL domain (identified as IgGFc-binding protein based on BLASTX), and AMOP-VWD domain (**Table 7**),

In summary, the common response to both treatments at 1d was similar to those activated at 3h, however, in a lower degree (lower number of DEGs). The transcriptomic response was potentially directed to differentiation, cell-cell communication, and mucus production. However, while grazing triggered the production of mucus, mechanical damage suppressed the mucus production and initiated protein synthesis and lipid transport. Similarly, fibrinogen was suppressed by

mechanical damage and activated by grazing. Moreover, grazing specifically modulated perception of stimulus and feeding suppressor against grazer, hinting to a specific response upon grazing.

3.4.6 Surveys of potential candidate genes related to enzymes for biosynthesis of brominated compounds

I explored the RNA-Seq data for genes potentially involved in the biosynthesis of brominated compounds in the sponge, in particular, in the following steps: (A) the biosynthesis pathway of tyrosines, (B) the biosynthesis of brominated precursors such as aerophobin-2, and (C) the biotransformation of these precursors into aeroplysinin-1 and, subsequently, into dienone (**Figure 21**). I also checked for regulation upon wounding and DEGs were detected only in mechanical damage group.

For (A), I found a putative main pathway to convert food-derived phenylalanine into tyrosine by phenylalanine-4-hydroylase-like genes with biopterin-dependent aromatic amino acid hydroxylase domain (PF00351; **Figure 21A, a**) and putative enzymes for the biosynthetic process of tetrahydrobiopterin (**THB; Figure 21A, b**) (i.e., sepiapterin reductase-like gene, GTP cyclohydrolase 1-like gene and 6-pyruvoyl tetrahydropterin synthase (PF01242)) – cofactor for phenylalanine-4-hydrolyase. Interestingly, I detected a potential alternative pathway for biosynthesis of tyrosine from glucose via the shikimate pathway which is well known in plants, bacteria, and fungi (Tzin & Galili, 2010), as well as its upstream and downstream pathways, i.e., enolase (PF03952 and PF00113) for the biosynthesis of phosphoenolpyruvate (**Figure 21A, c**), transaldolase (PF00923) for the biosynthesis of erythrose 4-phosphate involving in the pentose-phosphate shunt pathway (**Figure 21A, d**), type I 3-dehydroquinase (PF01487), shikimate/quinate 5-dehydrogenase (PF01488), and chorismate synthase-like gene (PF00425) for the shikimate pathway (**Figure 21A, e**), chorismate mutase type II (PF01817) for converting chorismate into prephenate (**Figure 21A, f**), prephenate dehydrogenase (**PDH;** PF02153) involving in tyrosine biosynthetic process (**Figure 21A, g**), and aminotransferase class I and II (**AT;** PF00155; Wang *et al.*, 2016b) for transamination through pyridoxal phosphate binding (**Figure 21A, h**). Most genes were shown to potentially localize in cytosol based on their GO

annotation. Two genes among step A were up-regulated in response to mechanical damage, i.e., PDH (at 1d) and AT (at 3h).

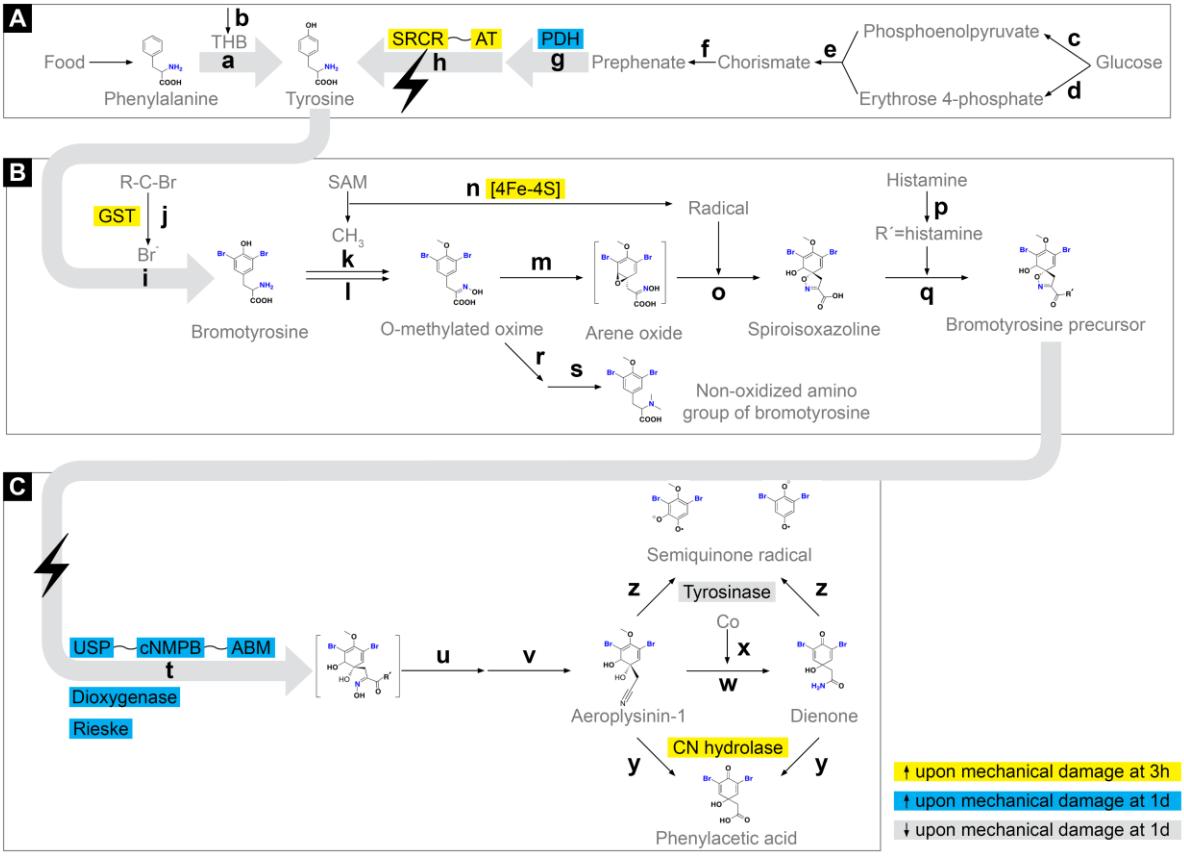

Figure 21. Proposed reaction mechanism of candidate pathways and genes for biosynthesis of brominated compounds. (**A**) The biosynthesis pathway of tyrosines from the main pathway (a-b) and the alternative pathway (c-h). (**B**) The biosynthesis pathway of bromotyrosine-derived precursors, for example aerophobin-2. (**C**) The biotransformation of precursors into aeroplysinin-1 and subsequent dienone, as well as conversion of both products into phenylacetic acids and semiquinone radicals. Dark lightning symbols showed putative stimulation responses according to SRCR, USP, and cNMPB domains. A total of 9 genes were specifically regulated upon mechanical damage and labeled with colored background. While AT, GST, [4Fe-4S], and CN hydrolase were up-regulated (↑) at 3h, PDH, ABM, dioxygenase, and rieske were up-regulated at 1d. Tyrosinase was the only one down-regulated (↓) at 1d. **ABM**: antibiotic biosynthesis monooxygenase; **AT**: aminotransferase class I and II; **CN hydrolase**: carbon-nitrogen hydrolase; **cNMPB**: cyclic nucleotide-binding domain; **Co**: cobalt ion; **Dioxygenase**: glyoxalase/bleomycin resistance protein/dioxygenase superfamily; **GST**: glutathione S-transferase; **PDH**: prephenate dehydrogenase; **Rieske**: Rieske [2Fe-2S] domain; **SAM**: S-adenosylmethionine; **SRCR**: scavenger receptor cystein-rich domain; **THB**: tetrahydrobiopterin; **[4Fe-4S]**: 4Fe-4S binding domain; **USP**: universal stress protein family.

For (B), I found several putative steps to form brominated precursors from tyrosine via bromination, O-methylation, oxime formation, epoxidation, and radical pathway. The genes likely locate in membrane compartiments, based on their GO annotation. First, flavin-dependent halogenase-like genes (Shepherd *et al.*, 2016; Neubauer *et al.*, 2018; Fraebel *et al.*, 2016; Gutleben *et al.*, 2019) with tryptophan halogenase

(PF04820) and FAD binding domain (PF01494) might be responsible for bromination of tyrosine (**Figure 21B, i**). Correspondent free bromides were likely provided by genes with alkylhalidase activity (GO: 0047651), e.g., glutathione S-transferase (**GST**; PF13417; PF02798; PF13409; PF14497; PF00043; **Figure 21B, j**). Second, O-methylation of bromotyrosine might be promoted by genes with O-methyltransferase activity (GO: 0008171; **Figure 21B, k**), e.g., (RS)-norcoclaurine 6-O-methyltransferase-like genes (PF00891; PF13649) which was identified to involve in alkaloid biosynthetic process (GO:0009821) based on GO approach, or probable caffeoyl-CoA O-methyltransferase 1-like gene (PF01596; PF13578). Correspondent methyl group (**Figure 21B, CH_3**) was likely provided by S-adenosylmethionine (**Figure 21B, SAM**). Oxime formation might be promoted by P450-containing genes (PF00067; **Figure 21B, l**) with secondary metabolite biosynthetic process (GO:0044550) and oxidoreductase activity (GO:0016709), e.g., cytochrome P450 3A, 71A or 78A family-like genes (Jørgensen *et al.*, 2011; Irmisch *et al.*, 2013). Third, formation of arene oxide intermediates (**Figure 21B, m**) might be addressed by cytochrome P450 2C family-like gene (Yan *et al.*, 2005) or flavin-dependent halogenase-like gene (PF04820; PF01494; Heine *et al.*, 2018). Fourth, formation of spiroisoxazoline might probably need a oxime radical generation (Zhu *et al.*, 2014) through radical pathway via radical SAM superfamily (PF04055) and its catalytic center [4Fe-4S] cluster with 4Fe-4S binding domain (PF12801; **Figure 21B, n**), and need a hydrolysis of arene (GO:0019439) by epoxide hydrolase 1-like gene (**Figure 21B, o**). Fifth, brominated precursors were likely synthesized by condensation of spiroisoxazoline unit(s) with amino acid unit(s), e.g., aerophobin-2 formation probably by a combination with histamine which derived from histidine via pyridoxal-dependent decarboxylase conserved domain-containing gene (PF00282; **Figure 21B, p and q**; Peng *et al.*, 2005). Two genes were found by mechanical damage, i.e., GST and [4Fe-4S]. I also found putative pathways for non-oxidized amino group of brominated compounds via mitochondrial amidoxime reducing component-like genes (PF03473; PF03476; Jakobs *et al.*, 2014) for reduction of oxime and phenylethanolamine N-methyltransferase-like genes with NNMT/PNMT/TEMT family (PF01234) for N-methylation (**Figure 21B, r and s**).

Finally, I searched for potential genes involved in the transformation of precursors into aeroplysinin-1 (C). This transformation would require the opening of spiro ring (**Figure 21C, t**). One of potential candidate genes for taking part in this step is

hydroxylation-exhibiting antibiotic biosynthesis monooxygenase (**ABM**; PF03992; Machovina *et al.*, 2016; Lyles and Eichenbaum, 2018). This gene had an upstream universal stress domain (**USP**; PF00582) and cyclic nucleotide-binding domain (**cNMPB**; PF00027). Other potential candidate genes were glyoxalase/bleomycin resistance protein/dioxygenase superfamily (PF00903) for aromatic compound catabolic process (GO:0019439), and rieske [2Fe-2S] domain (PF00355) for oxidation-reduction process (GO:0055114). In general, dioxygenases catalyze ring-opening of phenols with incorporation of one or two atoms of oxygen. For spiro ring, it was proposed here that dioxygenases broken the C-O bond of the isoxazoline ring (White and Flashman, 2016; Wang *et al.*, 2017). Interestingly, all three candidate genes for the last biotransformation step were up-regulated at 1d, indicating a strict control for an initiation to produce more toxic forms. Following the spiro ring opening, molecular intermediates would be recruited for further conversion steps, i.e., into nitriles probably via cytochrome P450 71A family-like genes (**Figure 21C, u**; Jørgensen *et al.*, 2011; Irmisch *et al.*, 2014). Converted intermediates would then be transported into a different water-rich microenvironment, which would induce rapid breaking down of C-C bond for the final transformation (**Figure 21C, v**; Murphy *et al.*, 2014). Aeroplysinin-1 could further be converted into dienone (**Figure 21C, w**). Lipowicz *et al.* (2013) identified a specific nitrile hydratase that would perform this step. In my dataset, I found nitrile hydratases (PF02979; PF02211; Lipowicz *et al.*, 2013; Martinez *et al.*, 2017) whose best hit (BLASTX) matched to the sequence probable nitrile hydratase from the choanoflagellate *Monosiga brevicollis* (Gene ID: 5892148; Foerstner *et al.*, 2008) and I also found putative transporter for its cofactor cobalt ion (**Co**; PF09490; PF01891; PF02361; **Figure 21C, x**). Both transformed products could be further converted into less toxic phenylacetic acid or more toxic semiquinone radical by carbon-nitrogen hydrolase (CN hydrolase; **Figure 21C, y**; Pace and Brenner, 2001; Bhalla *et al.*, 2018) and tyrosinase-like genes with monophenol monooxygenase activity (GO:0004503; **Figure 21C, z**; Koulman *et al.*, 1996; Song *et al.*, 2008), respectively. While the front one was up-regulated 3h after mechanical damage, the latter one was down-regulated at 1d. My findings suggest a potential participation of sponge enzymes rather than prokaryotic enzymes in the biosynthesis of brominated compounds. The sponge may likely control the synthesis and transformation of brominated compounds upon stimuli.

4. Discussion

As sessile animals, sponges are constantly exposed to diverse challenges including predators, competitors, pathogens, and environmental factors, but they lack behaviorally-mobile strategy to react quickly to such environmental pressure. Although secondary metabolism plays a role in defense against consumers, the sponge-opisthobranch (prey-grazer) interaction raises questions about the response of chemically-defended sponges to the counter-adaptation by spongivorous specialists. While a co-evolutionary arms race between terrestrial or marine plants and herbivores has been extensively studied (Baldwin, 1990; Toth and Pavia, 2007; Nylund *et al.*, 2011; Burkepile and Parker, 2017; Erb and Reymond, 2019), the knowledge of the sponges´ response to natural grazing is poor. I chose the sponge *Aplysina aerophoba* and its specialist grazer, the opisthobranch *Tylodina* (Willan, 1984; Becerro *et al.*, 2003a), as my case study due to the well-investigated chemistry in sponges of the order Verongiida (Lira *et al.*, 2011; Niemann *et al.*, 2015 and references therein), as well as the well-defined localization of brominated compounds in specialized sponge cells (Thompson *et al.*, 1983; Turon *et al.*, 2000). Here, I characterized, to my knowledge for the first time, the cellular, chemical, and molecular aspects of the response of sponges to grazing by application of multiple techniques, i.e., microscopy, MALDI-imaging MS, and RNA-Seq. The present study provides the first evidence that

(i) spherulous cells with electron-dense spherules were recruited to grazed surface in a time-dependent manner,

(ii) brominated alkaloids (i.e., aerophobin-2 and aeroplysinin-1) were allocated to the surface upon grazing, and

(iii) grazing induced cell migration, wound sealing, and immune response in a time-dependent manner.

Moreover, comparing the effect of grazing to mechanical damage revealed similar responses at the cellular, chemical, and molecular level. Both grazing and mechanical damage induced a resistance response by accumulating secondary

metabolites-carrying spherulous cells at wounded surface and triggering immune recognition, as well as a tolerance response by activating wound sealing and stress-induced pathways. However, the degree of cellular and molecular response was general lower upon grazing, suggesting a specific response to grazing.

4.1 Recruitment of spherulous cells to the wound

4.1.1 Cell migration in response to wounding

The specialized sponge cell population, spherulous cells, harbors brominated compounds in electron-dense spherules (Thompson *et al.*, 1983; Turon *et al.*, 2000) and relates with toxicity (Uriz *et al.*, 1996a, 1996b; Becerro *et al.*, 1997). However, no study has focused on functions of secondary metabolites-carrying spherulous cells after natural wounding, i.e., grazing. My findings of cellular response revealed that wounding, i.e., grazing or mechanical damage, induced a time-dependent recruitment of spherulous cells with electron-dense spherules to the wounded surface.

In the course of my PhD thesis, I showed that spherulous cells accumulated at the damaged surface. Treated samples from 1d-experiment had different distribution pattern of spherulous cells beyond the surface and the start of regenerated ectosome compared to treated samples from 3h. Thus, the spherulous cells actively accumulated at the surface and this is not an artifact caused by tissue loss. Otherwise, I would expect a similar patterning between samples from 3h- and 1d-experiments. My findings were consistent with a previous study by Smith and Hildemann (1986) that spherulous cells were found in mesohyl tracts which were directed to allograft zone and wounded surface in a demosponge. Moreover, my observation of spherulous cell population near spongin fibers and cell tract towards the wounded surface are reminiscent of laterally migrated cells from upwards moved blastemas (Boury-Esnault, 1976; Simpson, 1984; Coutinho *et al.*, 2017). Such strategic re-patterning of cells has been reported in regeneration of cnidarian and zebrafish (Bradshaw *et al.*, 2015; Romero *et al.*, 2018).

Few studies addressing the cellular response of sponges to wounding also suggest cell migration to the wound, however, no specific accumulation of spherulous cells

(Alexander *et al.*, 2015; Borisenko *et al.*, 2015; Ereskovsky *et al.*, 2015; 2017; Lavrov *et al.*, 2018). Ereskovsky *et al.* (2015) observed the migration of type 2 vacuolar cells to the wounded zone. This vacuolar cell population is conformed of special cells containing inclusions (Simpson, 1984; Ereskovsky, 2007). I observed also similar cellular debris as reported in plug formation during sponge regeneration by Borisenko *et al.* 2015. Apparently, to accomplish regeneration after wounding, sponges require different cell populations. Choanocytes, archeocytes, and pinacocytes migrated and formed blastemas for regeneration in the demosponge *Halisarca dujardini* via trans-differentiation (Borisenko *et al.*, 2015). And a remodeling process of pre-existing choanocytes and pinacocytes after wounding has been also reported in a homoscleromorph (Ereskovsky *et al.*, 2015) and two calcareous sponges (Ereskovsky *et al.*, 2017; Lavrov *et al.*, 2018).

The accumulation of spherulous cells at the wounded surface in my study is reminiscent of a wounding-caused infiltration of specialized cells from cnidarians to vertebrates: melanin-containing granular cells in cnidarians (Palmer *et al.*, 2011), spherule-containing cells in echinoderms (San Miguel-Ruize and García-Arraras, 2007; Vazzana *et al.*, 2015), and granulocytes in vertebrates (Christoffersson and Phillipson, 2018). Those cells are characterized by membrane-bound subcellular compartmentalization (i.e. spherules, inclusions, granules, or vesicles) and capacity to release subcellular, bioactive components (Maldonado, 2016; Ternon *et al.*, 2016; Palmer and Traylor-Knowles, 2012; Ramírez-Gómez and García-Arrarás, 2010; Yin and Heit, 2018). My findings revealed that the specialized spherulous cell population was not a set of loose cells, instead coordinately worked to increase the efficiency of allocation of secondary metabolites across the whole sponge body and probably form a temporally-protective boundary at the wounded surface. Beyond brominated alkaloids, spherulous cells at the wounded surface might also provide a physical support for ECM deposition (Bonasoro *et al.*, 2001; Wilkie *et al.*, 2006; Fassini *et al.*, 2012).

4.1.2 Molecular evidence for migration of spherulous cells

The observed transcriptomic responses agree with a scenario of migration of spherulous cells to the wounded surface. The TGM-mediated coagulant network

might provide a scaffold matrix for cell infiltration (reviewed in Richardson *et al.*, 2013; Perdomo-Morales, *et al.*, 2019). Besides, TGFß is well known to function as cytokines initiating cell migration. Components of two key signaling pathways, TGFß and wnt, were up-regulated in my experiments. These pathways mediate embryonic patterning and morphological polarity in sponges (reviewed in Borisenko *et al.*, 2019 and references therein; Borisenko *et al.*, 2016; Reid *et al.*, 2018; Kozin *et al.*, 2019). TGFß and wnt signaling likely provided also positional information for recruiting the spherulous cells to the wound. Two other gene groups, ephrin receptor-like (EphR-like) and Reeler domain-containing genes, further support the directed cell migration (Sentuerk *et al.*, 2011; Bouché, *et al.*, 2013).

4.2 Chemical responses

4.2.1 Strategic pre-positioning of brominated compounds concomitant with cellular features

In the course of my PhD thesis, a high variability of chemical distribution among control samples was revealed, which reflects the striking natural variability of absolute brominated compound concentrations commonly-observed in *Aplysina* sponges (Puyana *et al.*, 2003; Thoms *et al.*, 2006b; Gerçe *et al.,* 2009; Putz *et al.*, 2009; Sacristán-Soriano *et al.*, 2011). Owing to the spatially-resolved analysis of MALDI-imaging MS, it could be demonstrated that both aerophobin-2 and aeroplysinin-1 were most intensive at the sponge surface (within 2 mm depth from the surface) or at a dense mesohyl. The finding of brominated compounds mostly at the surface was similar to that in previous studies on *Aplysina* sponges by extraction methods (Kreuter *et al.*, 1992; Freemann and Gleason, 2010). However, Sacristán-Soriano *et al.* (2011) showed that aerophobin 2 and other brominated precursors mostly localized in the choanosome of *A. aerophoba* by extraction methods.

In general, distribution patterns of secondary metabolites depend on the sponge species considered (reviewed in Rhode and Schupp, 2018). The outer sponge tissue is maybe not the most “valuable” area, but is exposed to consumers and pathogens. The pattern observed in *A. aerophoba* control samples may provide a passive strategy to benefit the survival of sessile sponges, and may weigh more than costs of

constitutive production of brominated alkaloids as well as potential autotoxicity to sponges themselves. The specific depth of most intensive brominated compounds, i.e., aerophobin-2 and aeroplysinin-1, which were found to localize under subdermal spaces in the course of my PhD thesis enables the sponge to form a chemical boundary which facilitates defense against consumers and pathogens.

Due to antimicrobial activity of aeroplysinin-1 (reviewed in Lira *et al.*, 2011; Niemann *et al.*, 2015), its defensive role other than against consumers is expected, especially in areas where the ratio between the surface to the volume of pathogen-containing seawater is relatively high and the phagocytosis activity is relatively lower than that in the choanosome filled with choanocytes and nutrient digesting archeocytes. Moreover, this strategic distribution can also enable a tolerance of loss in the very superficial layer due to physical disturbances caused by natural abrasion wounding in the shallow water habitat (Shanks & Wright 1986), and the superficial damage can be recovered by rapid growth rate (Ayling, 1983; Duckworth, 2003). Although the control group showed a striking variability of distribution pattern, the highest intensity of aerophobin-2 and aeroplysinin-1 usually localized under the surface or near canals. Thus, my findings highlight a spatially-organized strategy in most control samples, which supports my hypothesis that brominated alkaloids mainly pre-localize at places where they are needed for constitutive defense – one of most vulnerable areas of sponges.

One limitation in the presented work was that the cell-resolution was not reached in MALDI-imaging MS. The balance between the resolution and the sensitivity of MALDI-imaging MS is indeed one of main challenges for the development of MALDI-imaging MS (Esquenazi *et al.*, 2008; Yarnold *et al.*, 2012). The longer the measuring time needs, the lower is the sensitivity for a detection of compounds and the replicability of results. This may result in a high variability in the measurement. To be able to compare relative intensity of compounds within three different treatment-sections each time (with a total measured area varying from 531 to 716 mm^2), the spatial resolution was compromised to 250 to 300 µm. Although this resolution was not comparable with the higher resolution by microscopy in the course of my PhD thesis, I observed that aerophobin-2 and aeroplysinin-1 were coincident with the spherulous cell tract in the grazed sample collected from the field at a higher resolution (20 to 100 µm).

4.2.2 Chemical defense by re-accumulation of brominated compounds compensating time for inducting secondary metabolism

Following grazing or mechanical damage in the course of my PhD thesis, the ectosome was destructed; thus, the intensity of both compounds at the surface was expected to be low directly after wounding compared with control. In contrast, both compounds were most intense at the surface and were missing in the center of sponge body among all wounded samples after 1 day. At the same time, the brominated alkaloids-carrying spherulous cells accumulated at the wounded surface. This distinct chemical and cellular patterning after wounding suggests a re-accumulation of brominated compounds at the damaged surface via cellular re-positioning. Interestingly, I observed that aerophobin-2 accumulated mainly at the damaged surface and less at the intact surface in wounded samples compared to aeroplysinin-1. This may suggest that the less toxic precursor aerophobin-2 was more transportable within spherulous cells. Thus, my findings of the co-localization of cells and chemicals as well as the re-accumulation of aerophobin-2 and aeroplysinin-1 at the surface of wounded sponges supports that the sponge activated a chemical defense trait at 1d after wounding by strategic re-accumulation at both chemical and cellular levels.

In general, the relative intensity of both compounds in wounding groups was lower than in control group. This may be contributed, in part, by a quick loss of brominated compounds via damage at the most chemically-intensive areas and the subsequent shedding of spherulous cells at 1d observed in the course of my PhD thesis. In addition to spherulous cells, I also observed the shedding of spongin fibers which have been reported to contain brominated compounds in Verongida sponges (Kunze *et al.*, 2013; Ueberlein *et al.*, 2017), pointing to an additional loss of chemical compounds. Chemicals can be released into surrounding seawater via spherulization in sponges upon disturbance (Ternon *et al.*, 2016) and via repeated disturbance in corals (Geffen *et al.*, 2009). In the latter case, it was suggested that a high capacity of repeated release of chemicals was correlated to a pre-existing reservoir of chemicals, but not to an induced synthesis of compounds after disturbance. Furthermore, only a few number of potential candidate genes related to enzymes for the biosynthesis of brominated compounds was differentially-expressed upon mechanical damage, but not upon grazing. Thus, my findings suggest that both

grazing and mechanical damage induced a re-distribution of the chemical reservoir, which may compensate the time needed for biosynthetic pathways of brominated alkaloids.

The present study focused on aerophobin-2 and aeroplysinin-1. By MALDI-imaging MS, I found other unknown brominated compounds, which were not yet reported in literature. Potential roles of other known and unknown brominated compounds, as well as potential synergistic effects of different secondary metabolites should be taken into account in the future. Nevertheless, generated spatial segmentation maps (**Figure Appendix B.4)** showed a distinct cluster of the first 200 spectrometric peaks at the surface upon wounding. This patterning was correspondent to the distribution pattern of aerophobin-2 and aeroplysinin-1. Thus, sponges responded to wounding by re-allocation of the major compounds that co-localized with the most abundant brominated alkaloids.

Unexpectedly, my findings suggest a constitutive transformation of aeroplysinin-1 from aerophobin-2. If sponges would respond to natural grazing or predation by a rapid transformation of chemical precursors into more toxic forms after cell disruption, so-called activated defense (Teeyapant and Proksch 1993; Ebel *et al.*, 1997; Thoms *et al.*, 2006b; Thoms and Schupp 2008; Rohde *et al.*, 2015), it is expected to detect a higher abundance of aeroplysinin-1 at the wounded surface compared to healthy sponges. In fact, disrupted cells would make up a relatively smaller portion at remained surface and their amount may be even diminished by shedding observed in the course of my PhD thesis. A relatively greater amount of cell disruption theoretically occurs in mouth of attackers, as the transformation has been shown to relate with the intensity of wounding types, i.e. stabbing, grinding, and longer grinding (Thoms *et al.*, 2006b).

Thus, the defense strategy of *A. aerophoba* involves: (i) constitutive production of brominated compounds, as well as constitutive transformation within sponge body at the vulnerable area against consumers and infections, and (ii) inducible defense by temporal and spatial coordination of spherulous cells to allocate brominated alkaloids to the wounded area. In addition, I did not observe the activated defense upon grazing. However, this could happen directly in mouth of grazers or in the surrounding seawater.

4.3 Sponge molecular response to grazing and mechanical damage

After wounding, the ability to maintain integrity, restore homeostasis, and functional multicellularity is essential for every multicellular organism (reviewed in Sonnemann and Bement, 2011). However, underlying molecular responses of sponges to wounding was previously restricted to artificial wounding and lacked replicability (Kenny *et al.*, 2018). I revealed a set of genes related to wound sealing in sponges predominantly at an early time point (3h) after wounding.

Transglutaminase (TGM)-mediated wound sealing was a general response to grazing and mechanical damage. TGM is a pleiotropic enzyme with calcium-dependent or –independent activity involving in many biological processes: the "coagulation" responsible for plug (clot) formation, immune response, and subsequent wound sealing in different invertebrates, including cnidarians (Cerenius *et al.*, 2010; Cerenius and Söderhäll, 2011; Palmer *et al.*, 2012; Palmer and Traylor-Knowles, 2018; Perdomo-Morales, *et al.*, 2019), and vertebrates (Tolentino *et al.*, 2002; Verderio *et al.*, 2005; Richardson *et al.*, 2013). Such coagulation-like process is further supported by alpha-2-macroglobulins which are known pro-coagulants (reviewed in Richardson *et al.*, 2013). This coagulation response via the cross-linking activity of TGM family common to both grazing and mechanical damage groups in agreement with reports in diverse animal groups (reviewed in Palmer and Traylor-Knowles, 2018 and references therein; Verderio *et al.*, 2005; van der Poll and Herwald, 2014; Rodrigues *et al.*, 2019) supports a highly-conserved role of TGM family.

My findings suggest a cross-talk between three key mediators – TGM, TGFß, and integrin –, which led to a coagulation-like event and initiation of immune response (reviewed in van der Poll and Herwald, 2014) at 3h (**Figure 22**). TGMs interact with TGFß and integrins: (i) TGM-mediated coagulation-like process stimulated TGFß-signaling for subsequent inflammation (reviewed in Sonnemann and Bement, 2011); (ii) vice versa, the activated TGFß-signaling enhanced the expression of TGM (Cao *et al.*, 2012; Yamaguchi *et al.*, 2017) probably through up-regulated AP-1 (Nsango *et al.*, 2013; Zhang *et al.*, 1998); (iii) TGM also involved in integrin-signaling or interacted with integrins (Park *et al.*, 2010; Yamaguchi *et al.*, 2017; Bagatur *et al.*, 2018); and (iv) integrins further played a role in the activation of TGFß (Margadant and Sonnenberg, 2010).

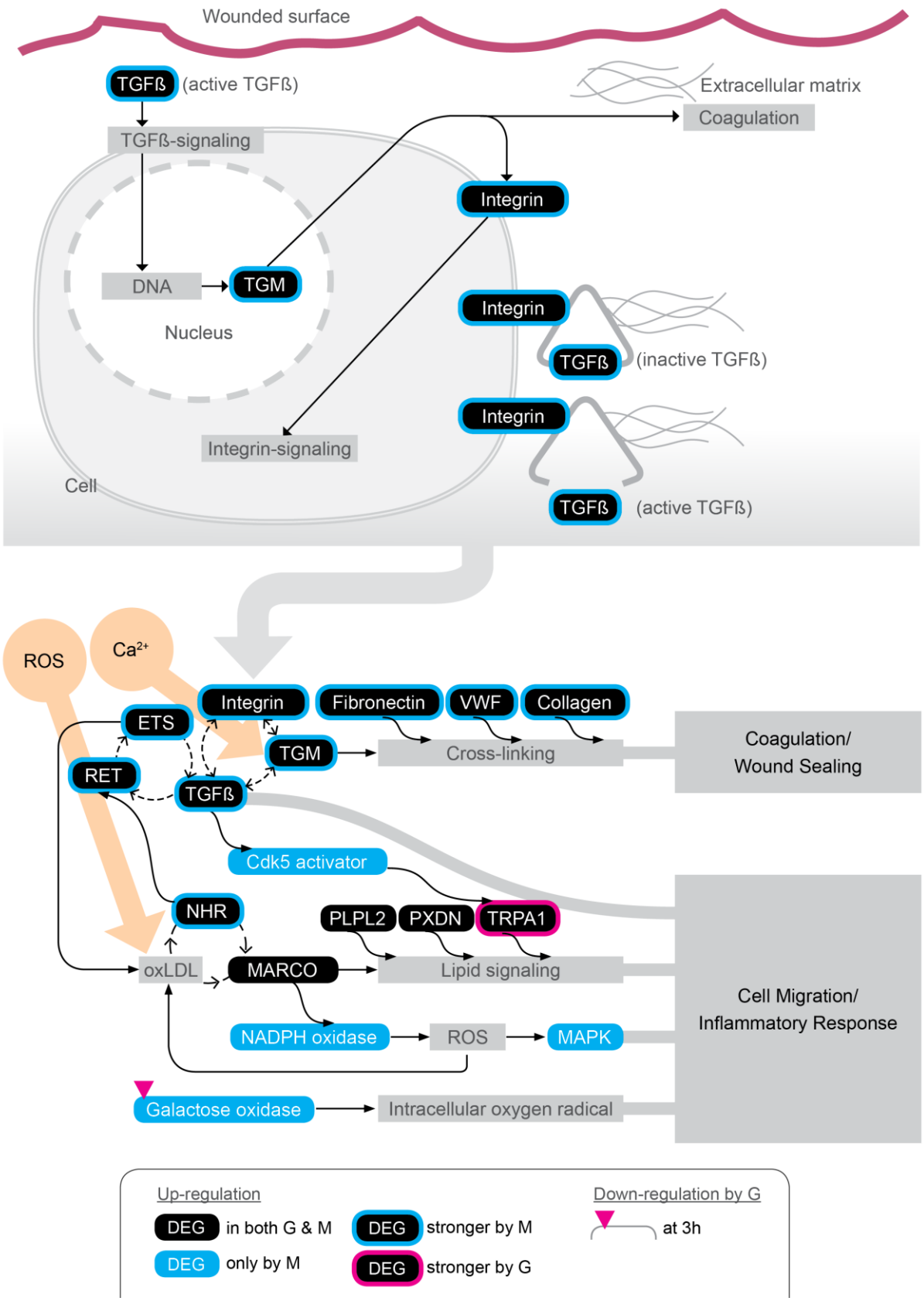

Figure 22. Proposed key molecular processes related to coagulation and cell migration induced by grazing or mechanical damage. A cross-talk between TGM, TGFß, and integrin was shown on top. Transcription-independent signals (labeled in yellow), i.e. calcium ions (**Ca^{2+}**) and reactive oxygen species (**ROS**) initiated TGM acitivity and oxLDL formation, respectively. The degree of cell migration and inflammatory response, coagulation and wound sealing was higher upon mechanical damage (**M**) then grazing (**G**).

The inflammatory response was initiated at 3h, by the activation of: (i) TGFß-mediated signaling, (ii) lipid signaling, (iii) MAPK pathway, and (iv) galactose oxidase-mediated oxygen radical pathway (**Figure 22**). A subsequent inflammatory response after TGM- and TGFß-mediated signaling is further supported by the activation of transcription factors such as ETS (Dumortier *et al.*, 2018) and AP-1 (Toggweiler *et al.*, 2016), extracellular matrix proteins such as tetraspanin (Adell *et al.*, 2004; reviewed in Zoeller, 2009; Saint-Pol *et al.*, 2017; Matthews *et al.*, 2017; Seipold *et al.*, 2018) and proteases (Reiss and Saftig, 2009; Dreymueller *et al.*, 2014; Giebeler and Zigrino, 2016; Reiss and Bhakdi, 2017; Bleibaum *et al.*, 2019).

Furthermore, the activation of SRCR and GPCR gene expression supports the initiation of a defense against potential pathogenic microorganisms in *A. aerophoba* (Pita *et al.*, 2018). Up-regulated fibrinogens were likely involved in defense response as well (Hanington and Zhang, 2011; Endo *et al.*, 2011; Gardères *et al.*, 2015; Perdomo-Morales, *et al.*, 2019). Another component of the immune response was the activation of c-type lectins and complement system (reviewed in Garderes *et al.*, 2015; reviewed in Brinchmann, 2016; Garneiro *et al.*, 2019). While mechanical damage triggered more genes coding SRCR and GPCR, grazing induced more genes related with fibrinogens and mucogenesis (**Figure 23**). Thus, I propose that grazing and mechanical damage triggered an immune defense to build a barrier against pathogens at the wound.

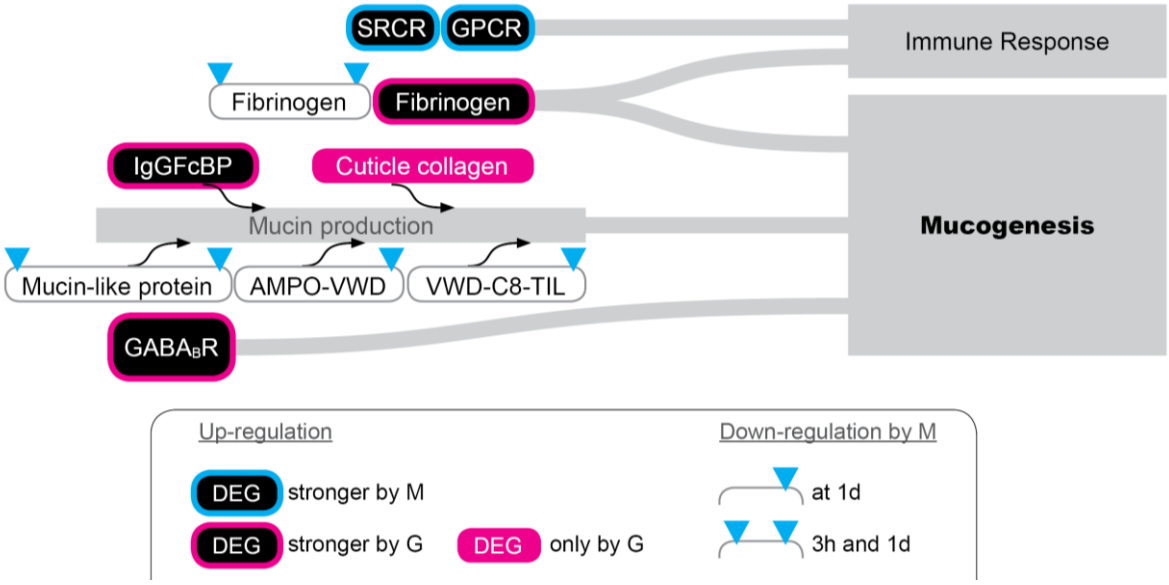

Figure 23. Comparison of the immune response and mucogenesis between treatments. While the degree of SRCR- and GPCR-mediated immune response was higher upon mechanical damage (**M**), the degree of mucogenesis was higher upon grazing (**G**).

The transcriptomic response suggests that calcium ions as key signal in the response to wounding (**Figure 22**). My findings of calcium-dependent genes in both groups (i.e. grazing and mechanical damage) suggest a wounding-induced calcium wave which likely activated TGM-mediated cross-linking, depolarized cell membranes, and amplified signaling (reviewed in Cordeiro and Jacinto, 2013; reviewed in Nakamura *et al.*, 2018; reviewed in Rodrigues *et al.*, 2019). The activation of calcium signaling pathways is a conserved feature during regenerative processes in different animal groups (Cary *et al.*, 2019).

In addition, reactive oxygen species (ROS) could also act as signal implicated in wounding response (**Figure 22**). My findings of up-regulated heat shock proteins (Vazzana *et al.*, 2015; reviewed in Yadav *et al.*, 2019) and BAG (reviewed in Behl, 2016) in both groups suggest that the sponge encountered wounding-induced oxidative stress. Oxidative stress leads to damage, such as formation of oxidized low density lipoprotein (oxLDL; reviewed in Kattoor *et al.*, 2017) which was likely recognized and uptaken by the up-regulated MARCO (Perez *et al.*, 2010). Interestingly, NHR was also up-regulated and might be responsible for the sense of oxidized lipids (Serbulea *et al.*, 2017; Sui *et al.*, 2011), and subsequently activated putative MARCO as oxLDL receptor (reviewed in Enciu *et al.*, 2018 and references therein). Besides, my findings of up-regulated TRPA1 provide a potential candidate gene involving in oxLDL uptake via calcium influx or matrix stiffness under pathogenic stress after wounding (Gupta *et al.*, 2019).

I propose that sponges activated PLPL9 to release arachidonic acids or polyunsaturated fatty acids from lipid membranes (Gramzow *et al.*, 1989; Park *et al.*, 2006). Released lipid molecules could serve for the synthesis of putative prostaglandin known as an inflammatory lipid mediator via up-regulated PXDN (Koljak *et al.*, 2000; Kawamura *et al.*, 2014; Zilietti *et al.*, 1989; Park *et al.*, 2006). Thus, activated TRPA1 could further stimulate a release of such inflammatory lipid mediators (reviewed in Fernandes *et al.*, 2012; Jain *et al.*, 2011). Vice versa, inflammatory mediators such as prostaglandin could activate TRPA1 (Taylor-Clark *et al.*, 2008; DallÁcqua *et al.*, 2014). In algae, prostaglandin production increased after wounding and played a role in defense (Hammann *et al.*, 2016). As the sponge activated MARCO, NHR, PLPL2, PXDN, and TRPA1 in response to grazing, but also to mechanical damage, it is attempting to suggest this putative lipid signaling and

lipid-derivatives initiated by ROS was general response to both wounding types at an early time point and might involve in defense of the sponge.

4.4 Comparison of the response to grazing *vs* the response to mechanical damage

Similar sponge responses to grazing and mechanical damage were observed at chemical, cellular, and molecular level. In marine algae, only grazing by gastropods (Pavia and Toth, 2000) or artificial enzymes related to gastropod salivary fluid (Coleman *et al.*, 2007) enhanced defensive compounds, while grazing by crustacean (Pavia and Toth, 2000) or mechanical damage (Pavia and Toth, 2000; Rohde *et al.*, 2004) did not. Nevertheless, induced defense has been demonstrated in algae without predator/or predator-derived elicitor, instead through oxidative burst via degradation of polysaccharide (i.e., alginate), a cell wand component, of marine algae (Küpper *et al.*, 2001, 2002). It is worth mentioning that induced defense was examined in 1-4 weeks after treatments (Pavia and Toth, 2000; Küpper *et al.*, 2002; Coleman *et al.*, 2007). The theoretical predictions suggested that due to high costs of induced defense, preys need to distinguish real danger (Harvell, 1990; Korth and Dixon, 1997; Agrawal and Karban 1999; Maffei *et al.*, 2004; Rohde and Schupp, 2018). In sponges, induced defense has also been reported by mechanical damage (clipping) mimicking fish bites (5 bites per day) for 2 week (Rohde *et al.*, 2015). My PhD thesis is the first study comparing the response of sponges to actual grazing *vs* mechanical damage and I observed a similar response at cellular, chemical, and molecular levels, at least within the first week after treatment.

Despite this overall similarity in the response to grazing and to mechanical damage, I also detected certain differences between treatments. Interestingly, the cell migration, inflammatory response, wound sealing, and immune response were activated at 3h by grazing and mechanical damage, but mostly stronger regulated by mechanical damage (**Figure 22** and **Figure 23**). DBH-like monooxygenase protein (MOXD)-mediated perception of stimulus (reviewed in Julliard *et al.*, 2017; Kondoh *et al.*, 2016) had also the same pattern, and was even suppressed by grazing at 1d (**Figure 24**). Potential suppression on predators feeding was also suppressed by grazing. While mechanical damage hypersensitized TRPA1 through an activation of a Cdk5

activator and an additional TGFß (Utreras *et al.*, 2012, 2013; Paulsen *et al.*, 2015; Hall *et al.*, 2018), grazing triggered a reduced sensitization of TRPA1 through an increase of both $GABA_BR$ and TRPA1 (Bell *et al.*, 2014; Hanack *et al.*, 2015). Interestingly, the striking activation of $GABA_BR$-mediated phagocytosis and the GPCR-perception of chemical molecules specifically-induced by grazing at both 3h and 1d suggest the perception of a signal specific to grazing.

The sponge response related with damage stimulus was relatively lower in grazing than that induced by mechanical damage. In my study, mechanical damage was intended to mimic natural grazing in terms of repeatedly clipping and similar size of damaged area. Nevertheless, it was challenging to mimic the feeding behavior of sea slugs, which is also the same challenges in study plant-herbivore interaction (reviewed in Baldwin, 1999). I observed differences in wounds caused by grazing *vs* the one caused by mechanical damage. First, the sea slugs covered the sponge surface for at least 1 - 3 hours by curving their foot and body during feeding, while mechanical damage caused remarkable darkening on the damaged surface. In the course of my PhD thesis, the level of this darkening after mechanical damage continuously increased for at least 2 hours. This indicates that this specialist spongivorous may reduce aeration and light condition to suppress further generation of ROS and aeroplysinin-1 production (Kreuter *et al.*, 1992) during grazing (**Figure 24**). In this way, sea slugs might reduce “sponge-self damaging” caused by activated defense during grazing-caused cell disruption and direct contact of the wounded surface to the environment. In contrast, mechanical damage probably resulted in additional oxidative stress, as suggested by the activation of oxidative stress-related and anti-oxidant genes and the stronger activation of inflammatory response. Thus, I propose that feeding behavior may partially attenuate the negative effect of grazing.

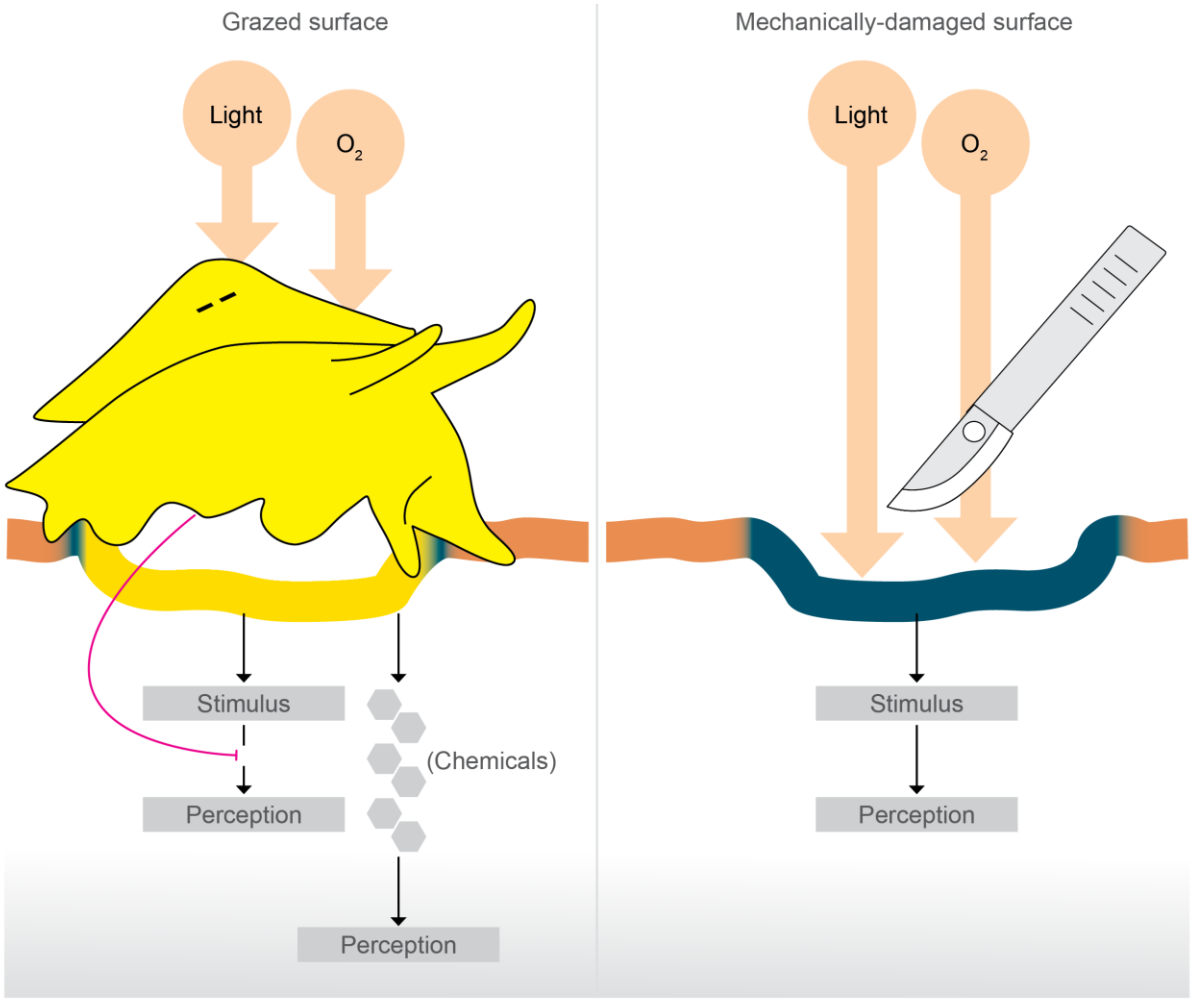

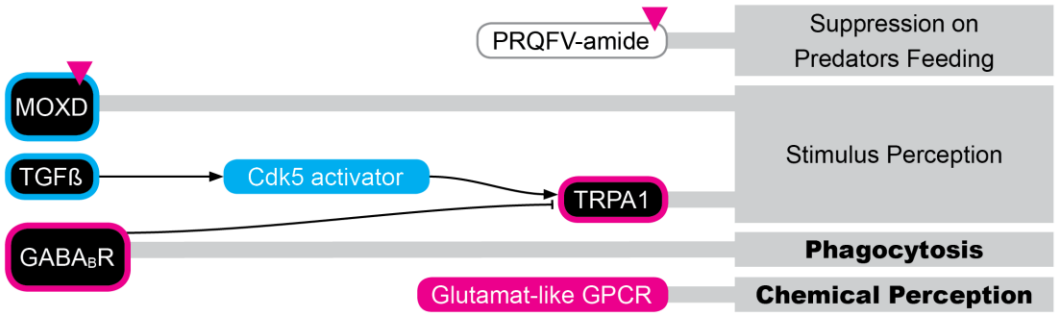

Figure 24. Comparison of the response to grazing *vs* the response to mechanical damage. While the degree of stimulus perception was higher upon mechanical damage (**M**), the degree of phagocytosis and chemical perception was higher upon grazing (**G**). Grazing further modulated the suppression on predators feeding.

4.5 Conclusion

This present PhD thesis revealed that grazing by the spongivorous sea slug *Tylodina perversa* constitutes a stressor to sponge *Aplysina aerophoba*. Grazing induced a wound-like response that was characterized by: (i) the accumulation of spherulous cells at the wounded surface and (ii) the molecular response including cell migration, inflammatory responses, wound sealing, immune defense, and stimulus perception. Thus, sponges activated an inducible defense which is recruited only when challenges exist, and diminished when challenges cease (reviewed by Harvell 1990; Cronin, 2001). The spatial distribution of spherulous cells and brominated alkaloids supports the optimal defense theory which suggests that defenses are costly (i.e., compromise other life history traits such as reproduction), so they are recruited only when they are needed and are allocated to the most vulnerable body parts to maximize the fitness.

My findings revealed that repeatedly wounding by either grazing or mechanical damage launched similar responses. The commonly temporal-spatial regulation at cellular, chemical, and molecular levels protected exposed sponge tissues against infections and damage. However, treatment-specific responses revealed that exogenous factors (i.e., wounding behavior) and endogenous factors (i.e., perception and evaluation of stimulus) had an influence on the degree of the responses in that mechanical damage triggered stronger oxidation stress and inflammatory responses than grazing by the sea slug.

4.6 Future perspectives

The induced response including chemical defense (recruitment of pre-existing brominated compounds and their carrier cells) and immune defense in sponges took place in a relatively short period (3h to 1d) compared to the time needed for an induced production of defensive compounds in marine algae and plants (4 days to 4 weeks). Moreover, the cellular, chemical, and molecular responses were not restricted to challenges from the specialist spongivorous sea slug, instead they were similar to repeatedly clipping (mechanical damage). Thus, it raises the question: whether the activation of the chemical and immune defenses at the early time point is

evolutionarily correlated to self-non-self-recognition. In other words, once the surface barrier is disrupted, then, foreign contact with the environment would stimulate the observed responses. It is also worth to investigate whether the metabolic costs of this induced response may be compromised by other benefits, in particular, as brominated alkaloids (pleiotropically defensive roles, inhibition, protection, perception, and oxidisalbe properties) and spherulous cells (toxicity, stiffening property, as well as secretion of collagen and lectin) have multiple functions.

Moreover, my investigations revealed potential candidate genes involving in pathways and regulation of brominated alkaloids synthesis. Quantification of their expression levels and investigation on their roles will be needed in the future to understand the implications of sponge chemical defenses to spongivorous predators. In particular, it is worth to investigate whether the concentration of chemical compounds is enhanced after a longer time interval than what was investigated in my study, and whether a shift of taste – high-dose-nasty – after possible inducible synthesis of defensive compounds may increase the movement of grazers and their risk to be found by their predators, and thus benefit the prey. It is also worth to address whether the biosynthesis of brominated compounds may take place far away from the wounded site, e.g., at base of sponge body, as I observed that sea slugs usually climbed up to top part of the sponge during feeding and brominated compounds-carrying spherulous cells have been reported to upward migrate during regeneration. Moreover, whether chemical compounds produced by symbiosis may play a role in chemical defense in context of a win-win-situation for both host and symbioses after wounding is still needed to be investigated.

The question should be explored, whether the enrichment of spherulous cells is a specific reaction within the family Aplysinellidae of the order Verongiida upon a “repeatedly” damaging within a given time interval which is caused probably only by this specialist grazer. Beyond spherulous cells, it is also worth to identify other cell types that are involved in wound response. My findings showed that chemically-defended sponges responded to wounding by the activation of TGM-mediated coagulation, mucogenesis, immunity, as well as inducible defense via cellular and chemical translocation at the first priority than the regeneration which is usually contributed by pluripotent cells (i.e., archeocytes and chanocytes), pointing to a co-ordination and an allocation of resources between different biological processes but

also between cell populations after wounding. Investigation on the localization of candidate genes related to transcription factors, calcium-dependent functions, lipid signaling, stimulus perception, immunity, stress response, mucogenesis, differentiation, and brominated alkaloid synthesis in sponge cell types is needed in the future to address how different sponge cell types co-ordinate upon wounding.

My study revealed a complex signaling network involved in cell migration and wound response, as well as provides candidates for studies on fundamental processes in multicellular organisms. Moreover, the potential correlation between the remarkable recruitment of “chemically-defended” cells and the activation of transcriptional expression of genes especially related to inflammatory response and oncogenic functions (e.g., TGM, TGFß, integrins, and ETS) indicates that pro-oncogenic genes already exist at the most ancient multicellularity and are regulated for embryogenesis, metaphogenesis, and wound response. Studying underlying molecular mechanisms is required to understand how those genes co-ordinate with each other in the ancient animals. Furthermore, it is worth to characterize the restoration process and underlying molecular response between the time interval 3d and 6d after wounding, as my findings revealed a recovery at 3d contaminant with a putative collagen network and no transcriptional activation after 6d.

My findings revealed a different degree of sponge response between grazing and mechanical damage, in particular, the degree of stimulus perception was lower and the degree of chemical perception, mucus production, and phagocytosis was higher upon grazing. It is worth to investigate candidate genes related with in particular, GABAergic and dopaminergic signaling pathways, TRPA1 sensitization, as well as ETS- and bHLH-mediated transcriptional regulation, to address if specialist grazers have co-evolved to regulate sponge perception through pro-neural pathways and which chemical(s) derived from grazer may serve as cue(s).

"Specific biological systems can provide exceptional experimental advantages.

Evolution has often resulted in variation in responses to special situations and demands.

Therefore, there are often variants of a general process or molecular organization.

Such variants can provide experimental possibilities

that are not easily achieved in the material or organism..."

-- Bjoerk and Wieslander, 2015

5. Summary

My study is the first report on the cellular, chemical, and molecular responses of sponges to spongivorous sea slugs. The findings provide evidence for an inducible defense which is composed (i) a recognition of cue meaning (within 3 hours) including potential pathogenesis and wounding-induced signals, (ii) an alteration of the phenotype for allocating resources to cell migration and wound sealing by activating key mediators (TGM, TGFß, and integrins), to the chemical defense trait by evoking patterning of pre-existing brominated alkaloids (i.e., aerophobin-2 and aeroplysinin-1) and their carrier cells (i.e., spherulous cells), and to the immune defense trait by activating recognition molecules, coagulation-, and mucogenesis-like processes to maximize the fitness upon reliable cues (from 3 hours to 1 day), and (iii) a reduction of the defense traits to fit the benefits-costs-balance in terms of starting regeneration (after 3 days) and abolishment of transcriptional activation back to an original state (after 6 days).

Compared to mechanical damage, grazing induced relatively fewer molecular transcripts that were related to cell migration, inflammatory response, immune and stress response, as well as perception of stimulus. Thus, the inducible response is consistent with optimal defense theory and provides candidate genes for studying prey-grazer interactions in context of consumer specialisation.

6. References

Adell, T., Gamulin, V., Perović-Ottstadt, S., Wiens, M., Korzhev, M., Mueller, I. M., & Mueller, W. E. G. (2004). Evolution of metazoan cell junction proteins: The scaffold protein MAGI and the transmembrane receptor tetraspanin in the demosponge *Suberites domuncula*. *Journal of Molecular Evolution*, *59*(1), 41–50. https://doi.org/10.1007/s00239-004-2602-2

Agrawal, A. A., & Karban, R. (1999). Why induced defenses may be favored over constitutive strategies in plants. *The Ecology and Evolution of Inducible Defenses*, 45–61.

Alexander, B. E., Achlatis, M., Osinga, R., van derGeest, H. G., Cleutjens, J. P. M., Schutte, B., & deGoeij, J. M. (2015). Cell kinetics during regeneration in the sponge *Halisarca caerulea* : how local is the response to tissue damage? *PeerJ*, *3*, e820. https://doi.org/10.7717/peerj.820

Alexandrov, T. (2012). MALDI imaging mass spectrometry: statistical data analysis and current computational challenges. *BMC Bioinformatics*, *13*(Suppl 16), S11. https://doi.org/10.1186/1471-2105-13-S16-S11

Andrews S. (2010). FastQC: a quality control tool for high throughput sequence data. Available online at: http://www.bioinformatics.babraham.ac.uk/projects/fastqc

Ayling, A. L. (1983). Growth and regeneration rates in thinly encrusting Demospongiae from temperate waters. *The Biological Bulletin*, *165*(2), 343–352. https://doi.org/10.2307/1541200

Bagatur, Y., Ilter Akulke, A. Z., Bihorac, A., Erdem, M., & Telci, D. (2018). Tissue transglutaminase expression is necessary for adhesion, metastatic potential and cancer stemness of renal cell carcinoma. *Cell Adhesion and Migration*, *12*(2), 138–151. https://doi.org/10.1080/19336918.2017.1322255

Bakus, G. J., & Green, G. (1974). Toxicity in sponges and holothurians: a geographic pattern. *Science*, *185*(4155), 951–953. https://doi.org/10.1126/science.185.4155.951

Baldwin, I. T. (1990). Herbivory simulations in ecologica. *Elsevier Science Ltd*, *5*(3), 3–5. https://doi.org/10.1016/0169-5347(90)90237-8

Baldwin, I. T. (1999). Inducible nicotine production in native *Nicotiana* as an example of adaptive phenotypic plasticity. *Journal of Chemical Ecology*, *25*(1), 3–30. https://doi.org/10.1023/A:1020880931488

Becerro, M. A., Uriz, M. J., & Turon, X. (1997). Chemically-mediated interactions in benthic organisms: The chemical ecology of *Crambe crambe* (Porifera, Poecilosclerida). *Hydrobiologia*, *355*, 77–89. https://doi.org/10.1023/A:1003019221354

Becerro, M. A., Paul, V. J., & Starmer, J. (1998). Intracolonial variation in chemical defenses of the sponge *Cacospongia* sp. and its consequences on generalist fish predators and the specialist nudibranch predator *Glossodoris pallida*. *Marine Ecology Progress Series*, *168*, 187–196. https://doi.org/10.3354/meps168187

Becerro, M. A., Thacker, R. W., Turon, X., Uriz, M. J., & Paul, V. J. (2003a). Biogeography of sponge chemical ecology: Comparisons of tropical and temperate defenses. *Oecologia*, *135*(1), 91–101. https://doi.org/10.1007/s00442-002-1138-7

Becerro, M. A., Turon, X., Uriz, M. J., & Templado, J. (2003b). Can a sponge feeder be a herbivore? *Tylodina perversa* (Gastropoda) feeding on *Aplysina aerophoba* (Demospongiae). *Biological Journal of the Linnean Society*, *78*, 429–438. https://doi.org/10.1046/j.0024-4066.2002.00165.x

Behl, C. (2016). Breaking BAG: the co-chaperone BAG3 in health and disease. *Trends in Pharmacological Sciences*, *37*(8), 672–688. https://doi.org/10.1016/j.tips.2016.04.007

Bell, J. J. (2008). The functional roles of marine sponges. *Estuarine, Coastal and Shelf Science*, *79*(3), 341–353. https://doi.org/10.1016/j.ecss.2008.05.002

Bell, J. T., Loomis, A. K., Butcher, L. M., Gao, F., Zhang, B., Hyde, C. L., Sun, J., Wu, H., Ward, K., Harris, J., Scollen, S., Davies, M. N., Schalkwyk, L. C., Mill, J., Williams, F. M. K., Li, N., Deloukas, P., Beck, S., McMahon, S. B., Wang, J., John, S. L., & Spector, T. D. (2014). Differential methylation of the TRPA1 promoter in pain sensitivity. *Nature Communications*, *5*. https://doi.org/10.1038/ncomms3978

Bhalla, T. C., Kumar, V., Kumar, V., Thakur, N., & Savitri. (2018). Nitrile metabolizing enzymes in biocatalysis and biotransformation. *Applied Biochemistry and Biotechnology*, *185*(4), 925–946. https://doi.org/10.1007/s12010-018-2705-7

Bleibaum, F., Sommer, A., Veit, M., Rabe, B., Andrae, J., Kunzelmann, K., Nehls, C., Correa, W., Gutsmann, T., Groetzinger, J., Bhakdi, S., & Reiss, K. (2019). ADAM10 sheddase activation is controlled by cell membrane asymmetry. *Journal of Molecular Cell Biology*, 1–15. https://doi.org/10.1093/jmcb/mjz008

Blunt, J. W., Carroll, A. R., Copp, B. R., Davis, R. A., Keyzers, R. A., & Prinsep, M. R. (2018). Marine natural products. *Natural Product Reports*, 8–53. https://doi.org/10.1039/C7NP00052A

Bolger, A. M., Lohse, M., & Usadel, B. (2014). Trimmomatic: a flexible trimmer for Illumina Sequence Data. *Bioinformatics*, btu170.

Bonasoro, F., Wilkie, I. C., Bavestrello, G., Cerrano, C., & Carnevali, M. D. C. (2001). Dynamic structure of the mesohyl in the sponge *Chondrosia reniformis* (Porifera, Demospongiae). *Zoomorphology*, *121*(2), 109–121. https://doi.org/10.1007/PL00008497

Borisenko, I. E., Adamska, M., Tokina, D. B., & Ereskovsky, A.V. (2015). Transdifferentiation is a driving force of regeneration in *Halisarca dujardini* (Demospongiae, Porifera). *PeerJ*, *3*, e1211. https://doi.org/10.7717/peerj.1211

Borisenko, I., Adamski, M., Ereskovsky, A., & Adamska, M. (2016). Surprisingly rich repertoire of Wnt genes in the demosponge *Halisarca dujardini*. *BMC Evolutionary Biology*, *16*(1), 123. https://doi.org/10.1186/s12862-016-0700-6

Borisenko, I., Podgornaya, O. I., & Ereskovsky, A.V. (2019). From traveler to homebody: which signaling mechanisms sponge larvae use to become adult sponges? In *Advances in Protein Chemistry and Structural Biology* (1st ed., Vol. 116). https://doi.org/10.1016/bs.apcsb.2019.02.002

Bornancin, L., Bonnard, I., Mills, S. C., & Banaigs, B. (2017). Chemical mediation as a structuring element in marine gastropod predator-prey interactions. *Natural Product Reports*, *34*, 644–676. https://doi.org/10.1039/C6NP00097E

Boury-Esnault, N. (1976). Morphogenese experimentale des papilles inhalantes de l'eponge *Polymastia mamillaris* (Muller). *Archives de Zoologie Expérimentale et Générale*, *117*(2), 181–196.

Bradshaw, B., Thompson, K., & Frank, U. (2015). Distinct mechanisms underlie oral *vs* aboral regeneration in the cnidarian *Hydractinia echinata*. *ELife*, *2015*(4), 1–19. https://doi.org/10.7554/eLife.05506

Braekman, J. C., & Daloze, D. (1986). Chemical defence in sponges. *Pure and Applied Chemistry*, *58*(3), 357–364. https://doi.org/10.1351/pac198658030357

Bryant, D. M., Johnson, K., DiTommaso, T., Tickle, T., Couger, M. B., Payzin-Dogru, D., Lee, T. J., Leigh, N. D., Kuo, T. H., Davis, F. G., Bateman, J., Bryant, S., Guzikowski, A. R., Tsai, S. L., Coyne, S., Ye, W. W., Freeman, R. M., Peshkin, L., Tabin, C. J., Regev, A., Haas, B. J., & Whited, J. L. (2017). A tissue-mapped axolotl *de novo* transcriptome enables identification of limb regeneration factors. *Cell Reports*, *18*(3), 762–776. https://doi.org/10.1016/j.celrep.2016.12.063

Burkepile, D. E., & Parker, J. D. (2017). Recent advances in plant-herbivore interactions. *F1000Research*, *6*(0), 119. https://doi.org/10.12688/f1000research.10313.1

Cao, L., Shao, M., Schilder, J., Guise, T., Mohammad, K. S., & Matei, D. (2012). Tissue transglutaminase links TGF-beta, epithelial to mesenchymal transition and a stem cell phenotype in ovarian cancer. *Oncogene*, *31*(20), 2521–2534. https://doi.org/10.1038/onc.2011.429

Carpenter, R. C. (1986). Partitioning herbivory and its effects on coral reef algal communities. *Ecological Monographs*, *56*(4), 345–363.

Cary, G. A., Wolff, A., Zueva, O., Pattinato, J., & Hinman, V. F. (2019). Analysis of sea star larval regeneration reveals conserved processes of whole-body regeneration across the metazoa. *BMC Biology*, *17*(1), 1–19. https://doi.org/10.1186/s12915-019-0633-9

Cavalier-Smith, T. (2017). Origin of animal multicellularity: precursors, causes, consequences—the choanoflagellate/sponge transition, neurogenesis and the

Cambrian explosion. *Philosophical Transactions of the Royal Society B: Biological Sciences*, *372*(1713). https://doi.org/10.1098/rstb.2015.0476

Cerenius, L., Kawabata, S. ichiro, Lee, B. L., Nonaka, M., & Soederhaell, K. (2010). Proteolytic cascades and their involvement in invertebrate immunity. *Trends in Biochemical Sciences*, *35*(10), 575–583. https://doi.org/10.1016/j.tibs.2010.04.006

Cerenius, L., & Soederhaell, K. (2011). Coagulation in invertebrates. *Journal of Innate Immunity*, *3*(1), 3–8. https://doi.org/10.1159/000322066

Christoffersson, G., & Phillipson, M. (2018). The neutrophil: one cell on many missions or many cells with different agendas? *Cell and Tissue Research*, *371*(3), 415–423. https://doi.org/10.1007/s00441-017-2780-z

Cimino, G., De Rosa, S., De Stefano, S., Spinella, A., & Sodano, G. (1984). The zoochrome of the sponge *Verongia aerophoba* ("Uranidine"). *Tetrahedron letters*, 25(27), 2925-2928.

Coleman, R. A., Ramchunder, S. J., Moody, A. J., & Foggo, A. (2007). An enzyme in snail saliva induces herbivore-resistance in a marine alga. *Functional Ecology*, *21*(1), 101–106. https://doi.org/10.1111/j.1365-2435.2006.01210.x

Coutinho, C. C., Rosa, I. D. A., Douglas, J., Teixeira, D. O., Andrade, L. R., Costa, M. L., & Mermelstein, C. (2017). Cellular migration, transition and interaction during regeneration of the sponge *Hymeniacidon heliophila*. *PLoS ONE*, *12*(5), 1–25.

Cronin, G. (2001). Resource allocation in seaweeds and marine invertebrates: chemical defense patterns in relation to defense theories. *Marine chemical ecology*, 325–353.

Dall'Acqua, M. C., Bonet, I. J. M., Zampronio, A. R., Tambeli, C. H., Parada, C. A., & Fischer, L. (2014). The contribution of transient receptor potential ankyrin 1 (TRPA1) to the *in vivo* nociceptive effects of prostaglandin E2. *Life Sciences*, *105*(1–2), 7–13. https://doi.org/10.1016/j.lfs.2014.02.031

De Luca, V., & Laflamme, P. (2001). The expanding universe of alkaloid biosynthesis. *Current Opinion in Plant Biology*, *4*(3), 225–233. https://doi.org/10.1016/s1369-5266(00)00165-5

De Vos, L., Ruetzler, K., Boury-esnault, N., Donadey, C., & Vacelet, J. (1991). *Atlas of sponge morphology*. Smithsonian Institution.

Delolme, F., Anastasi, C., Alcaraz, L. B., Mendoza, V., Vadon-Le Goff, S., Talantikite, M., Capomaccio, R., Mevaere, J., Fortin, L., Mazzocut, D., Damour, O., Zanella-Cléon, I., Hulmes, D. J. S., Overall, C. M., Valcourt, U., Lopez-Casillas, F., & Moali, C. (2015). Proteolytic control of TGF-ß co-receptor activity by BMP-1/ tolloid-like proteases revealed by quantitative iTRAQ proteomics. *Cellular and Molecular Life Sciences*, *72*(5), 1009–1027. https://doi.org/10.1007/s00018-014-1733-x

Dreymueller, D., Uhlig, S., & Ludwig, A. (2014). ADAM-family metalloproteinases in lung inflammation: potential therapeutic targets. *American Journal of Physiology-Lung*

Cellular and Molecular Physiology, *308*(4), L325–L343. https://doi.org/10.1152/ajplung.00294.2014

Duckworth, A. R. (2003). Effect of wound size on the growth and regeneration of two temperate subtidal sponges. *Journal of Experimental Marine Biology and Ecology*, *287*(2), 139–153. https://doi.org/10.1016/S0022-0981(02)00552-X

Dumortier, M., Ladam, F., Damour, I., Vacher, S., Bièche, I., Marchand, N., deLaunoit, Y., Tulasne, D., & Chotteau-Lelièvre, A. (2018). ETV4 transcription factor and MMP13 metalloprotease are interplaying actors of breast tumorigenesis. *Breast Cancer Research*, *20*(1), 1–18. https://doi.org/10.1186/s13058-018-0992-0

Dunn, C. W., Leys, S. P., & Haddock, S. H. D. (2015). The hidden biology of sponges and ctenophores. *Trends in Ecology and Evolution*, *30*(5), 282–291. https://doi.org/10.1016/j.tree.2015.03.003

Ebel, R., Brenzinger, M., Kunze, A., Gross, H. J., & Proksch, P. (1997). Wound activation of protoxins in marine sponge *Aplysina aerophoba*. *Canadian Field-Naturalist*, *111*(1), 1451–1462. https://doi.org/10.1023/B:JOEC.0000006475.10310.3a

Ebel, R., Marin, A., & Proksch, P. (1999). Organ-specific distribution of dietary alkaloids in the marine opisthobranch *Tylodina perversa*. *Biochemical Systematics and Ecology*, *27*(8), 769–777. https://doi.org/10.1016/S0305-1978(99)00024-1

El-Demerdash, A., Atanasov, A. G., Horbanczuk, O. K., Tammam, M. A., Abdel-Mogib, M., Hooper, J. N. A., Sekeroglu, N., Al-Mourabit, A., & Kijjoa, A. (2019). Chemical diversity and biological activities of marine sponges of the genus *Suberea*: a systematic review. *Marine Drugs*, *17*(2), 115. https://doi.org/10.3390/md17020115

El-Gebali, S., Mistry, J., Bateman, A., Eddy, S. R., Luciani, A., Potter, S. C., Qureshi, M., Richardson, L. J., Salazar, G. A., Smart, A., Sonnhammer, E. L. L., Hirsh, L., Paladin, L., Piovesan, D., Tosatto, S. C. E., & Finn, R. D. (2019). The Pfam protein families database in 2019. *Nucleic Acids Research*, *47*(D1), D427–D432. https://doi.org/10.1093/nar/gky995

Enciu, A. M., Radu, E., Popescu, I. D., Hinescu, M. E., & Ceafalan, L. C. (2018). Targeting CD36 as biomarker for metastasis prognostic: how far from translation into clinical practice? *BioMed Research International*, *2018*. https://doi.org/10.1155/2018/7801202

Endo, Y., Matsushita, M., & Fujita, T. (2011). The role of ficolins in the lectin pathway of innate immunity. *International Journal of Biochemistry and Cell Biology*, *43*(5), 705–712. https://doi.org/10.1016/j.biocel.2011.02.003

Erb, M., & Reymond, P. (2019). Molecular interactions between plants and insect herbivores. *Annual Review of Plant Biology*, *70*(1), 527–557. https://doi.org/10.1146/annurev-arplant-050718-095910

Ereskovsky, A.V. (2007). A new species of *Halisarca* (Demospongiae: Halisarcida) from the Sea of Okhotsk, North Pacific. *Zootaxa*, (1432), 57–66. https://doi.org/10.5281/zenodo.175835

Ereskovsky, A.V. (2010). *The comparative embryology of sponges*. Springer Science & Business Media.

Ereskovsky, A.V., Borisenko, I. E., Lapébie, P., Gazave, E., Tokina, D. B., Borchiellini, C., & Singh, S. R. (2015). *Oscarella lobularis* (Homoscleromorpha, Porifera) regeneration: epithelial morphogenesis and metaplasia. *PLoS ONE*, *10*(8), 1–28. https://doi.org/10.1371/journal.pone.0134566

Ereskovsky, A.V., Lavrov, A. I., Bolshakov, F.V., & Tokina, D. B. (2017). Regeneration in white sea sponge *leucosolenia complicata* (Porifera, calcarea). *Invertebrate Zoology*, *41*(2), 108–113. https://doi.org/10.15298/invertzool.14.2.02

Esquenazi, E., Coates, C., Simmons, L., Gonzalez, D., Gerwick, W. H., & Dorrestein, P. C. (2008). Visualizing the spatial distribution of secondary metabolites produced by marine cyanobacteria and sponges via MALDI-TOF imaging. *Molecular BioSystems*, *4*(6), 562–570. https://doi.org/10.1039/b720018h

Fassini, D., Parma, L., Wilkie, I. C., Bavestrello, G., Bonasoro, F., & Candia Carnevali, M. D. (2012). Ecophysiology of mesohyl creep in the demosponge *Chondrosia reniformis* (Porifera: Chondrosida). *Journal of Experimental Marine Biology and Ecology*, *428*, 24–31. https://doi.org/10.1016/j.jembe.2012.05.025

Faulkner, D., & Ghiselin, M. (1983). Chemical defense and evolutionary ecology of dorid nudibranchs and some other opisthobranch gastropods. *Marine Ecology Progress Series*, *13*, 295–301. https://doi.org/10.3354/meps013295

Fernandes, E. S., Fernandes, M. A., & Keeble, J. E. (2012). The functions of TRPA1 and TRPV1: moving away from sensory nerves. *British Journal of Pharmacology*, *166*(2), 510–521. https://doi.org/10.1111/j.1476-5381.2012.01851.x

Firn, R. D., & Jones, C. G. (2009). A Darwinian view of metabolism: molecular properties determine fitness. *Journal of Experimental Botany*, *60*(3), 719–726. https://doi.org/10.1093/jxb/erp002

Foerstner, K. U., Doerks, T., Muller, J., Raes, J., & Bork, P. (2008). A nitrile hydratase in the eukaryote *Monosiga brevicollis*. *PLoS ONE*, *3*(12). https://doi.org/10.1371/journal.pone.0003976

Fraebel, S., Krischke, M., Staniek, A., & Warzecha, H. (2016). Recombinant flavin-dependent halogenases are functional in tobacco chloroplasts without co-expression of flavin reductase genes. *Biotechnology Journal*, *11*(12), 1586–1594. https://doi.org/10.1002/biot.201600337

Freeman, C. J., & Gleason, D. F. (2010). Chemical defenses, nutritional quality, and structural components in three sponge species: *Ircinia felix*, *I. campana*, and *Aplysina fulva*. *Marine Biology*, *157*(5), 1083–1093. https://doi.org/10.1007/s00227-010-1389-5

Funayama, N. (2010). The stem cell system in demosponges: insights into the origin of somatic stem cells. *Development Growth and Differentiation*, *52*(1), 1–14. https://doi.org/10.1111/j.1440-169X.2009.01162.x

Funayama, N. (2018). The cellular and molecular bases of the sponge stem cell systems underlying reproduction, homeostasis and regeneration. *The International Journal of Developmental Biology*, *62*(3-7–8), 513–525. https://doi.org/10.1387/ijdb.180016nf

Furukawa, Y., Nakamaru, K., Sasaki, K., Fujisawa, Y., Minakata, H., Ohta, S., Morishita, F., Matsushima, O., Li, L., Alexeeva, V., Ellis, T. A., Dembrow, N. C., Jing, J., Sweedler, J.V, Weiss, K. R., & Vilim, F. S. (2003). PRQFVamide , a novel pentapeptide identified from the CNS and gut of *Aplysia*. *Journal of Neurophysiology*, *89*(6), 3114–3127. https://doi.org/10.1152/jn.00014.2003

Gardères, J., Bourguet-Kondracki, M. L., Hamer, B., Batel, R., Schroeder, H. C., & Mueller, W. E. G. (2015). Porifera lectins: diversity, physiological roles and biotechnological potential. *Marine Drugs*, *13*(8), 5059-5101. https://doi.org/10.3390/md13085059

Geffen, Y., Ron, E. Z., & Rosenberg, E. (2009). Regulation of release of antibacterials from stressed scleractinian corals. *FEMS Microbiology Letters*, *295*(1), 103–109. https://doi.org/10.1111/j.1574-6968.2009.01590.x

Gemballa, S., & Schermutzki, F. (2004). Cytotoxic haplosclerid sponges preferred: a field study on the diet of the dotted sea slug *Peltodoris atromaculata* (Doridoidea: Nudibranchia). *Marine Biology*, *144*(6), 1213–1222. https://doi.org/10.1007/s00227-003-1279-1

Gerçe, B., Schwartz, T., Voigt, M., Ruehle, S., Kirchen, S., Putz, A., Proksch, P., Obst, U., Syldatk, C., & Hausmann, R. (2009). Morphological, bacterial, and secondary metabolite changes of *Aplysina aerophoba* upon long-term maintenance under artificial conditions. *Microbial Ecology*, *58*(4), 865–878. https://doi.org/10.1007/s00248-009-9560-6

Giebeler, N., & Zigrino, P. (2016). A disintegrin and metalloprotease (ADAM): historical overview of their functions. *Toxins*, *8*(4), 122. https://doi.org/10.3390/toxins8040122

Grabherr, M. G., Haas, B. J., Yassour, M., Levin, J. Z., Thompson, D. A., Amit, I., Adiconis, X., Fan, L., Raychowdhury, R., Zeng, Q., Chen, Z., Mauceli, E., Hacohen, N., Gnirke, A., Rhind, N., DiPalma, F., Birren, B. W., Nusbaum, C., Lindblad-Toh, K., Friedman, N., & Regev, A. (2011). Full-length transcriptome assembly from RNA-Seq data without a reference genome. *Nature Biotechnology*, *29*(7), 644–652. https://doi.org/10.1038/nbt.1883

Gotsbacher, M. P., & Karuso, P. (2015). New antimicrobial bromotyrosine analogues from the sponge *Pseudoceratina purpurea* and its predator *Tylodina corticalis*. *Marine Drugs*, *13*(3), 1389–1409. https://doi.org/10.3390/md13031389

Goetz, S., García-Gómez, J. M., Terol, J., Williams, T. D., Nagaraj, S. H., Nueda, M. J., Robles, M., Talón, M., Dopazo, J., & Conesa, A. (2008). High-throughput functional annotation and data mining with the Blast2GO suite. *Nucleic Acids Research*, *36*(10), 3420–3435. https://doi.org/10.1093/nar/gkn176

Gramzow, M., Schroeder, H. C., Fritsche, U., Kurelec, B., Robitzki, A., Zimmermann, H., Friese, K., Kreuter, M. H., & Mueller, W. E. G. (1989). Role of phospholipase A2 in the stimulation of sponge cell proliferation by homologous lectin. *Cell*, *59*(5), 939–948. https://doi.org/10.1016/0092-8674(89)90616-8

Gupta, N., Goswami, R., Alharbi, M. O., Biswas, D., & Rahaman, S. O. (2019). TRPV4 is a regulator in *P. gingivalis* lipopolysaccharide- induced exacerbation of macrophage foam cell formation. *Physiological Reports*, *7*(7), e14069. https://doi.org/10.14814/phy2.14069

Gutleben, J., Koehorst, J. J., McPherson, K., Pomponi, S., Wijffels, R. H., Smidt, H., & Sipkema, D. (2019). Diversity of tryptophan halogenases in sponges of the genus *Aplysina*. *FEMS Microbiology Ecology*, *95*(8), 1–15. https://doi.org/10.1093/femsec/fiz108

Gvaramia, D., Blaauboer, M. E., Hanemaaijer, R., & Everts, V. (2013). Role of caveolin-1 in fibrotic diseases. *Matrix Biology*, *32*(6), 307–315. https://doi.org/10.1016/j.matbio.2013.03.005

Haas, B. J., Papanicolaou, A., Yassour, M., Grabherr, M., Blood, P. D., Bowden, J., Couger, M. B., Eccles, D., Li, B., Lieber, M., Macmanes, M. D., Ott, M., Orvis, J., Pochet, N., Strozzi, F., Weeks, N., Westerman, R., William, T., Dewey, C. N., Henschel, R., Leduc, R. D., Friedman, N., & Regev, A. (2013). *De novo* transcript sequence reconstruction from RNA-seq using the Trinity platform for reference generation and analysis. *Nature Protocols*, *8*(8), 1494–1512. https://doi.org/10.1038/nprot.2013.084

Hall, B. E., Prochazkova, M., Sapio, M. R., Minetos, P., Kurochkina, N., Binukumar, B. K., Amin, N. D., Terse, A., Joseph, J., Raithel, S. J., Mannes, A. J., Pant, H. C., Chung, M. K., Iadarola, M. J., & Kulkarni, A. B. (2018). Phosphorylation of the transient receptor potential ankyrin 1 by cyclin-dependent kinase 5 affects chemo-nociception. *Scientific Reports*, *8*(1), 1177. https://doi.org/10.1038/s41598-018-19532-6

Hammann, M., Rempt, M., Pohnert, G., Wang, G., Boo, S. M., & Weinberger, F. (2016). Increased potential for wound activated production of prostaglandin E2 and related toxic compounds in non-native populations of *Gracilaria vermiculophylla*. *Harmful Algae*, 51, 81-88. https://doi.org/10.1016/j.hal.2015.11.009

Hanack, C., Moroni, M., Lima, W. C., Wende, H., Kirchner, M., Adelfinger, L., Schrenk-Siemens, K., Tappe-Theodor, A., Wetzel, C., Kuich, P. H., Gassmann, M., Roggenkamp,

D., Bettler, B., Lewin, G. R., Selbach, M., & Siemens, J. (2015). GABA blocks pathological but not acute TRPV1 pain signals. *Cell*, *160*(4), 759–770. https://doi.org/10.1016/j.cell.2015.01.022

Hanington, P. C., & Zhang, S. M. (2011). The primary role of fibrinogen-related proteins in invertebrates is defense, not coagulation. *Journal of Innate Immunity*, *3*(1), 17–27. https://doi.org/10.1159/000321882

Hansen, R. L., Dueñas, M. E., & Lee, Y. J. (2019). Sputter-coated metal screening for small molecule analysis and high-spatial resolution imaging in laser desorption ionization mass spectrometry. *Journal of the American Society for Mass Spectrometry*, *30*(2), 299–308. https://doi.org/10.1007/s13361-018-2081-0

Harvell, C. D. (1990). The ecology and evolution of inducible defenses. *The Quarterly Review of Biology*, *65*(3), 323–340.

Hay, M. E. (1996). Marine chemical ecology: what' s known and what' s next ? *Journal of Experimental Marine Biology and Ecology*, *200*, 103–134. https://doi.org/10.1016/S0022-0981(96)02659-7

Hay, M. E. (2009). Marine chemical ecology: chemical signals and cues structure marine populations, communities, and ecosystems. *Annual Review of Marine Science*, *1*(1), 193–212. https://doi.org/10.1146/annurev.marine.010908.163708

Heine, T., Tischler, D., vanBerkel, W., vanPée, K.-H., & Gassner, G. (2018). Two-component FAD-dependent monooxygenases: current knowledge and biotechnological opportunities. *Biology*, *7*(3), 42. https://doi.org/10.3390/biology7030042

Hentschel, U., Piel, J., Degnan, S. M., & Taylor, M. W. (2012). Genomic insights into the marine sponge microbiome. *Nature Reviews Microbiology*, *10*(9), 641–654. https://doi.org/10.1038/nrmicro2839

Hooper, J. N., & Van Soest, R. W. (2002). Systema Porifera. a guide to the classification of sponges. In *Systema Porifera*. Springer, Boston, MA.

Huerta-Cepas, J., Szklarczyk, D., Forslund, K., Cook, H., Heller, D., Walter, M. C., Rattei, T., Mende, D. R., Sunagawa, S., Kuhn, M., Jensen, L. J., VonMering, C., &Bork, P. (2016). EGGNOG 4.5: a hierarchical orthology framework with improved functional annotations for eukaryotic, prokaryotic and viral sequences. *Nucleic Acids Research*, *44*(D1), D286–D293. https://doi.org/10.1093/nar/gkv1248

Irmisch, S., McCormick, A. C., Boeckler, G. A., Schmidt, A., Reichelt, M., Schneider, B., Block, K., Schnitzler, J-P., Gershenzon, J., Unsicker, S. B., & Köllner, T. G. (2013). Two herbivore-induced cytochrome P450 enzymes CYP79D6 and CYP79D7 catalyze the formation of volatile aldoximes involved in poplar defense. *The Plant Cell*, *25*(11), 4737–4754. https://doi.org/10.1105/tpc.113.118265

Irmisch, S., Clavijo McCormick, A., Guenther, J., Schmidt, A., Boeckler, G. A., Gershenzon, J., Unsicker, S. B., & Koellner, T. G. (2014). Herbivore-induced poplar cytochrome P450

enzymes of the CYP71 family convert aldoximes to nitriles which repel a generalist caterpillar. *Plant Journal*, *80*(6), 1095–1107. https://doi.org/10.1111/tpj.12711

Jain, A., Broenneke, S., Kolbe, L., Staeb, F., Wenck, H., & Neufang, G. (2011). TRP-channel-specific cutaneous eicosanoid release patterns. *Pain*, *152*(12), 2765–2772. https://doi.org/10.1016/j.pain.2011.08.025

Jakobs, H. H., Froriep, D., Havemeyer, A., Mendel, R. R., Bittner, F., & Clement, B. (2014). The mitochondrial amidoxime reducing component (mARC): involvement in metabolic reduction of N-oxides, oximes and N-hydroxyamidinohydrazones. *ChemMedChem*, *9*(10), 2381–2387. https://doi.org/10.1002/cmdc.201402127

Jørgensen, K., Morant, A. V., Morant, M., Jensen, N. B., Olsen, C. E., Kannangara, R., Motawia, M. S., Møller, B. L., & Bak, S. (2011). Biosynthesis of the cyanogenic glucosides linamarin and lotaustralin in cassava: isolation, biochemical characterization, and expression pattern of CYP71E7, the oxime-metabolizing cytochrome P450 enzyme. *Plant Physiology*, *155*(1), 282–292. https://doi.org/10.1104/pp.110.164053

Julliard, A. K., AlKoborssy, D., Fadool, D. A., & Palouzier-Paulignan, B. (2017). Nutrient sensing: another chemosensitivity of the olfactory system. *Frontiers in Physiology*, *8*, 1–16. https://doi.org/10.3389/fphys.2017.00468

Kanehisa, M. & Goto, S. (2000). KEGG: kyoto encyclopedia of genes and genomes. *Nucleic Acids Research*, *28*, 27-30

Kanehisa, M. (2019). Toward understanding the origin and evolution of cellular organisms. *Protein Science*, *28*(11), 1947-1951. https://doi.org/10.1002/pro.3715

Kanehisa, M., Sato, Y., Furumichi, M., Morishima, K., & Tanabe, M. (2019). New approach for understanding genome variations in KEGG. *Nucleic Acids Research*, *47*(D1), D590–D595. https://doi.org/10.1093/nar/gky962

Kattoor, A. J., Pothineni, N. V. K., Palagiri, D., & Mehta, J. L. (2017). oxidative stress in atherosclerosis. *Current Atherosclerosis Reports*, *19*(11), 42. https://doi.org/10.1007/s11883-017-0678-6

Kawamura, M., Inaoka, H., Obata, S., & Harada, Y. (2014). Why do a wide variety of animals retain multiple isoforms of cyclooxygenase? *Prostaglandins and Other Lipid Mediators*, *109–111*, 14–22. https://doi.org/10.1016/j.prostaglandins.2014.03.002

Kenny, N. J., de Goeij, J. M., de Bakker, D. M., Whalen, C. G., Berezikov, E., & Riesgo, A. (2018). Towards the identification of ancestrally shared regenerative mechanisms across the Metazoa: a transcriptomic case study in the Demosponge *Halisarca caerulea*. *Marine Genomics*, *37*, 135–147. https://doi.org/10.1016/j.margen.2017.11.001

Knowlton, A. L., & Highsmith, R. C. (2000). Convergence in the time-space continuum: A predator-prey interaction. *Marine Ecology Progress Series*, *197*(May 2000), 285–291. https://doi.org/10.3354/meps197285

Kossel, A. (1891). Über die chemische Zusammensetzung der Zelle. *Archives of Analytical Physiology, Physiol Abteilung*, 181-186.

Koljak, R., Jaerving, I., Kurg, R., Boeglin, W. E., Varvas, K., Valmsen, K., Ustav, M., Brash, A. R., & Samel, N. (2001). The basis of prostaglandin synthesis in coral: molecular cloning and expression of a cyclooxygenase from the arctic soft coral *Gersemia fruticosa*. *Journal of Biological Chemistry*, *276*(10), 7033–7040. https://doi.org/10.1074/jbc.M009803200

Kondoh, K., Lu, Z., Ye, X., Olson, D. P., Lowell, B. B., & Buck, L. B . (2016). A specific area of olfactory cortex involved in stress hormone responses to predator odours. *Nature*, *532*(7597), 103–106. https://doi.org/10.1038/nature17156

Korth, K. L., & Dixon, R. a. (1997). Evidence for chewing insect-specific molecular events distinct from a general wound response in leaves. *Plant Physiology*, *115*(4), 1299–1305. https://doi.org/10.1104/pp.115.4.1299

Koulman, A., Proksch, P., Ebel, R., Beekman, A. C., VanUden, W., Konings, A. W. T., Pedersen, J. A., Pras, N., & Woerdenbag, H. J. (1996). Cytoxicity and mode of action of aeroplysinin-1 and a related dienone from the sponge *Aplysina aerophoba*. *Journal of Natural Products*, *59*(6), 591–594. https://doi.org/10.1021/np960167z

Kozin, V.V., Borisenko, I. E., & Kostyuchenko, R. P. (2019). Establishment of the axial polarity and cell fate in metazoa via canonical Wnt signaling: new insights from sponges and annelids. *Biology Bulletin*, *46*(1), 14–25. https://doi.org/10.1134/s1062359019010035

Kreuter, M. H., Robitzki, A., Chang, S., Steffen, R., Michaelis, M., Kljajić, Z., Bachmann, M., Schroeder, H. C., & Mueller, W. E. G. (1992). Production of the cytostatic agent aeroplysinin by the sponge *Verongia aerophoba* in *in vitro* culture. *Comparative Biochemistry and Physiology. Part C, Comparative*, *101*(1), 183–187. https://doi.org/10.1016/0742-8413(92)90217-U

Krogh, A., Larsson, B., VonHeijne, G., & Sonnhammer, E. L. L. (2001). Predicting transmembrane protein topology with a hidden Markov model: application to complete genomes. *Journal of Molecular Biology*, *305*(3), 567–580. https://doi.org/10.1006/jmbi.2000.4315

Kunze, K., Niemann, H., Ueberlein, S., Schulze, R., Ehrlich, H., Brunner, E., Proksch, P., & VanPée, K. H. (2013). Brominated skeletal components of the marine demosponges, *Aplysina cavernicola* and *Ianthella basta*: analytical and biochemical investigations. *Marine Drugs*, *11*(4), 1271–1287. https://doi.org/10.3390/md11041271

Küpper, F. C., Kloareg, B., Guern, J., & Potin, P. (2001). Oligoguluronates elicit an oxidative burst in the brown algal kelp *Laminaria digitata*. *Plant Physiology*, *125*(1), 278–291. https://doi.org/10.1104/pp.125.1.278

Küpper, F. C., Müller, D. G., Peters, A. F., Kloareg, B., & Potin, P. (2002). Oligoalginate recognition and oxidative burst play a key role in natural and induced resistance of sporophytes of *Laminariales*. *Ournal of Chemical Ecology*, *28*(10), 2057–2081. https://doi.org/10.1023/A

Lavrov, A. I., Bolshakov, F.V., Tokina, D. B., & Ereskovsky, A.V. (2018). Sewing up the wounds : the epithelial morphogenesis as a central mechanism of calcaronean sponge regeneration. *Journal of Experimental Zoology Part B: Molecular and Developmental Evolution*, *330*(6–7), 351–371. https://doi.org/10.1002/jez.b.22830

Li, C., Hancock, M. A., Sehgal, P., Zhou, S., Reinhardt, D. P., & Philip, A. (2016). Soluble CD109 binds TGF-ß and antagonizes TGF-ß signalling and responses. *Biochemical Journal*, *473*(5), 537–537. https://doi.org/10.1042/BJ20141488

Li, C.-W., Chen, J.-Y., & Hua, T.-E. (1998). Precambrian sponges with cellular structures. *Science*, *279*(5352), 879–882. https://doi.org/10.1126/science.279.5352.879

Lipowicz, B., Hanekop, N., Schmitt, L., & Proksch, P. (2013). An aeroplysinin-1 specific nitrile hydratase isolated from the marine sponge *Aplysina cavernicola*. *Marine Drugs*, *11*(8), 3046–3067. https://doi.org/10.3390/md11083046

Lira, N. S., Montes, R. C., Tavares, J. F., Da Silva, M. S., Da Cunha, E. V. L., De Athayde-Filho, P. F., Rodrigues, L. C., Da Silva Dias, C., & Barbosa-Filho, J. M. (2011). Brominated compounds from marine sponges of the genus *Aplysina* and a compilation of their 13C NMR spectral data. *Marine Drugs*, *9*(11), 2316–2368. https://doi.org/10.3390/md9112316

Loh, T. L., & Pawlik, J. R. (2014). Chemical defenses and resource trade-offs structure sponge communities on Caribbean coral reefs. *Proceedings of the National Academy of Sciences of the United States of America*, *111*(11), 4151–4156. https://doi.org/10.1073/pnas.1321626111

Lyles, K.V., & Eichenbaum, Z. (2018). From host heme to iron: the expanding spectrum of heme degrading enzymes used by pathogenic bacteria. *Frontiers in Cellular and Infection Microbiology*, *8*(June), 1–13. https://doi.org/10.3389/fcimb.2018.00198

Machovina, M. M., Usselman, R. J., & DuBois, J. L. (2016). Monooxygenase substrates mimic flavin to catalyze cofactorless oxygenations. *Journal of Biological Chemistry*, *291*(34), 17816–17828. https://doi.org/10.1074/jbc.M116.730051

Maffei, M., Bossi, S., Spiteller, D., Mithoefer, A., & Boland, W. (2004). Effects of feeding *Spodoptera littoralis* on lima bean leaves. I. membrane potentials, intracellular calcium variations, oral secretions, and regurgitate components. *Plant Physiology*, *134*(4), 1752–1762. https://doi.org/10.1104/pp.103.034165

Maldonado, M. (2016). Sponge waste that fuels marine oligotrophic food webs: a re-assessment of its origin and nature. *Marine Ecology*, *37*(3), 477–491. https://doi.org/10.1111/maec.12256

Man, X. Y., Finnson, K. W., Baron, M., & Philip, A. (2012). CD109, a TGF-beta co-receptor, attenuates extracellular matrix production in scleroderma skin fibroblasts. *Arthritis Research and Therapy*, *14*(3), R144. https://doi.org/10.1186/ar3877

Margadant, C., & Sonnenberg, A. (2010). Integrin–TGF-β crosstalk in fibrosis, cancer and wound healing. *EMBO Reports*, *11*(2), 97–105. https://doi.org/10.1038/embor.2009.276

Martinez, S., Yang, X., Bennett, B., & Holz, R. C. (2017). A cobalt-containing eukaryotic nitrile hydratase. *Biochimica et Biophysica Acta - Proteins and Proteomics*, *1865*(1), 107–112. https://doi.org/10.1016/j.bbapap.2016.09.013

Matthews, A. L., Noy, P. J., Reyat, J. S., & Tomlinson, M. G. (2017). Regulation of a disintegrin and metalloproteinase (ADAM) family sheddases ADAM10 and ADAM17: the emerging role of tetraspanins and rhomboids. *Platelets*, *28*(4), 333–341. https://doi.org/10.1080/09537104.2016.1184751

McClintock, J. B., & Baker, B. J. (2001). *Marine chemical ecology*. CRC press.

McKey, D. (1974). Adaptive patterns in alkaloid physiology. *The American Naturalist*, *108*(961), 305–320. https://doi.org/10.1086/282909

McKey, D. (1979). The distribution of secondary compounds within plants. *Herbivores: Their Interaction with Secondary Plant Metabolites*, 55–133.

Menzel P., Ng K.L., & Krogh A. (2016) Fast and sensitive taxonomic classification for metagenomics with Kaiju. *Nature Communications*, 7, 11257.

Moroz, L. L., & Kohn, A. B. (2016). Independent origins of neurons and synapses: Insights from ctenophores. *Philosophical Transactions of the Royal Society B: Biological Sciences*, *371*(1685). https://doi.org/10.1098/rstb.2015.0041

Murphy, L. J., Robertson, K. N., Harroun, S. G., Brosseau, C. L., Werner-Zwanziger, U., Moilanen, J., Tuononen, H. M., & Clyburne, J. A. (2014). A simple complex on the verge of breakdown: isolation of the elusive cyanoformate ion. *Science*, *344*(6179), 75–78. https://doi.org/10.1126/science.1250808

Nakamura, M., Dominguez, A. N. M., Decker, J. R., Hull, A. J., Verboon, J. M., & Parkhurst, S. M. (2018). Into the breach : how cells cope with wounds. *Open Biology*, *8*, 180135. https://doi.org/10.1098/rsob.180135

Neubauer, P. R., Widmann, C., Wibberg, D., Schroeder, L., Frese, M., Kottke, T., Kalinowski, J., Niemann, H. H., & Sewald, N. (2018). A flavin-dependent halogenase from metagenomic analysis prefers bromination over chlorination. *PLoS ONE*, *13*(5), 1–21. https://doi.org/10.1371/journal.pone.0196797

Niemann, H., Marmann, A., Lin, W., & Proksch, P. (2015). Sponge derived bromotyrosines: structural diversity through natural combinatorial chemistry. *Natural Product Communications*, *10*(1), 219–231.

Nsango, S. E., Pompon, J., Xie, T., Rademacher, A., Fraiture, M., Thoma, M., Awono-Ambene, P. H., Moyou, R. S., Morlais, I., & Levashina, E. A. (2013). AP-1/Fos-TGase2

axis mediates wounding-induced *Plasmodium falciparum* killing in *Anopheles gambiae*. *Journal of Biological Chemistry*, *288*(22), 16145–16154. https://doi.org/10.1074/jbc.M112.443267

Nylund, G. M., Weinberger, F., Rempt, M., & Pohnert, G. (2011). Metabolomic assessment of induced and activated chemical defence in the invasive red alga *Gracilaria vermiculophylla*. *PLoS ONE*, *6*(12): e29359. https://doi.org/10.1371/journal.pone.0029359

Pace, H. C., & Brenner, C. (2016). The nitrilase superfamily: classification, structure and function. *Genome Biology*, *2*(1), 1–9. https://doi.org/10.1186/gb-2001-2-1-reviews0001

Palmer, C.V., Traylor-Knowles, N. G., Willis, B. L., & Bythell, J. C. (2011). Corals use similar immune cells and wound-healing processes as those of higher organisms. *PLoS ONE*, *6*(8), 1–11. https://doi.org/10.1371/journal.pone.0023992

Palmer, C.V., Bythell, J. C., & Willis, B. L. (2012). Enzyme activity demonstrates multiple pathways of innate immunity in Indo-Pacific anthozoans. *Proceedings of the Royal Society B: Biological Sciences*, *279*(1743), 3879–3887. https://doi.org/10.1080/13504630.2013.789209

Palmer, C.V., & Traylor-Knowles, N. (2012). Towards an integrated network of coral immune mechanisms. *Proceedings of the Royal Society B: Biological Sciences*, *279*(1745), 4106–4114. https://doi.org/10.1098/rspb.2012.1477

Palmer, C. V., & Traylor-Knowles, N. (2018). Cnidarian immunity: anthozoans in the hot seat. In *Advances in Comparative Immunology*. https://doi.org/10.1007/978-3-319-76768-0_3

Park, D., Choi, S. S., & Ha, K. S. (2010). Transglutaminase 2: A multi-functional protein in multiple subcellular compartments. *Amino Acids*, *39*(3), 619–631. https://doi.org/10.1007/s00726-010-0500-z

Park, J. Y., Pillinger, M. H., & Abramson, S. B. (2006). Prostaglandin E2 synthesis and secretion: the role of PGE2 synthases. *Clinical Immunology*, *119*(3), 229–240. https://doi.org/10.1080/10407780600602374

Paulsen, C. E., Armache, J. P., Gao, Y., Cheng, Y., & Julius, D. (2015). Structure of the TRPA1 ion channel suggests regulatory mechanisms. *Nature*, *520*(7548), 511–517. https://doi.org/10.1038/nature14367

Pavia, H., & Toth, G. B. (2000). Inducible chemical resistance to herbivory in the brown seaweed Ascophyllum nodosum. *Ecology*, *81*(3), 3212–3225. https://doi.org/10.1890/0012-9658(2000)081

Pawlik, J. R. (1993). Marine invertebrate chemical defenses. *Chemical Reviews*, 1911–1922. https://doi.org/10.1021/cr00021a012

Pawlik, J. R. (2011). The chemical ecology of sponges on caribbean reefs: natural products shape natural systems. *BioScience*, *61*(11), 888–898. https://doi.org/10.1525/bio.2011.61.11.8

Pawlik, J. R., & McMurray, S. E. (2020). The emerging ecological and biogeochemical importance of sponges on coral reefs. *Annual Review of Marine Science*, *12*(1), 1–23. https://doi.org/10.1146/annurev-marine-010419-010807

Peng, J., Li, J., & Hamann, M. T. (2005). The marine bromotyrosine derivatives. In *The Alkaloids: Chemistry and Biology* (Vol. 61, pp. 59-262). Academic Press.

Perdomo-Morales, R., Montero-Alejo, V., & Perera, E. (2019). The clotting system in decapod crustaceans: history, current knowledge and what we need to know beyond the models. *Fish and Shellfish Immunology*, *84*, 204–212. https://doi.org/10.1016/j.fsi.2018.09.060

Perez, A., Wright, M. B., Maugeais, C., Braendli-Baiocco, A., Okamoto, H., Takahashi, A., Singer, T., Mueller, L., & Niesor, E. J. (2010). MARCO, a macrophage scavenger receptor highly expressed in rodents, mediates dalcetrapib-induced uptake of lipids by rat and mouse macrophages. *Toxicology in Vitro*, *24*(3), 745–750. https://doi.org/10.1016/j.tiv.2010.01.002

Pita, L., Hoeppner, M. P., Ribes, M., & Hentschel, U. (2018). Differential expression of immune receptors in two marine sponges upon exposure to microbial-associated molecular patterns. *Scientific Reports*, *8*(1), 16081. https://doi.org/10.1038/s41598-018-34330-w

Proksch, P. (1994). Defensive role for secondary metabolites from marine sponges and sponge-feeding nudibranchs. *Toxicon*, *32*, 639–655. https://doi.org/10.1016/0041-0101(94)90334-4

Putz, A., Kloeppel, A., Pfannkuchen, M., Briimmer, F., & Proksch, P. (2009). Depth-related alkaloid variation in mediterranean *Aplysina* sponges. *Zeitschrift Fur Naturforschung - Section C Journal of Biosciences*, *64*, 279–287.

Puyana, M., Fenical, W., & Pawlik, J. R. (2003). Are there activated chemical defenses in sponges of the genus *Aplysina* from the Caribbean? *Marine Ecology Progress Series*, *246*, 127–135. https://doi.org/10.3354/meps246127

R Core Team (2019). R: A language and environment for statistical computing. R Foundation for Statistical Computing, Vienna, Austria. http://www.R-project.org/.

RStudio Team (2019). RStudio: integrated development for R. RStudio, Inc., Boston, MA. http://www.rstudio.com/.

Ramírez-Gómez, F., & García-Arrarás, J. E. (2010). Echinoderm immunity. *Invertebrate Survival Journal*, *7*(2), 211–220.

Randall, J. E., & Hartman, W. D. (1968). Sponge-feeding fishes of the West Indies. *Marine Biology*, *1*(3), 216–225. https://doi.org/10.1007/BF00347115

Reid, P. J. W., Matveev, E., McClymont, A., Posfai, D., Hill, A. L., & Leys, S. P. (2018). Wnt signaling and polarity in freshwater sponges. *BMC Evolutionary Biology*, *18*(1), 12. https://doi.org/10.1186/s12862-018-1118-0

Reiss, K., & Bhakdi, S. (2017). The plasma membrane: Penultimate regulator of ADAM sheddase function. *Biochimica et Biophysica Acta - Molecular Cell Research*, *1864*(11), 2082–2087. https://doi.org/10.1016/j.bbamcr.2017.06.006

Reiss, K., & Saftig, P. (2009). The “A Disintegrin And Metalloprotease” (ADAM) family of sheddases: physiological and cellular functions. *Seminars in Cell and Developmental Biology*, *20*(2), 126–137. https://doi.org/10.1016/j.semcdb.2008.11.002

Rhoades, D. F. (1979). Evolution of plant chemical defense against herbivores. In *Herbivores: their interaction with secondary plant metabolites* (pp. 3–54).

Richardson, V. R., Cordell, P., Standeven, K. F., & Carter, A. M. (2013). Substrates of Factor XIII-A: roles in thrombosis and wound healing. *Clinical Science*, *124*(3), 123–137. https://doi.org/10.1042/cs20120233

Rodrigues, M., Kosaric, N., Bonham, C. A., & Gurtner, G. C. (2019). Wound healing: a cellular perspective. *Physiological Reviews*, *99*(1), 665–706. https://doi.org/10.1152/physrev.00067.2017

Rohde, S., Molis, M., & Wahl, M. (2004). Regulation of anti-herbivore defence by *Fucus vesiculosus* ln response to varlous cues. *Journal of Ecology*, *92*(6), 1011–1018.

Rohde, S., Nietzer, S., & Schupp, P. J. (2015). Prevalence and mechanisms of dynamic chemical defenses in tropical sponges. *PLoS ONE*, *10*(7), 1–19. https://doi.org/10.1371/journal.pone.0132236

Rohde, S., & Schupp, P. (2018). Spatial and temporal variability in sponge chemical defense. In *Chemical Ecology:The Ecological Impacts of Marine Natural Products* (pp. 373–395). Taylor & Francis.

Romero, M. M. G., McCathie, G., Jankun, P., & Roehl, H. H. (2018). Damage-induced reactive oxygen species enable zebrafish tail regeneration by repositioning of Hedgehog expressing cells. *Nature Communications*, *9*(1), 4010. https://doi.org/10.1038/s41467-018-06460-2

Sacristán-Soriano, O., Banaigs, B., Casamayor, E. O., & Becerro, M. A. (2011). Exploring the links between natural products and bacterial assemblages in the sponge *Aplysina aerophoba*. *Applied and Environmental Microbiology*, *77*(3), 862–870. https://doi.org/10.1128/aem.00100-10

Saint-Pol, J., Billard, M., Dornier, E., Eschenbrenner, E., Danglot, L., Boucheix, C., Charrin, S., & Rubinstein, E. (2017). New insights into the tetraspanin tspan5 using novel monoclonal antibodies. *Journal of Biological Chemistry*, *292*(23), 9551–9566. https://doi.org/10.1074/jbc.M116.765669

San Miguel-Ruiz, J. E., & García-Arrarás, J. E. (2007). Common cellular events occur during wound healing and organ regeneration in the sea cucumber *Holothuria glaberrima*. *BMC Developmental Biology*, *7*, 1–19. https://doi.org/10.1186/1471-213X-7-115

Schindelin, J., Arganda-carreras, I., Frise, E., Kaynig, V., Pietzsch, T., Preibisch, S., Rueden, C., Saalfeld, S., Schmid, B., Tinevez, J., White, D. J., Hartenstein, V., Tomancak, P., & Cardona, A. (2019). Fiji - an open source platform for biological image analysis. *Nature Methods*, *9*(7). https://doi.org/10.1038/nmeth.2019

Schneider, C. A., Rasband, W. S., & Eliceiri, K. W. (2012). NIH Image to ImageJ: 25 years of image analysis. *Nature Methods*, *9*(7), 671–675. https://doi.org/10.1038/nmeth.2089

Schuman, M. C., & Baldwin, I. T. (2016). The layers of plant responses to insect herbivores. *Annual Review of Entomology*, *61*(1), 373–394. https://doi.org/10.1146/annurev-ento-010715-023851

Seipold, L., Altmeppen, H., Koudelka, T., Tholey, A., Kasparek, P., Sedlacek, R., Schweizer, M., Baer, J., Mikhaylova, M., Glatzel, M., & Saftig, P. (2018). *In vivo* regulation of the A disintegrin and metalloproteinase 10 (ADAM10) by the tetraspanin 15. *Cellular and Molecular Life Sciences*, *75*(17), 3251–3267. https://doi.org/10.1007/s00018-018-2791-2

Sentuerk, A., Pfennig, S., Weiss, A., Burk, K., & Acker-Palmer, A. (2011). Ephrin Bs are essential components of the Reelin pathway to regulate neuronal migration. *Nature*, *472*(7343), 356–360. https://doi.org/10.1038/nature09874

Serbulea, V., DeWeese, D., & Leitinger, N. (2017). The effect of oxidized phospholipids on phenotypic polarization and function of macrophages. *Free Radical Biology and Medicine*, *111*, 156–168. https://doi.org/10.1016/j.freeradbiomed.2017.02.035

Shady, N. H., Fouad, M. A., Kamel, M. S., Schirmeister, T., & Abdelmohsen, U. R. (2019). Natural product repertoire of the genus *Amphimedon*. *Marine Drugs*, *17*(1). https://doi.org/10.3390/md17010019

Shanks, A. L., & Wright, W. G. (1986). Adding teeth to wave action: the destructive effects of wave-borne rocks on intertidal organisms. *Oecologia*, *69*(3), 420–428. https://doi.org/10.1007/BF00377065

Simão, F. A., Waterhouse, R. M., Ioannidis, P., Kriventseva, E.V., & Zdobnov, E. M. (2015). BUSCO: Assessing genome assembly and annotation completeness with single-copy orthologs. *Bioinformatics*, *31*(19), 3210–3212. https://doi.org/10.1093/bioinformatics/btv351

Simpson, T. L. (1984). *The cell biology of sponges*. Springer Science & Business Media.

Smith, L. C., & Hildemann, W. H. (1986). Allograft rejection, autograft fusion and inflammatory responses to injury in *Callyspongia diffusa* (Porifera; Demospongia). *Proceedings of the Royal Society of London. Series B. Biological Sciences*, *226*(1245), 445–464.

Smith-Unna, R., Boursnell, C., Patro, R., Hibberd, J. M., & Kelly, S. (2016). TransRate: reference-free quality assessment of de novo transcriptome assemblies. *Genome Research*, *26*(8), 1134–1144. https://doi.org/10.1101/gr.196469.115

Song, Y., Wagner, B. A., Lehmler, H. J., & Buettner, G. R. (2008). Semiquinone radicals from oxygenated polychlorinated biphenyls: electron paramagnetic resonance studies. *Chemical Research in Toxicology*, *21*(7), 1359–1367. https://doi.org/10.1021/tx8000175

Sonnemann, K. J., & Bement, W. M. (2011). Wound repair: toward understanding and integration of single-cell and multicellular wound responses. *Annual Review of Cell and Developmental Biology*, *27*, 237–263. https://doi.org/10.1146/annurev-cellbio-092910-154251

Stewart, F. J., Ottesen, E. A., & Delong, E. F. (2010). Development and quantitative analyses of a universal rRNA-subtraction protocol for microbial metatranscriptomics. *ISME Journal*, *4*(7), 896–907. https://doi.org/10.1038/ismej.2010.18

Sui, Y., Xu, J., Rios-pilier, J., & Zhou, C. (2011). Deficiency of PXR decreases atherosclerosis in apoE-deficient mice. *Journal of Lipid Research*, *52*(9), 1652–1659. https://doi.org/10.1194/jlr.M017376

Supek, F., Bošnjak, M., Škunca, N., & Šmuc, T. (2011). Revigo summarizes and visualizes long lists of gene ontology terms. *PLoS ONE*, *6*(7). https://doi.org/10.1371/journal.pone.0021800

Taylor-Clark, T. E., Undem, B. J., MacGlashan, D. W., Ghatta, S., Carr, M. J., & McAlexander, M. A. (2008). Prostaglandin-induced activation of nociceptive neurons via direct interaction with transient receptor potential A1 (TRPA1). *Molecular Pharmacology*, *73*(2), 274–281. https://doi.org/10.1124/mol.107.040832

Teeyapant, R., & Proksch, P. (1993). Biotransformation of the brominated compounds in the marine sponge *Verongia aerophoba*: evidence for an induced chemical defense? *Naturwissenschaften*, *80*, 369–370.

Teeyapant, R., Kreis, P., Wray, V., Witte, L., & Proksch, P. (1993a). Brominated secondary compounds from the marine sponge *Verongia aerophoba* and the sponge feeding gastropod *Tylodina perversa*. *Zeitschrift Fuer Naturforschung*, *48*c, 640–644.

Teeyapant, R., Woerdenbag, H. J., Kreis, P., Hacker, J., Wray, V., Witte, L., & Proksch, P. (1993b). Antibiotic and cytotoxic activity of brominated compounds from the marine sponge *Verongia aerophoba*. *Zeitschrift Fuer Naturforschung*, *48c*, 939–945. https://doi.org/10.1515/znc-1993-11-1218

Ternon, E., Zarate, L., Chenesseau, S., Croué, J., Dumollard, R., Suzuki, M. T., & Thomas, O. P. (2016). Spherulization as a process for the exudation of chemical cues by the encrusting sponge *C. crambe*. *Scientific Reports*, *6*, 29474. https://doi.org/10.1038/srep29474

The Gene Ontology Consortium: Ashburner, M., Ball, C. A., Blake, J. A., Botstein, D., Butler, H., Cherry, J. M., Davis, A. P., Dolinski, K., Dwight, S. S., Eppig, J. T., Harris, M. A., Hill, D. P., Issel-Tarver, L., Kasarskis, A., Lewis, S., Matese, J. C., Richardson, J. E.,

Ringwald, M., Rubin, G. M., & Sherlock, G. (2000). Gene Ontology: tool for the unification of biology. *Nature Genetics*, *25*(1), 25–29. https://doi.org/10.1038/75556

The Gene Ontology Resource (2018). 20 years and still GOing strong. *Nucleic Acids Research*, *47*(D1), D330–D338. https://doi.org/10.1093/nar/gky1055

The UniProt Consortium (2019) UniProt: a worldwide hub of protein knowledge. Nucleic Acids Research. 47: 506-515

Thompson, J. E., Barrow, K. D., & Faulkner, D. J. (1983). Localization of two brominated metabolites, aerothionin and homoaerothionin, in spherulous cells of the marine sponge *Aplysina fistularis* (=*Verongia thiona*). *Acta Zoologica*, *64*(4), 199–210. https://doi.org/10.1111/j.1463-6395.1983.tb00801.x

Thoms, C., & Schupp, P. J. (2007). Chemical defense strategies in sponges: a review. *Porifera Research: Biodiversity, Innovation and Sustainability*, 627–637.

Thoms, C., & Schupp, P. J. (2008). Activated chemical defense in marine sponges-a case study on *Aplysinella rhax*. *Journal of Chemical Ecology*, *34*(9), 1242–1252. https://doi.org/10.1007/s10886-008-9518-z

Thoms, C., Ebel, R., Hentschel, U., & Proksch, P. (2003). Sequestration of dietary alkaloids by the spongivorous marine mollusc *Tylodina perversa*. *Zeitschrift Fur Naturforschung - Section C Journal of Biosciences*, *58*(5–6), 426–432.

Thoms, C., Wolff, M., Padmakumar, K., Ebel, R., & Proksch, P. (2004). Chemical defense of mediterranean sponges *Aplysina cavernicola* and *Aplysina aerophoba*. *Zeitschrift Fur Naturforschung - Section C Journal of Biosciences*, *59*(1–2), 113–122.

Thoms, C., Ebel, R., & Proksch, P. (2006a). Sequestration and possible role of dietary alkaloids in the sponge-feeding mollusk *Tylodina perversa*. *Progress in Molecular and Subcellular Biology*, *43*, 261–275.

Thoms, C., Ebel, R., & Proksch, P. (2006b). Activated chemical defense in *Aplysina* sponges revisited. *Journal of Chemical Ecology*, *32*(1), 97–123. https://doi.org/10.1007/s10886-006-9355-x

Toggweiler, J., Willecke, M., & Basler, K. (2016). The transcription factor Ets21C drives tumor growth by cooperating with AP-1. *Scientific Reports*, *6*, 1–10. https://doi.org/10.1038/srep34725

Tolentino, P. J., DeFord, S. M., Notterpek, L., Glenn, C. C., Pike, B. R., Wang, K. K. W., & Hayes, R. L. (2002). Up-regulation of tissue-type transglutaminase after traumatic brain injury. *Journal of Neurochemistry*, *80*(4), 579–588. https://doi.org/10.1046/j.0022-3042.2001.00726.x.

Toth, G. B., & Pavia, H. (2007). Induced herbivore resistance in seaweeds: a meta-analysis. *Journal of Ecology*, *95*(3), 425–434. https://doi.org/10.1111/j.1365-2745.2007.01224.x

Turon, X., Becerro, M. A., & Uriz, M. J. (2000). Distribution of brominated compounds within the sponge *Aplysina aerophoba*: Coupling of X-ray microanalysis with cryofixation

techniques. *Cell and Tissue Research*, *301*(2), 311–322. https://doi.org/10.1007/s004410000233

Tzin, V., & Galili, G. (2010). New Insights into the shikimate and aromatic amino acids biosynthesis pathways in plants. *Molecular Plant*, *3*(6), 956–972. https://doi.org/10.1093/mp/ssq048

Ueberlein, S., Machill, S., Schupp, P. J., & Brunner, E. (2017). Determination of the halogenated skeleton constituents of the marine demosponge *Ianthella basta*. *Marine Drugs*, *15*(2). https://doi.org/10.3390/md15020034

Uriz, M. J., Turon, X., Becerro, M. A., & Galera, J. (1996a). Feeding deterrence in sponges. The role of toxicity, physical defenses, energetic contents, and life-history stage. *Journal of Experimental Marine Biology and Ecology*, *205*(1–2), 187–204. https://doi.org/10.1016/S0022-0981(96)02609-3

Uriz, M. J., Becerro, M. A., Tur, J. M., & Turon, X. (1996b). Location of toxicity within the Mediterranean sponge *Crambe crambe* (Demospongiae: Poecilosclerida). *Marine Biology*, *124*(4), 583–590. https://doi.org/10.1007/BF00351039

Utreras, E., Keller, J., Terse, A., Prochazkova, M., Iadarola, M. J., & Kulkarni, A. B. (2012). Transforming growth factor-β1 regulates Cdk5 activity in primary sensory neurons. *Journal of Biological Chemistry*, *287*(20), 16917–16929. https://doi.org/10.1074/jbc.M111.329979

Utreras, E., Prochazkova, M., Terse, A., Gross, J., Keller, J., Iadarola, M. J., & Kulkarni, A. B. (2013). TGF-β1 sensitizes TRPV1 through Cdk5 signaling in odontoblast-like cells. *Molecular Pain*, *9*(1), 1. https://doi.org/10.1186/1744-8069-9-24

Vacelet, J. (1967). Les cellules a inclusions de leponge cornee *Verongia cavernicola* vacelet. *Journal of Microscopy-Oxford*, 6(2), 237–240.

van der Poll, T., & Herwald, H. (2014). The coagulation system and its function in early immune defense. *Thrombosis and Haemostasis*, *112*(10), 640–648. https://doi.org/10.1160/TH14-01-0053

Van Soest, R. W. M., Boury-Esnault, N., Vacelet, J., Dohrmann, M., Erpenbeck, D., DeVoogd, N. J., Santodomingo, N., Vanhoorne, B., Kelly, M., & Hooper, J. N. A. (2012). Global diversity of sponges (Porifera). *PLoS ONE*, *7*(4), e35105. https://doi.org/10.1371/journal.pone.0035105

Van Soest, R.W.M., Boury-Esnault, N., Hooper, J.N.A., Ruetzler, K., de Voogd, N.J., Alvarez, B., Hajdu, E., Pisera, A.B., Manconi, R., Schoenberg, C., Klautau, M., Kelly, M., Vacelet, J., Dohrmann, M., Díaz, M.-C., Cárdenas, P., Carballo, J.L., Ríos, P., Downey, R., & Morrow, C.C. (2019). World Porifera Database. http://www.marinespecies.org/porifera

Vazzana, M., Siragusa, T., Arizza, V., Buscaino, G., & Celi, M. (2015). Cellular responses and HSP70 expression during wound healing in *Holothuria tubulosa* (Gmelin, 1788). *Fish and Shellfish Immunology*, *42*(2), 306–315. https://doi.org/10.1016/j.fsi.2014.11.010

Verderio, E. A. ., Johnson, T. ., & Griffin, M. (2005). Transglutaminases in Wound Healing. In *Transglutaminases* (Vol. 38, pp. 89–114). Karger Publishers.

Waterhouse, R. M., Seppey, M., Simao, F. A., Manni, M., Ioannidis, P., Klioutchnikov, G., Kriventseva, E.V., & Zdobnov, E. M. (2018). BUSCO applications from quality assessments to gene prediction and phylogenomics. *Molecular Biology and Evolution*, *35*(3), 543–548. https://doi.org/10.1093/molbev/msx319

Wang, J., Zhao, Y., Ray, I., & Song, M. (2016a). Transcriptome responses in alfalfa associated with tolerance to intensive animal grazing. *Scientific Reports*, *6*(1), 19438. https://doi.org/10.1038/srep19438

Wang, M., Toda, K., & Maeda, H. A. (2016b). Biochemical properties and subcellular localization of tyrosine aminotransferases in *Arabidopsis thaliana*. *Phytochemistry*, *132*, 16–25. https://doi.org/10.1016/j.phytochem.2016.09.007

Wang, Y., Li, J., & Liu, A. (2017). Oxygen activation by mononuclear nonheme iron dioxygenases involved in the degradation of aromatics. *JBIC Journal of Biological Inorganic Chemistry*, *22*(2–3), 395–405. https://doi.org/10.1007/s00775-017-1436-5

Weiss, B., Ebel, R., Elbrächter, M., Kirchner, M., & Proksch, P. (1996). Defense metabolites from the marine sponge *Verongia aerophoba*. *Biochemical Systematics and Ecology*, *24*(1), 1-12.

White, M. D., & Flashman, E. (2016). Catalytic strategies of the non-heme iron dependent oxygenases and their roles in plant biology. *Current Opinion in Chemical Biology*, *31*, 126–135. https://doi.org/10.1016/j.cbpa.2016.02.017

Wilkie, I. C., Parma, L., Bonasoro, F., Bavestrello, G., Cerrano, C., & Carnevali, M. D. C. (2006). Mechanical adaptability of a sponge extracellular matrix: evidence for cellular control of mesohyl stiffness in *Chondrosia reniformis* Nardo. *Journal of Experimental Biology*, *209*(22), 4436–4443. https://doi.org/10.1242/jeb.02527

Willan, R. C. (1984). A review of diets in the Notaspidea (Mollusca: Opisthobranchia). *Journal of the Malacological Society of Australia*, *6*(3–4), 125–142. https://doi.org/10.1080/00852988.1984.10673965

Wulff, J. L. (2006). Ecological interactions of marine sponges. *Canadian Journal of Zoology*, *84*, 146–166. https://doi.org/10.1139/z06-019

Yadav, K., Yadav, A., Priyanka, Pandey, V. P., & Dwivedi, U. N. (2019). Protein misfolding diseases and therapeutic approaches. *Current Protein & Peptide Science*, *20*, 1–21. https://doi.org/10.2174/1389203720666190610092840

Yamaguchi, H., Kuroda, K., Sugitani, M., Takayama, T., Hasegawa, K., & Esumi, M. (2017). Transglutaminase 2 is upregulated in primary hepatocellular carcinoma with early recurrence as determined by proteomic profiles. *International Journal of Oncology*, *50*(5), 1749–1759. https://doi.org/10.3892/ijo.2017.3917

Yan, Z., Li, J., Huebert, N., Caldwell, G. W., Du, Y., & Zhong, H. (2005). Detection of a novel reactive metabolite of diclofenac: Evidence for CYP2C9-mediated bioactivation via arene oxides. *Drug Metabolism and Disposition*, *33*(6), 706–713. https://doi.org/10.1124/dmd.104.003095

Yarnold, J. E., Hamilton, B. R., Welsh, D. T., Pool, G. F., Venter, D. J., & Carroll, A. R. (2012). High resolution spatial mapping of brominated pyrrole-2-aminoimidazole alkaloids distributions in the marine sponge *Stylissa flabellata* via MALDI-mass spectrometry imaging. *Molecular BioSystems*, *8*(9), 2249–2259. https://doi.org/10.1039/c2mb25152c

Yin, Z., Zhu, M., Davidson, E. H., Bottjer, D. J., Zhao, F., & Tafforeau, P. (2015). Sponge grade body fossil with cellular resolution dating 60 Myr before the Cambrian. *Proceedings of the National Academy of Sciences*, 201414577. https://doi.org/10.1073/pnas.1414577112

Zhang, Y., Feng, X. H., & Derynck, R. (1998). Smad3 and Smad4 cooperate with c-Jun/c-Fos to mediate TFG-beta-induced transcription. *Nature*, *394*(6696), 909–913.

Zhu, L., Yu, H., Xu, Z., Jiang, X., Lin, L., & Wang, R. (2014). Copper-catalyzed oxyazidation of unactivated alkenes: A facile synthesis of isoxazolines featuring an azido substituent. *Organic Letters*, *16*(6), 1562–1565. https://doi.org/10.1021/ol403687k

Zoeller, M. (2009). Tetraspanins: Push and pull in suppressing and promoting metastasis. *Nature Reviews Cancer*, *9*(1), 40–55. https://doi.org/10.1038/nrc2543

7. Curriculum Vitae

NAME

EMAIL

Yu-Chen Wu (born in Taipei city, Taiwan) yuchen.wu.m@gmail.com

EDUCATION

10/2015–current: Promotion at the research group Marine Symbioses, GEOMAR, Kiel, Germany. Supervisor: Prof. Dr. Ute Hentschel Humeida and Dr. Lucía Pita Galán

10/2011–03/2015: Master of Science in Biology at the research group Biochemical Ecology and Molecular Evolution, Kiel University, Kiel, Germany. Supervisor: Prof. Dr. Dietrich Ober

RESEARCH INTERESTS

Environmental stresses can influence species response. I am particularly interested in species-specific interactions. My PhD thesis focused on the interaction between two animals: the sponge *Aplysina aerophoba* (Phylum Porifera: Class Demospongiae) and the sea slug *Tylodina perversa* (Phylum Mollusca: Class Opistobranchia). I aimed to understand the cellular, chemical, and molecular response of the sponge *A. aerophoba* to sea slug grazing, by ways of modern techniques: microscopic technologies, MALDI-imaging mass spectrometry, and RNA-Seq-based transcriptomics, respectively. A specialized cell population – spherulous cells – in genus *Apylsina* harbors bioactive secondary metabolites. My research goals were to understand sponge response in facing specialist consumers by studying testable hypotheses and provide insights into underlying mechanisms. I hypothesized that grazing can induce signaling pathways for a recruitment of spherulous cells with secondary metabolites. An accumulation of spherulous cells and brominated alkaloids at grazed surface, as well as an activation of genes related with cell migration were identified in the course of my PhD thesis. These allow us to explore broader themes such as inflammatory response, immune response, wound sealing, and regeneration in basal animal phyla.

PUBLICATIONS

Helber, S. B., Steinert, G., **Wu, Y. C.**, Rohde, S., Hentschel, U., Muhando, C. A., & Schupp, P. J. (2019). Sponges from Zanzibar host diverse prokaryotic communities with potential for natural product synthesis. *FEMS microbiology ecol*ogy, 95(4), fiz026.

Rubin-Blum, M., Antony, C. P., Sayavedra, L., Martínez-Pérez, C., Birgel, D., Peckmann, J., **Wu, Y. C.**, Cardenas, P., MacDonald, I., Marcon, Y., Sahling, H., Hentschel, U., & Dubilier, N. (2019). Fueled by methane: deep-sea sponges from asphalt seeps gain their nutrition from methane-oxidizing symbionts. *The ISME journal*, 13(5), 1209.

Moitinho-Silva, L., Steinert, G., Nielsen, S., Hardoim, C. C., **Wu, Y. C.**, McCormack, G. P., López-Legentil, S., Marchant, R., Webster, N., Thomas, T., & Hentschel, U. (2017). Predicting the HMA-LMA status in marine sponges by machine learning. *Frontiers in microbiology*, 8, 752.

PRESENTATIONS

Poster: **Wu, Y. C.**, García-Altares, M., Ribes, M., Hentschel, U., & Pita, L.: The response of the Mediterranean sponge *Aplysina aerophoba* to grazing by the sea slug *Tylodina perversa*. Life sciences student symposium. Kiel, Germany, 2018

Talk: **Wu, Y. C.**, García-Altares, M., Ribes, M., Hentschel, U., & Pita, L.: The response of the Mediterranean sponge *Aplysina aerophoba* to grazing by the sea slug *Tylodina perversa*. YOUMARES 9 conference for young marine researchers. Oldenburg, Germany, 2018

Talk: **Wu, Y. C.**, Pita, L., & Hentschel, U. (2017) Unravelling the interactions between the sponge *Aplysina aerophoba* and the snail *Tylodina perversa*. NextGen@Helmholtz conference. Kiel, Germany, 2017

FIELD WORK

Aquarium experiments in the Institute of Marine Sciences (ICM-CSIC, Barcelona, Spain), 2016 and 2017

8. Appendixes

8.1 Appendix A: Relative position of sample collection.

Example of grazed specimens collected at 1d-2016 (**2016**) and 1d-2017 (**2017**) showing their osculum and grazed scar (**Photographically recording**), as well as their relative sampling position for microscopy, MALDI-imaging MS, and RNA-Seq (**Sampling position**). Yellow-labeled area denotes a grazed scar.

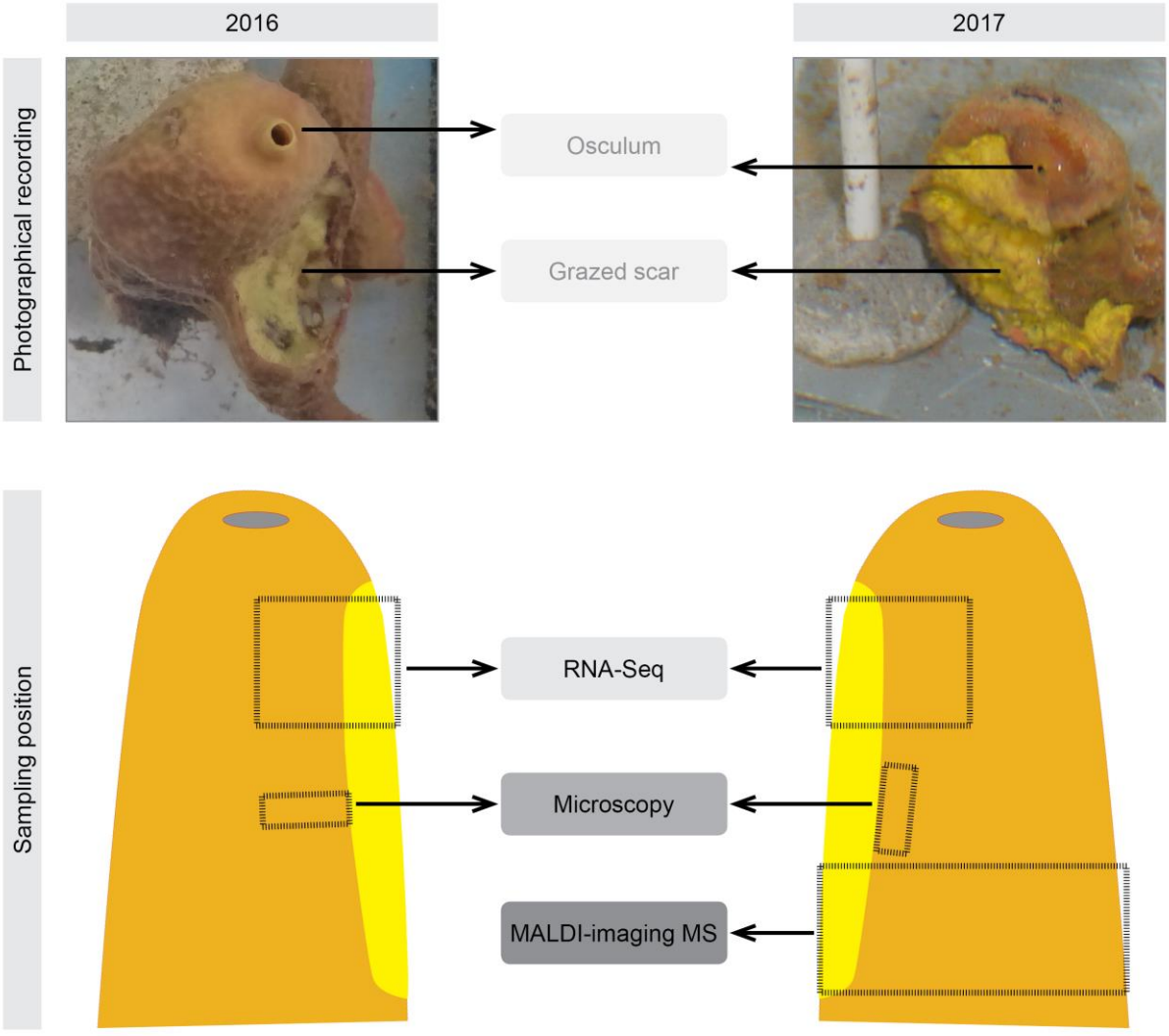

Figure Appendix A. Relative position of sample collection.

8.2 Appendix B: Optimization of the MALDI-imaging MS protocol and expanded investigations on the spatial distribution of brominated compounds by multivariate statistics

8.2.1 Appendix B-1: Sample collection in the field

Three individuals of *Aplysina aerophoba* being grazed by *Tylodina perversa* and presenting a clear grazed scar were sampled by scuba diving in February 2017 in the north western Mediterranean coast of Spain (42.1145863 N, 3.168486 E) at a depth between 2 to 10 m. In addition, one sample without presence of *T. perversa* or scars was taken as control. The tissue (ca. 1 cm^3) of each sample was collected directly in the field, wrapped individually in aluminum with a clear annotation of the location of the grazed side, stored immediately at 4 °C, and transported to the ZAE at the ICM-CSIC in Barcelona. All 4 field sponge samples were then snap-frozen in liquid nitrogen, and immediately stored at -20 °C. The following sample preparation was performed by Yu-Chen Wu and the analysis was performed by María García-Altares.

8.2.2 Appendix B-2: Optimizing sample preparation for MALDI-imaging MS

The sponge samples collected directly from the field (three grazed and one control) and the specimens corresponding to 2 sponge individuals from 1d-2017 experiment were used for optimizing the sample preparation for MALDI-imaging MS after cryosectioning. To remove embedding medium on ITO glass slides for further MALDI-imaging MS measurement, Yarnold *et al.* (2012) performed a wash step with Milli-Q water. However, in the course of my PhD thesis, the wash step led to a morphological alteration of all sample sections, which caused an artifact in distribution of compounds (**Figure Appendix B.1, A**). Therefore, in order to remove embedding medium while maintaining sample morphology, I tested a double-sided adhesive conductive carbon tape (Plano, Germany) as described by Goodwin *et al.* (2012) (abbreviated as tape-attached method).

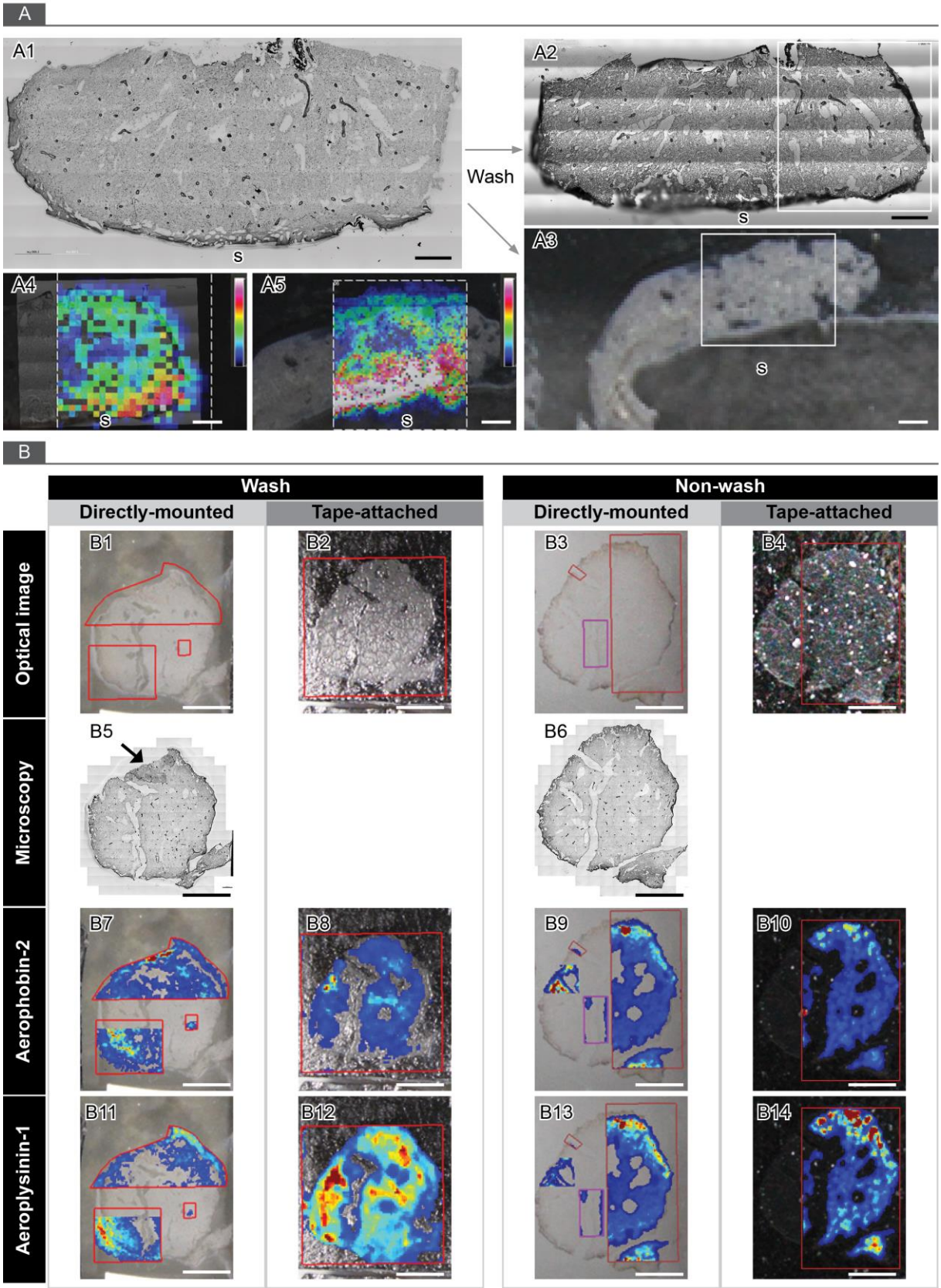

Figure Appendix B.1. Optimizing sample preparation for MALDI-imaging MS by directly-mounted method and non-wash step. (**A**) Example of wash-effect. Three almost-identical sections (**A1-A3**) from the non-grazed sample collected from the field were mounted onto slides. Compared with non-washed (**A1**), edges of sections became floating after 1x wash (**A2**) and the morphology altered completely after 3x wash (**A3**). Chemical patterns of aeroplysinin-1 in both morphologically-altered sections confirmed a great difference of aeroplysinin-1 intensity at the surface (**s**) between these two morphologically-altered sections, and for A3 delocalization of the analyte (i.e., aeroplysinin-

1 was found outside of the tissue in the surroundings of the sample, since the compound had partially dissolved in water and migrated to the borders of the tissue) was observed. (**A4** corresponding to the insert in A2; **A5** corresponding to the insert in A3). Scale bar= 1 mm. (**B**) Four almost-identical sections from a control specimen collected at 1d-2017 were directly-mounted (**B1, B3**) or tape-attached (**B2, B4**) onto slides. 1x wash was applied to the first slide (**B1** and **B2**), while the second slide (**B3** and **B4**) was not washed. For each section, optical image (**Optical image**), microscopic images (**Microscopy**), and relative intensity of aerophobin-2 (**Aerophobin-2**) as well as aeroplysinin-1 (**Aeroplysinin-1**) are shown. A folded edge was observed clearly under microscope of washed and directly-mounted section (**B5, black arrow**) compared to other three sections (**B2**, **B4,** and **B6**). Scale bar= 0.5 cm. The relative intensity of each compound is depicted in a color scale (blue as low intensity, red as high intensity).

For comparison, I tested the preparation of sample by thaw-mounting onto the same ITO glass slide without the conductive carbon tape (abbreviated as directly-mounted method). A second ITO glass slide was prepared with the same methodology (one section attached and one directly-mounted) and was used to test the protocol without the wash step (abbreviated as non-wash) (**Figure Appendix B.1, B**). The results showed that (i) the directly-mounted method provided an advantage for taking microscopic images compared to the tape-attached method, but caused alterations in the morphology of the tissue after washing, and (ii) the non-wash step provided a more consistent pattern of chemical distribution between both directly-mounted and tape-attached methods compared to the wash step. Thus, for my PhD thesis, I applied direct-mounting of sponge sections onto ITO glass slides which were not washed with water. Washing steps are usually performed to reduce potential signal inhibition caused by embedding medium, but in the course of my PhD thesis the *m/z* signals generated by the embedding medium (a polymeric pattern between 1000 to approximately 3000 Da) did not interfere with my range of interest (200 to 800 Da). The embedding medium signals were excluded when performing multivariate statistics.

8.2.3 Appendix B-3: Choosing the suitable matrix solvent

A 1:1 mixture of 2,5-dihydroxybenzoic acid and α-cyano-4-hydroxy-cinnamic acid (Bruker Daltonics) was used as matrix for the measurements, since it was able to successfully ionize both aerophobin-2 and aeroplysinin-1 reference compounds (Santa Cruz Biotechnology, Germany). Two different matrix solvents for compound ionization that differed in their water content on almost-identical consecutive tissue

sections were tested: (i) water-containing matrix (20 mg/mL of 1:1 mixture of 2,5-dihydroxybenzoic acid and α-cyano-4-hydroxy-cinnamic acid in acetonitrile/methanol/water (70:25:5, v/v/v)), or (ii) non-water-containing matrix (20 mg/mL of 1:1 mixture of 2,5-dihydroxybenzoic acid and α-cyano-4-hydroxy-cinnamic acid in acetonitrile/methanol (70:30, v/v)). The influence of water in the matrix solvent had an important effect in the ionization efficiency of aeroplysinin-1 and aerophobin-2, most like due to their different polarities (**Figure Appendix B.2**). Since the solvent with 5 % water inhibited the ionization of aerophobin-2, the non-water-containing matrix was opted to perform MALDI-imaging MS analysis.

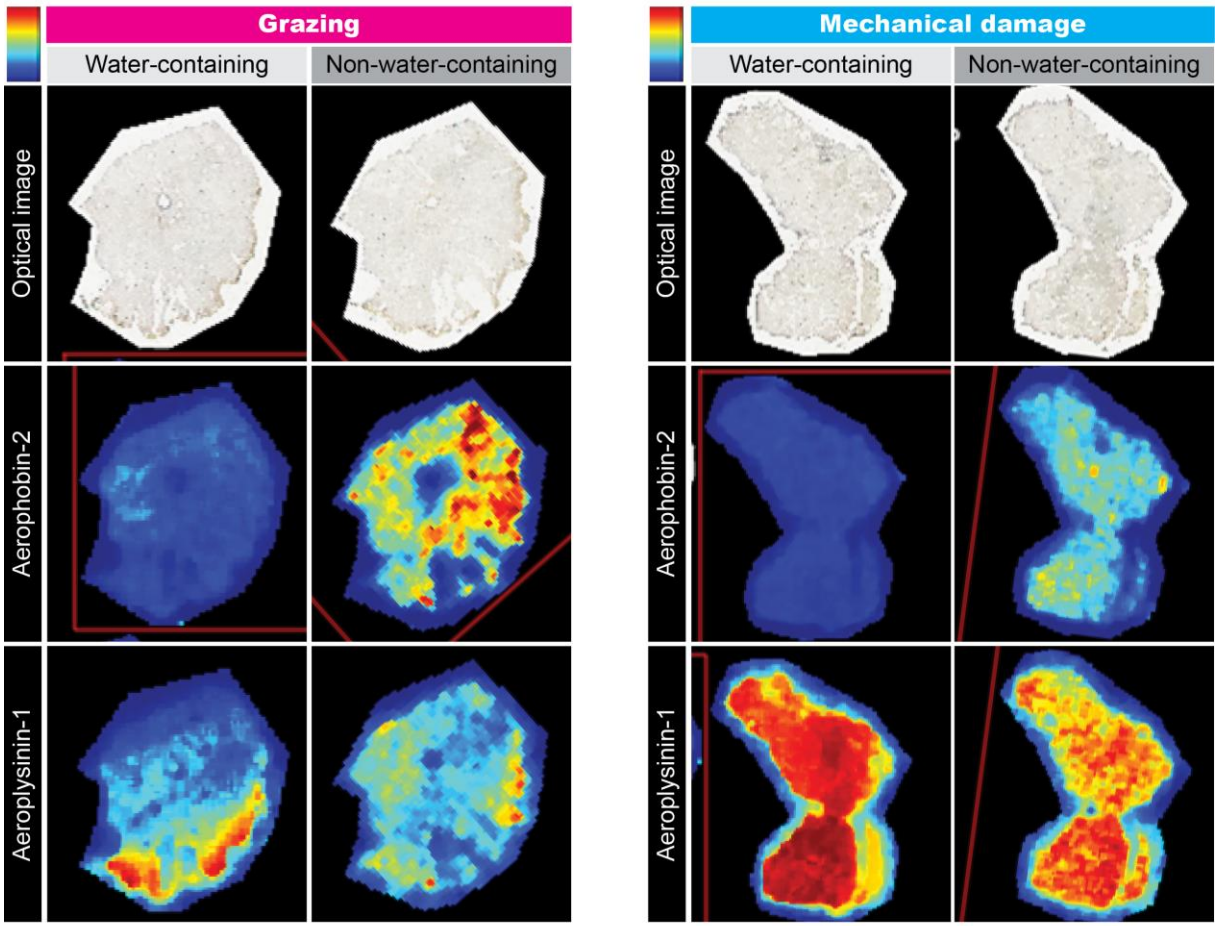

Figure Appendix B.2. Optimizing MALDI-imaging MS protocol and selection of non-water-containing matrix solvent. For each treatment (**Grazing** or **Mechanical damage**), two almost-identical consecutive sections were prepared on the same ITO glass slide (**Optical image**). The 2D-MALDI-image of aerophobin-2 (**Aerophobin-2**) and aeroplyinin-1 (**Aeroplysinin-1**) was showed by using different matrix solvents (**Water-containing** vs **Non-water-containing**), respectively. Red color represents a relatively higher intensity, while blue color represents a relatively lower intensity of each compound.

8.2.4 Appendix B-4: Raster size determination

A balance between the raster size (spatial resolution) and the signal intensity (sensitivity) is one of main technical challenges for the development of MALDI-imaging MS protocols (Hansen *et al.*, 2019). Longer measurement times are required for big sections and/or for high spatial resolution. For example, an area of 33 mm^2 at a raster size of 20 µm would take more than 46 hours to be measured, whereas the same area at a raster size of 200 µm in approximately 30 min with the instrument and protocol used in my PhD thesis. Long measurement times may compromise sensitivity and replicability of results due to loss of signal, caused by matrix evaporation and residues accumulating on the P2 plate in the ion source. Therefore, the balance between raster size (i.e., resolution) and measuring time should be chosen to avoid sensitivity problems. Samples for this study were measured at a MALDI-imaging MS raster size ranging from 20 x 20 to 300 x 300 $µm^2$ according to the total measured area of sponge tissues on each ITO glass slide to avoid a measurement times longer than 5 hours.

8.2.5 Appendix B-5: Reproducibility and selection of the normalization algorithm

Three different normalization algorithms to process my MALDI-imaging MS datasets were compared: (i) No Normalization (NN), (ii) Total Ion Count (TIC), and (iii) Root Mean Square (RMS). Three almost-identical consecutive sections were used to evaluate the reproducibility of the measurements, by comparing the spatial distribution and intensity of aeroplysinin-1. The aim was to select the normalization algorithm that provided the relative standard deviation (RSD) of aeroplysinin-1 and aerophobin-2 intensities among the three consecutive sections. Lower RSD values were provided by using RMS normalization (**Figure Appendix B.3**). It was confirmed that RMS did not created artifacts in the ion images by visual examination, as recommended in Alexandrov *et al.* (2012).

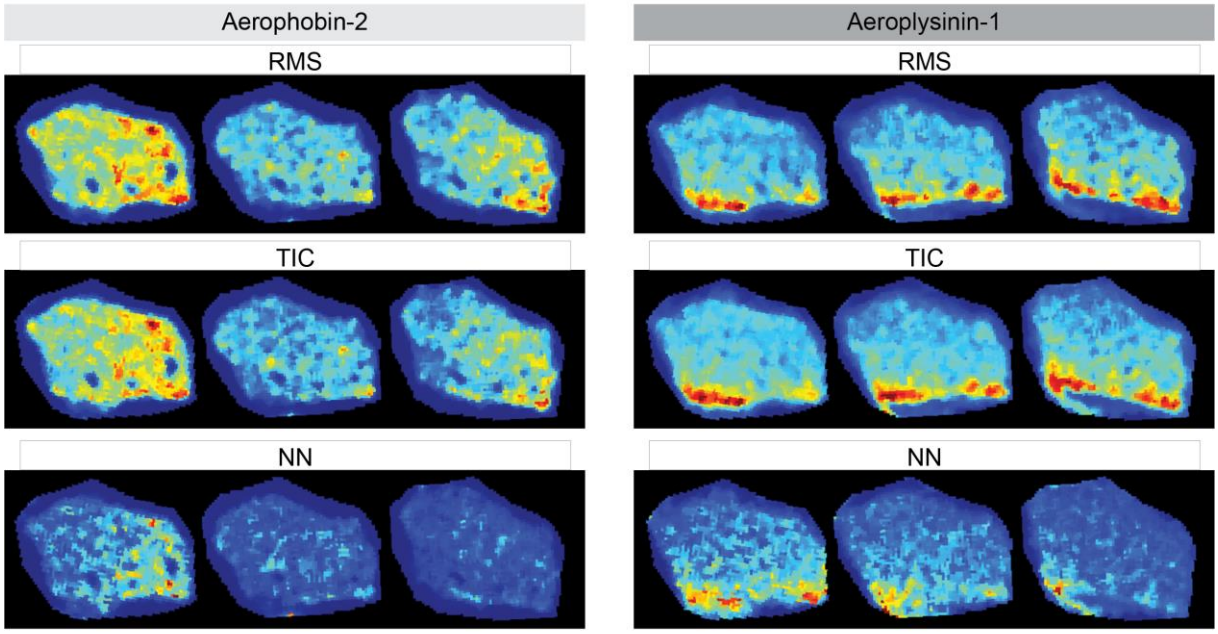

Figure Appendix B.3. Optimizing MALDI-imaging MS protocol and selection of Root Mean Square (RMS) normalization. Comparison between MALDI-imaging MS normalization methods (**RMS**, Root Mean Square; **TIC**, Total Ion Count; **NN**, No Normalization) on spatial distribution of aerophobin-2 (**Aerophobin-2**) and aeroplysinin-1 (**Aeroplysinin-1**). Three almost-identical sections of one sponge specimen collected at 1d-2017 were mounted on a same ITO glass slide. The relative intensity of each compound is depicted in a color scale (**top left**). Red color represents a relatively higher intensity, while blue color represents a relatively lower intensity of each compound.

8.2.6 Co-localization of aeroplysinin-1 with aerophobin-2 across sponge cross-sections of 1d-2017 samples

To investigate the co-localization relationship between aerophobin-2 and aeroplysinin-1, ion images were exported as greyscale images in SCiLS Lab 2016b. Thus, the absolute intensity of each compound in each pixel was computed as relative values of a gradient grayscale (0 to 255). Greyscale images were imported in Fiji (Schindelin *et al.*, 2019). Images that showed (i) on which pixels both compounds co-localized (abbreviated AND, aerophobin-2 ∧ aeroplysinin-1) and (ii) on which pixels at least one compound was detected (abbreviated OR, aerophobin-2 ∨ aeroplysinin-1) were calculated. The results showed two consistent patterns among all control, grazed, and mechanically damaged samples: (i) the co-localization maps (**Figure Appendix B.4, AND**) were correlated with the spatial distribution of aerophobin-2 (**Figure 15**), and (ii) areas with the highest intensity in the maps with at least one compound (**Figure Appendix B.4, OR**) showed usually no signals in the co-localization maps (**Figure Appendix B.4, AND**). These spatial associations

suggest that: (i) aeroplysinin-1 correlated with aerophobin-2 (i.e., when aerophobin-2 is detected, aeroplysinin-1 is usually detected as well), and (ii) a higher intensity of one compound was coincident with decreased intensity of another compound, which suggests interconversion. These two phenomena took place independently from the treatments.

It is worth noticing that mass spectrometric techniques are not absolutely quantitative, since under a given set of conditions different molecules ionize to different extents according to their physicochemical properties. For the same concentration of analyte (1 mM), aeroplysinin-1 and aerophobin-2 showed different intensities in MALDI-TOF (**Figure Appendix B.5**). For that reason, the intensity (relative intensity) of each compound between treatments was qualitatively compared.

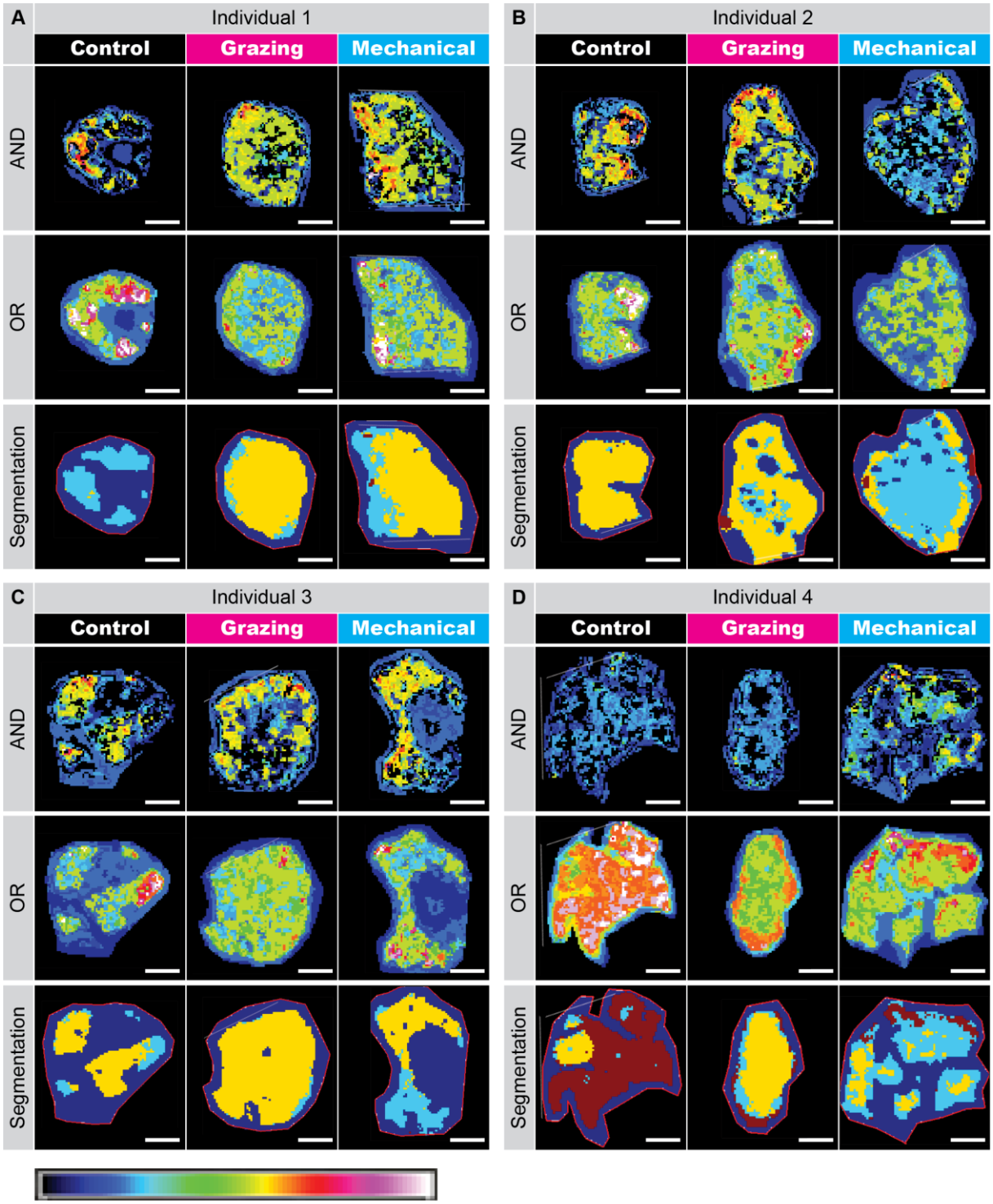

Figure Appendix B.4. Co-localization maps and segmentation maps of sponges collected from 1d-2017. (**A, B, C, D**) Each box shows the results corresponding to the three different treatments of one biological replicate (i.e., specimens of a same sponge individual): **Control** (left panel), **Grazing** (middle panel), and **Mechanical** (mechanical damage: right panel). For each sample, the correspondent co-localization of aerophobin-2 and aeroplysinin-1 (**AND**), the distribution pattern of at least one of the compounds aerophobin-2 or aeroplysinin-1 (**OR**), and a segmentation map (**Segmentation**) are shown. The relative intensity in AND and OR is depicted in a color scale (**bottom left**). White color represents a relatively higher intensity, while blue color represents a relatively lower intensity. **White-dotted line**= broken or cut edges; scale bar = 5 mm.

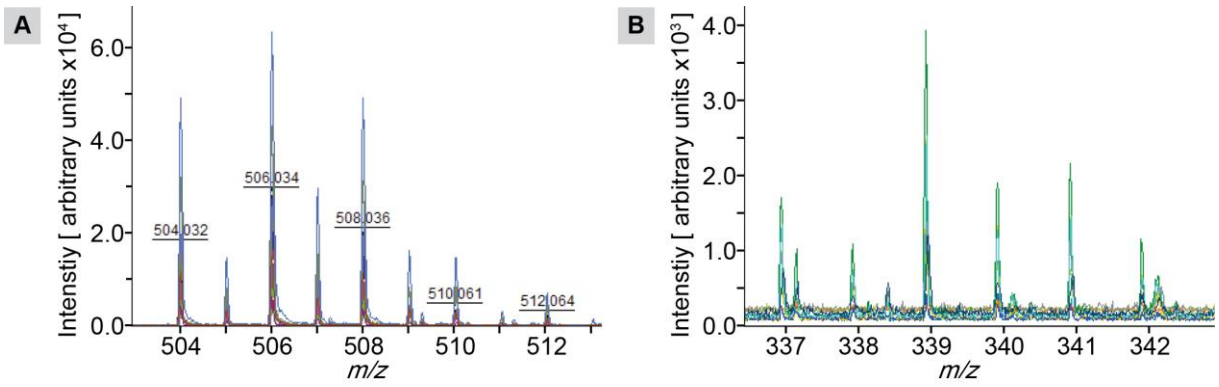

Figure Appendix B.5. Comparison of ionization yield of aerophobin-2 and aeroplysinin-1 at the same concentration (1 mM). Aerophobin-2 (**A**) showed one order of magnitude in intensity compared with aeroplysinin-1 (**B**).

8.2.7 Multivariate statistics to investigate sponge cross-sections of 1d-2017 samples

In my PhD thesis, the MALDI-imaging MS measurements generated a large and complex datasets with thousands of spectra per sample, each spectrum containing hundreds of compounds including my target compounds aerophobin-2 and aeroplysinin-1 (**Figure 15**), more brominated compounds, and other unidentified compounds.

The datasets were analyzed and interpreted by applying spatial multivariate statistics. Specifically, spatial segmentation on the MALDI-imaging MS data was applied by clustering of spectra by their similarity, generating an unsupervised spatial segmentation map of the tissue section where regions of similar chemical compositions were revealed. Thus, in segmentation maps regions of distinct molecular composition are color coded. SCiLS Lab 2015b was used to calculate segmentation maps using the following parameters: in peak picking workflow, 200 peaks (every 2 spectra) were selected; segmentation maps were calculated by bisecting k-means using correlation distance, weak denoising, and RMS normalization.

In samples of the control group, two spatial patterns were found: (i) a homogeneous pattern in individual 1 and 2 (i.e., most spectra from the sections belong to the same “chemical region”), and (ii) a heterogeneous pattern (i.e., marked two to three colored-clusters) in individual 3 and 4 (**Figure Appendix B.4, Segmentation**). In contrast, the grazing and mechanical damage groups had only a heterogeneous

pattern in which one distinct cluster localized at the surface (**Figure Appendix B.4, Segmentation**). The segmentation maps highlighted (i) high variability among the control samples and (ii) distinct patterning among the wounding groups, which suggests that the surface of wounded samples has a distinct chemical composition. In general, the unsupervised segmentation maps show correspondence to the distribution of aerphobin-2 and aeroplysin-1, which suggests that the presence of brominated alkaloids are important to define the chemical regions on the sponge sections.

9. Publications

In the course of my PhD thesis, I performed a part of microscopic research in the following publications which can be found at the links provided below.

Helber, S. B., Steinert, G., **Wu, Y. C.**, Rohde, S., Hentschel, U., Muhando, C. A., & Schupp, P. J. (2019). Sponges from Zanzibar host diverse prokaryotic communities with potential for natural product synthesis. *FEMS microbiology ecology*, *95*(4), fiz026. https://doi.org/10.1093/femsec/fiz026

Rubin-Blum, M., Antony, C. P., Sayavedra, L., Martínez-Pérez, C., Birgel, D., Peckmann, J., **Wu, Y. C.**, Cardenas, P., MacDonald, I., Marcon, Y., Sahling, H., Hentschel, U., & Dubilier, N. (2019). Fueled by methane: deep-sea sponges from asphalt seeps gain their nutrition from methane-oxidizing symbionts. *The ISME journal*, *13*(5), 1209. https://doi.org/10.1038/s41396-019-0346-7

Moitinho-Silva, L., Steinert, G., Nielsen, S., Hardoim, C. C., **Wu, Y. C.**, McCormack, G. P., López-Legentil, S., Marchant, R., Webster, N., Thomas, T., & Hentschel, U. (2017). Predicting the HMA-LMA status in marine sponges by machine learning. *Frontiers in microbiology*, *8*, 752. https://doi.org/10.3389/fmicb.2017.00752